

PROFESSOR JÉRÔME CHEVALIER (Orcid ID : 0000-0001-8546-6149)

Article type : Invited Feature Article

Fourty years after the promise of « ceramic steel? »: zirconia-based composites with a metal-like mechanical behavior.

Jérôme Chevalier^{a,*}, Aléthéa Liens^a, Helen Reveron^a, Fei Zhang^a, Pascal Reynaud^a, Thierry Douillard^a, Laura Preiss^a, Valter Sergio^{b,c}, Vanni Lughì^b, Mike Swain^{d,e}, Nicolas Courtois^f

^a Université de Lyon, INSA-Lyon, UMR CNRS 5510 MATEIS, 20 Avenue Albert Einstein, 69621 Villeurbanne Cedex, France

^b Engineering and Architecture Dept., University of Trieste, Italy

^c Faculty of Health Sciences, University of Macau, SAR Macau, China

^d AMME, University of Sydney, NSW 2006 Australia

^e Engineering, Don State Technical University, Rostov-on Don, Russia.

^f Anthogyr SAS, 2237 avenue A. Lasquin 74700 Sallanches, France

Abstract

* Corresponding author : jerome.chevalier@insa-lyon.fr

This article has been accepted for publication and undergone full peer review but has not been through the copyediting, typesetting, pagination and proofreading process, which may lead to differences between this version and the [Version of Record](#). Please cite this article as [doi: 10.1111/JACE.16903](https://doi.org/10.1111/JACE.16903)

This article is protected by copyright. All rights reserved

40 years ago, Garvie and his Australian co-workers reported that the stress induced transformation of metastable tetragonal zirconia grains to the monoclinic symmetry could give rise to a powerful toughening mechanism. Their results even led them to consider zirconia systems as analogues of certain steels. This seminal paper generated extraordinary excitement in the ceramic community and it is still the subject of extensive research. Transformation toughening is widely used in zirconia materials and results in an increase in strength and toughness when compared to non-transformable ceramics, but the implementation into strong, tough, and sufficiently stable materials has not been fully reached. Zirconia ceramics generally fail at low strains with a much larger scatter in the strength values than metals and require statistical approaches to failure. Here we describe in details the mechanical behavior laws of ceria-doped zirconia composites exhibiting a high degree of stress-induced transformation. They present, to some extent, mechanical behavior analogous to a metal, displaying, *i)* significant amount of transformation-induced plasticity without damage, *ii)* very high flaw tolerance and *iii)* almost no dispersion in strength data. They potentially open new application avenues in situations where the advantages of ceramics were dampened by their brittle failure behavior. In particular, the consequences of such behavior for dental implants and additive-manufactured structures are highlighted.

I. Introduction

Zirconia (ZrO_2) was first identified by the German chemist Martin Heinrich Klaproth in 1789 [1] as a reaction product of heating zirconium. In 1892, a more abundant source was discovered in the mineral Baddeleyite (80-98% of zirconia) [2]. An important step in the development of zirconia was published just a century ago in the *Journal of the American Ceramic Society* during its inaugural year in 1918, by Phillips, who proposed a procedure for the purification of zirconium dioxide [3]. However, it was not until 1928 that the first commercial zirconia-based product appeared, in the form of MgO-stabilized ZrO_2 crucibles for metal melts [4]. Because of the tetragonal (*t*) to monoclinic (*m*) martensitic phase transformation that occurs during cooling at $\sim 950^\circ\text{C}$ (temperature referred to as M_s , *Martensitic-Start*), accompanied by approximately 5% of volume increase [5], pure zirconia was indeed unsuitable for numerous technical applications, due to the impossibility of full-densification without catastrophic failure upon cooling and/or its poor stability when cycling at high temperatures (in the range $900\text{-}1200^\circ\text{C}$). However, it was shown that certain oxides could be added to zirconia and stabilize the high-temperature phases (cubic or tetragonal) at room temperature (see **Panel A**), thus allowing the use of this ceramic in a wide range of application fields. Nevertheless, for many years the use of CaO or MgO-stabilized zirconia was limited to the refractory industry. The discovery of the phase transformation toughening mechanism by Garvie and co-authors in 1975 [6] created new visions for high-performance zirconia applications. It was stated that ‘*The presence of a tetragonal phase that can revert to the stable monoclinic form has a number of important consequences. The first is a significant-increase in strength [...]. A more important contribution comes from the absorption of energy during the martensitic transformation of tetragonal particles, as in the TRIP steels*’. In other words, the *t-m* transformation at the crack tip could lead to an important transformation-induced absorption of energy. Their results, including the fact that the phase diagrams showed similar features to the one of Fe-C, even led them to consider zirconia systems as analogues of certain steels. This seminal paper created extraordinary excitement in the ceramic community and zirconia is still the subject of extensive research, debates and controversies. From a practical point of view, zirconia finds applications in a number of technical fields such as in Thermal Barrier Coatings (TBCs), bearings, fuel cell membranes, oxygen sensors, optical ferrules, and, most recently, biomedical devices. Today stabilized-zirconia is without doubt one of the most important ceramic materials because of its unique combination of properties such as high strength and

fracture toughness at room temperature, high density, hardness, wear resistance, high temperature stability and low thermal conductivity. However, it must be recognized that transformation toughening leads to an increase in strength when compared to non-transformable ceramics, but the translation into tough, strong and sufficiently stable materials has not been fully accomplished. For most industrial applications, zirconia ceramics fail by crack extension at low strains along with much larger scatter in strength than metals and this behavior imposes the use of statistical failure approaches. This is the case of the most common zirconia ceramic, stabilized with Yttria (*Y-TZP*, for *Yttria-Tetragonal Zirconia Polycrystal*). On the other hand, in the past [7-10] and more recently [11, 12], some Ceria-doped zirconia (*Ce-TZP*) based ceramics and composites were shown to exhibit significant amount of transformation-induced plasticity and almost no dispersion in strength data. Such materials could open new possibilities for applications where the limits of the failure properties of ceramics could be overcome, provided their mechanical behavior laws are well understood and described. The aim of the present paper is thus to describe in details the mechanical behavior of ceria-doped zirconia composites in relation to their transformation characteristics, and to discuss the transition from a conventional brittle behavior to a transformation induced ductility and, finally, to highlight the positive impact of genuine ductility on future potential applications. We here take the example of dental implants and additive-manufactured materials, for which a certain ductility and defect tolerance would be utterly beneficial.

II. Where are we?

Based on the established linear elastic fracture mechanics and Griffith equation, it is well known that there are two approaches to obtain reliable structural ceramic materials: controlling flaw size and/or increasing toughness and crack resistance. Indeed, for brittle materials, it is generally considered that strength σ_R is given by:

$$\sigma_R \sim \frac{K_{IC}}{\sqrt{\pi c}} \quad (1)$$

Where K_{IC} is the toughness and c is the size of the most critical defect.

With the continuing trend of seeking ever stronger materials, previous studies in the 80's proceeded to identify and reduce strength-reducing flaws by improving processing [13], for

example through colloidal approaches to remove powder agglomeration and/or to induce microstructure refinement. Nevertheless, these strength enhancements were limited, as in the case of alumina ceramics, which barely exceed 600 MPa, even with careful control of grain size and processing defects. Subsequently in the 90's, researches placed emphasis on improving the toughness of brittle ceramics. Various methods were developed such as; *i*) phase transformation toughening in zirconia ceramics, *ii*) bridging via larger grains along with elongated morphology, *iii*) reinforcement by dispersing particles, whiskers and/or fibers, etc. [14-19]. Ceramics are not intrinsically tough as metals (where dislocation-based plasticity ahead of the crack tip is the key factor), but can be extrinsically toughened at the crack tip wake. This results in the generation of a crack-resistance curve (rising R-curve), which means that the toughness increases as the crack grows, eventually reaching a plateau value. However, unfortunately, strength is influenced by short-crack extension behavior and the optimal conditions (composition, grain size, transformability...) that maximize ceramic strength and toughness are not usually coincident. Consequently, the design of strong and tough materials is inevitably a matter of compromise. Therefore, over the last two decades, studies focused on strategies to obtain a better balance between strength and toughness in ceramic materials [5, 11, 12, 20-45].

Following the extensive research studies on the development of tough and strong ceramics, bio-inspired materials have been also investigated, such as the damage-resistant materials containing a large inorganic content that widely exist in nature for structural purposes, including bone, nacre or enamel. Bio-inspired materials are tailored to have similar specific hierarchical structures as biological materials at multiple length scales [46-49]. Some remarkable enhancements in toughness were indeed achieved, for example, nacre-like 'brick-and-mortar' structures made from hybrid materials (alumina-polymethyl methacrylate) or in artificial mineral constituents, resulting in materials having long-crack fracture toughness of $\geq 20 \text{ MPa}\cdot\sqrt{\text{m}}$ and strength of 200-500 MPa [46, 47]. By looking at the fracture behavior, the fracture resistance of these bio-inspired ceramics is derived from a series of extrinsic toughening mechanisms acting at various length-scales and developing a substantial R-curve effect [46-50]. These mechanisms are related to damage extension and development of a 'process zone' in which crack bridging, deflection and branching act to increase the crack resistance. Apart from the case of metal- or polymer-impregnated bio-inspired ceramics, ceramics remain 'brittle' in the sense that no ductility is observed. The term

ductility is meant to convey, from a mechanical point of view, that a permanent strain remains after unloading with minimal loss in stiffness and no associated damage.

Considering the development of ‘traditional’ zirconia ceramics, the capability of obtaining genuinely “ductile” ceramics from transformation-induced plasticity has been under-explored. Some zirconia indeed exhibit pronounced R-curve behavior (high fracture toughness ≥ 20 MPa $\cdot\sqrt{m}$ reported in some cases [14]) and a few studies have shown that Ce-TZP based ceramics might be considered as ‘ductile’, with a certain degree of transformation-induced plasticity before failure [6-10, 20, 21, 51-57 and Figure 1]. Recent studies on micro-pillars have also reported that some Y-TZP ceramics exhibit transformation-induced plasticity [58], provided the size of the tested samples was small enough and free of processing defects. Transformation-induced plasticity is thus more limited in 3Y-TZP than in Ce-TZP and has never been reported on large-sized samples.

Zirconia offers the possibility of utilizing different stabilizers [13, 22]. As explained in Panel A, metastable tetragonal zirconia can be retained at room temperature by alloying with Y_2O_3 , CeO_2 or other rare earth oxides. 3 mol.% yttria-stabilized zirconia (3Y-TZP) possesses the highest strength (800-1200 MPa) among all single-phase oxide ceramics, but only moderate fracture toughness (~ 6 MPa $\cdot\sqrt{m}$). Ce-TZP (typically 10 and 12 mol.% Ce-TZP) on the other hand exhibits higher toughness (15-20 MPa $\cdot\sqrt{m}$) but lower strength (typically less than 600 MPa). The strength difference between Y-TZP and Ce-TZP is in part related to the fact that fully dense 3Y-TZP can be easily sintered while retaining a relatively small grain size (submicron grain size, typically as low as 0.3 μm), whereas the grain size of Ce-TZP generally lies above 1.5-2.0 μm . Indeed, the mobility of grain boundaries during sintering is much higher in Ce-TZP than in Y-TZP and it is thus difficult to obtain a fine-grained, fully dense Ce-TZP. Furthermore, compared to Y-TZP, Ce-TZP has a lower critical transformation stress (σ_c^{t-m}) and a higher spontaneous tetragonal-monoclinic transformation temperature T_0^{t-m} , which is associated with a larger transformation zone size around a crack [59]. Depending on the dopant concentration and the final grain size, the width of the transformation zone (h) in Ce-TZP is in the range of 100 μm while the transformation zone of Y-TZP is much smaller, typically a few micrometers [60]. Regarding the R-curve behavior, as shown in Figure 2 [5, 23-24], the extent of transformation toughening is proportional to $h^{1/2}$, while the crack extension to achieve a plateau value is a multiple (4 to 6 times) of h . In the case of Ce-TZP ceramics, this results in having a high saturation level (K_{Rmax}). Furthermore, a crack can

stably grow several times larger than the maximum transformation zone size, and, hence, Ce-TZP has high flaw tolerance characteristics [61]. Nevertheless, as explained above, since high strength can only be obtained for materials with high toughness at small crack length, the gradual increase of crack resistance (small initial slope of R-curve) in Ce-TZP gives rise to relatively modest strength compared to Y-TZP.

As a consequence, thanks to their high strength, 3Y-TZP ceramics (especially 3 mol.%) have found various high-performance applications, such as in the biomedical field, initially for hip joints (almost abandoned after 2001, due to a failure episode associated to the issue of aging described below), then for dental prostheses and implants. Moreover, high-quality commercial 3Y-TZP powders are readily available, and these ceramics can be quite easily machined at different steps of the process (either in green, pre-sintered or sintered stage) and can be made more translucent. However, Y-TZP based systems may suffer from hydrothermal aging in the presence of water [59]. Aging of 3Y-TZP may be a critical concern in certain cases: this phase destabilization, occurring spontaneously (without the need of applied stresses) at room temperature and in presence of water had clearly a negative impact in the orthopedic community because of the failure of more than eight hundred 3Y-TZP Prozyr® femoral heads in 2000, commencing within months after implantation [59]. Nevertheless, the use of yttria-stabilized zirconia is booming in dental fields to make crowns, bridges and even implants, for which the optical properties (color and translucency) is another important driving force. Research is also ongoing to improve the aging resistance of 3Y-TZP ceramics. Recent literature shows that adding alumina as dopant, increasing the homogeneity of the yttria content in the grains or playing with grain boundaries can strongly delay hydrothermal aging [62-65]. Obtaining completely aging-free 3Y-TZP seems to be a difficult task due to the inherent presence of oxygen vacancies generated when Y^{3+} replaces Zr^{4+} in the cationic sub-lattice, in order to achieve charge neutrality. It is now well accepted that the presence of oxygen vacancies, stabilizing the tetragonal phase in Yttria-Zirconia system, are also the origin of aging, since they can be re-filled by hydroxyl groups in the presence of water [59]. This is in contrast to Ce-TZP, where tetragonal zirconia is stabilized by a tetravalent dopant (Ce^{4+}) thanks to a steric effect and the absence of oxygen vacancies make this system very stable in the presence of water [59, 61]. It is worth recalling that, as explained before, not only having a high strength is important but, today, the quest is also to obtain materials with an optimal balance between strength, toughness and long-term stability, a balance that, ideally,

should be tailored for each specific application. Ce-TZP systems can benefit from a high degree of transformation-induced plasticity and high toughness [5, 23-25, 51], making them highly suitable for obtaining such balance between strength, toughness and long-term stability in water-rich environments. The most critical challenges in these systems is thus to refine the microstructure, optimize the degree of phase transformation and better understand the mechanical behavior laws [66].

It is well known that processing nanocomposites is a promising strategy for inhibiting grain growth. Introducing an immiscible second phase like alumina to pin the grain boundaries can control the grain growth of zirconia. Finer microstructures lead to higher σ_c^{t-m} and steeper R-curves slopes, but higher σ_c^{t-m} may compromise the toughening extent in zirconia ceramics. In this sense, it may be advantageous to have additional toughening effects, like adding elongated phases which can also hinder the zirconia grain growth and further improve the toughness by crack deflection [26, 67-70]. The challenge of incorporating elongated third phases is to retain the fine and uniform microstructure without turning themselves into “critical defects”. Such Ce-TZP based-composites, with high flaw tolerance and narrow strength distributions, have been reported [11, 12, 21, 22, 25-42, 71]. Without achieving the very high strength of 3Y-TZP, Ce-TZP based composites can be made strong enough for most engineering applications, with a higher toughness and reliability (*i.e.* high Weibull Modulus) and a certain degree of plasticity [5, 12, 22-25]. However, it has to be admitted that, 40 years after the introduction of the concept of ‘Ceramic steels’ and 30 years after the first studies on ductile Ce-TZP [6-10, 20, 21, 51-57], their potential has not been fully exploited. There is indeed no application of this transformation-induced plasticity feature into real ceramic products.

This paper therefore attempts to address the following issues:

- How can we process ultra-fine Ce-TZP based composites and how can we reach the highest degree of strength and toughness?
- What is the mechanical behavior law of a highly transformable (ductile) zirconia composite and what can be the extent of plasticity achievable with such materials?
- Can we talk about transformation-induced plasticity?
- What are the benefits and drawbacks of highly transformable zirconia systems and what can be the targeted future applications?

III. Processing challenges and experimental methods (Ce-TZP composites)

General challenges in processing ultrafine ceramic composites

Over the past few decades, the mechanical properties of structural ceramics have been substantially improved thanks to the development of ceramic nanocomposites [15]. These composite materials are typically processed by adding fine particles/whiskers/elongated phases to different ceramic matrix (oxides and non-oxides) with the aim of refining the microstructure (increasing strength and hardness) and/or to promote other toughening or high temperature strengthening mechanisms [16-19].

In the case of zirconia-based composites, the progress made to combine strength and toughness in a unique material stems not only from a better understanding of toughening/strengthening mechanisms but also from improvements achieved in the processing of nano-powders and the capability of developing complex microstructures at the nanoscale.

Typically, ceramic composites are processed by mixing appropriate quantities of commercial or synthesized powders in aqueous suspensions. After the dispersion step (through ball-milling, attrition milling, planetary milling, etc.), the slurry can be slip-casted onto a porous mold and then sintered (natural sintering usually at $T > 0.5T_{\text{melting}}$) or dried (spray-drying or natural drying followed by dry-milling) in order to obtain a granulated powder. The latter is then pressed (by uniaxial pressing or cold isostatic pressing) and sintered or pressed and sintered at once (by hot pressing, hot isostatic pressing, Spark Plasma Sintering etc.). Ultimately, preparing ceramic composites with homogenous and controlled microstructure requires optimizing both powder synthesis and processing.

Zirconia-based composites can be prepared from milling and mixing powders [72]. However, this processing route often yields to materials with coarser microstructures than those obtained with bottom-up approaches. The so-called colloidal processing based on sol-gel methods enables development of ultrafine materials, but it is more complex and, frequently, the use of expensive organic precursors such as metal alkoxides is required [73]. Since 2000 onwards various surface modification techniques have been used to produce composite powders from pure zirconia powders and inexpensive inorganic salts [74, 75]. Starting from a commercial powder, the surface

of particles is first coated by precursors of second phases which are then crystallized during thermal treatment. In this manner, the mixing between the matrix ceramic particles and the precursor is realized at the nano/atomic level and composite materials with a very homogenous second phase distribution can be obtained [74, 76].

In the case of alumina-rich composites, a modified processing route which consists in doping a commercial alumina powder with alkoxides has been used to process very homogeneous alumina-based composites. These have a relatively low quantity (< 5 wt.%) of secondary intergranular nanophases of zirconia, yttrium aluminium perovskite (YAP), yttrium aluminium garnet (YAG) and/or mullite, thereby increasing the effectiveness of the reinforcement mechanisms operating in these nanocomposites and also the creep resistance [77, 78].

Previous attempts and state of the art: processing of Ce-TZP based composites

Table 1 shows the properties of some Ce-TZP composites developed these past 30 years. The concept of “ceramic composite” was for the first time applied in 1989 to Ce-TZP ceramics with the aim of increasing the hardness and Young modulus by adding alumina particles [32]. Since then, several authors have developed alumina/Ce-TZP composites from in-lab synthesized powders or pre-mixed and spray-dried commercial powders, which were often subjected to Cold Isostatic Pressing (CIP) and conventional sintering and in some cases to Hot Isostatic Pressing (HIP) [11, 12, 21, 25, 26, 32, 37, 38, 43, 45]. It was observed that when 20 wt.% of Al_2O_3 is added to 12 mol.% Ce-TZP, the presence of alumina particles of $0.5 \mu\text{m}$ limited the zirconia grain size from 3 to about $1 \mu\text{m}$ [33, 34]. Very high toughness and strength values ($9.8 \text{ MPa}\cdot\sqrt{\text{m}}$ and bending strength of 950 MPa) have been also reported in 1998 [35] for an intra-granular type 10Ce-TZP/30vol.% Al_2O_3 / 0.05 mol.% TiO_2 composite in which 10-100 nm sized Al_2O_3 particles were trapped within the ZrO_2 grains and vice versa [36] (**Figure 3**).

The above 10Ce-TZP based materials were classically processed from dispersed commercial powders, which were subsequently dried, calcined, sieved, uniaxially and CIP pressed and conventionally sintered at $T < 1550^\circ\text{C}$ for 2h. Thanks to strict control of the composition, the mechanical properties were optimized, giving rise to the US patent 7928028 and the commercial product named NANOZR (Panasonic Electric Works, Japan) with a reported bending strength of 1290 MPa and a toughness of $8.6 \text{ MPa}\cdot\sqrt{\text{m}}$ [37]. More recently, a composite of 10Ce-TZP/16vol%

MgAl₂O₄ combining high strength (~900 MPa) and very high toughness (15 MPa·√m) was also successfully developed [38]. According to the authors, the grain size reduction achieved by developing inter-intragranular composites (10Ce-TZP and Mg-spinel grain sizes were 0.5 and 0.2 μm respectively) increases the critical stress to induce *t-m* zirconia phase transformation, while still maintaining a high level of transformability. A further increase in toughness achieved by activating additional bridging/crack deflection mechanisms is also expected with the use of elongated second phases (SrAl₁₂O₁₉, LaAl₁₁O₁₈, MgAl₂O₄...) [41]. Nevertheless, the exact role of such platelets on toughness, even if quite obvious in principle, has not been fully elucidated and quantified.

In the case of alumina-rich systems, the commercial product named BIOLOX Delta (CeramTec AG, Germany) which is a Zirconia Toughened Alumina (ZTA) consisting of 80 vol.% Al₂O₃, 17 vol.% ZrO₂ and 3 vol.% SrAl₁₂O₁₉ platelets shows excellent stability, wear resistance and mechanical properties. Flexural strength of 1150 MPa and toughness of 5.9 - 8.5 MPa·√m were reported [79, 80]. Small quantities of Y₂O₃ (0.6 wt.%) and Cr₂O₃ (0.3 wt.%) are also added to the raw materials in order to increase zirconia stability, and hardness and wear resistance, respectively [71] (Figure 4). Ceria has also been used to improve the stability of zirconia in ZTA materials [40] as well as other elongated phases such as CeMgAl₁₁O₁₉ (obtained by co-precipitation methods and mixed with zirconia and alumina powders [41]) or LaAl₁₁O₁₈ (crystallized in-situ during sintering from La₂O₃ [42]).

In the case of zirconia-rich systems, Cutler et al. developed in the 90's tri-phasic 12Ce-TZP/Al₂O₃/SrAl₁₂O₁₉ composites, with Ce-TZP grains of 1-3 μm, equiaxed Al₂O₃ grains of 0.1-1 μm and SrAl₁₂O₁₉ platelets of 1-3 μm in length [21]. Depending on the composition, fracture strength in the range 500-700 MPa and fracture toughness of 10-15 MPa·√m were measured. These composites were processed by mixing Al₂O₃, Ce-TZP (12 mol.%) and SrZrO₃, the latter being the source of SrAl₁₂O₁₉ platelets. Zirconia-based composites may be also processed by the alkoxide route described above, allowing a fine tuning of microstructure and composition [77, 81-83].

At this stage, it is pertinent to address the issue of the redox behavior of Cerium. Cerium ions can present both the Ce⁺⁴ and Ce⁺³ oxidation state. As stabilizing agent for zirconia, for reasons already recalled in section II, Ce⁺⁴ is preferred to Ce⁺³ [84-86]. The internal part of ceria/zirconia composites can however undergo the Ce⁺⁴/Ce⁺³ reduction even when sintered in air, and this may

be detrimental for the structural stability of the component (this fact can be detected even with the naked eye, since the zirconia parts with Cerium oxide in the Ce^{+3} state (Ce_2O_3) tend to have a greyish color rather than the pale yellow of Ce-TZP with Ce^{+4} ; ultimately, though, the presence of Ce^{+3} can be confirmed by X-Ray Photoelectron Spectroscopy (XPS) analysis [87]. Indeed all processing/firing conditions of Ce-TZP composites must be designed in order to avoid Ce^{+3} appearance, but practically, the issue is relevant only for dense pieces thicker than about 1 cm: below this dimension, if sintered in air with a convenient cooling rate, Ce^{+4} is the dominant oxidation state.

The two approaches to process Ce-TZP - Al_2O_3 - $SrAl_{12}O_{19}$ composites presented in this work

The above-mentioned literature shows that tri-phasic systems are promising to obtain Ce-TZP-based composites with high toughness and high strength, thanks to a careful microstructural engineering. The combination of this approach with surface-coating strategies (e.g. surface modification of a Ce-TZP powder with inorganic precursors, which then gives rise to composite nano-powders) allows a further degree of refinement, as shown in previous studies [11, 12, 74, 75, 77]. We thus decided to work in the Ce-TZP – Alumina – Strontium Aluminate system to take benefit and tailor the transformation features of the zirconia phase (by tailoring the amount of Ceria in the zirconia phase) and to refine the microstructure by the addition of two additional phases. The strontium aluminate phase ($SrAl_{12}O_{19}$) was added to benefit from the potential additional crack-deviation mechanism mentioned in previous literature (e.g. in [41]), but also to induce tensile residual stresses in the zirconia matrix [88] and trigger the t-m transformation, in order to compensate for the small zirconia grain sizes.

Surface-coating route

In order to obtain ultrafine tri-phasic ceramics, composite powders were prepared by an innovative surface coating route, developed at the Politecnico di Torino by Palmero et al. [11]: commercial zirconia powders were coated by inorganic precursors of the second phases which crystallize on the surface of the zirconia particles under appropriate thermal treatment. basically, a commercial 10 mol.% ceria-stabilized zirconia powder (Daiichi Kigenso Kagaku Kogyo Co. LTD, Japan), referred to as 10Ce-TZP, was employed as raw material. The powder was then dispersed in a water-based slurry, which was then doped by a drop-wise addition of nitrates of Aluminum,

Strontium and Cerium to obtain composite powders having the following composition after thermal treatments: 84 vol.% ZrO₂, 8 vol.% Al₂O₃, 8 vol.% SrAl₁₂O₁₉ (referred to as ZA₈Sr₈) and with different degrees of ceria in the zirconia phase. Composite powders were then obtained by drying the slurry with the precursors attached at the surface of the zirconia particles and then with further thermal treatments yielding the secondary alumina and aluminate phases. The powders were then dispersed in water and slip-casted, under conditions reported in [11]. An example of the microstructure obtained with these composite powders is shown in **Figure 5**: zirconia grains (Z) of $0.6 \pm 0.2 \mu\text{m}$, alumina grains (A) of $0.3 \pm 0.1 \mu\text{m}$ and strontium aluminate grains (S) with a mean length of $0.6 \pm 0.2 \mu\text{m}$ and aspect ratio (length/width) of 5 ± 2 were developed after conventional sintering at 1450°C-1h. The method thus allows a very precise and easy tuning of the ceria content, as well as ultrafine microstructures not previously achieved, and it has been patented [89]. However, industrial needs require easier processing, with more conventional powder-mixing and pressing techniques: therefore a more standard route was also attempted as a benchmark, as explained below.

Standard powder-mixing route

Zirconia-based composites with 11.0 and 11.5 mol.% CeO₂ contents obtained by industrial processing (*i.e.* isostatic pressing of a spray dried composite powder composed of 84 vol.% Ce-TZP, 8 vol.% Al₂O₃ and 8 vol.% SrAl₁₂O₁₉ and conventional sintering) were also investigated [22]. For all the composites sintered conventionally at 1450°C-1h (**Figure 6**), the grain size of zirconia (Z) was $1.0 \pm 0.3 \mu\text{m}$, the grain size of alumina (A) was $0.3 \pm 0.1 \mu\text{m}$, the length of the aluminate platelets was $1.7 \pm 0.5 \mu\text{m}$ and their aspect ratio (length/width) 5 ± 2 [22]. The industrial processing of the studied composites led to a larger size of the zirconia and aluminate elongated phases, in comparison to those developed by a surface modification strategy and slip-casting.

Choice of samples for testing

Due to the difficulty in obtaining large batches of materials through the surface-coating method, the characterization of these samples was limited to: *i*) spontaneous transformation temperatures T_{t-m} , *ii*) biaxial bending strength and *iii*) toughness (Single-Edge-V-Notched Beam (SENVB)). The effect of the composition (mainly the Ceria content) and of the sintering temperature on these properties were also thoroughly investigated.

On the other hand, to determine the mechanical behavior laws of more transformable composites and to characterize the mechanical properties with different testing geometries (biaxial bending, four-point bending, pure tension, load to failure of dental implants, compression of additive-manufactured samples), a large series of samples was processed by the powder-mixing route, in a pilot-plant.

Piston-on-three balls biaxial bending strength was determined from samples with a diameter of 15 mm machined on both sides in order to have opposing flat surfaces, with a thickness of 1.2 ± 0.2 mm. For toughness and four-point bending strength measurements, ceramics were machined on all sides to a rectangular cross section of $(4.0 \times 3.0) \pm 0.2$ mm x 50 mm. Final machining of tensile surfaces was performed by grinding with a 16 μ m diamond grinding tools (CNC with DMU60 mono BLOCK®, DMG, Germany). The notches (SENVB) were introduced using a diamond-loaded cutting wheel 300 μ m in thickness across the 3 mm wide surface perpendicular to the length of the bar, and then sharpened using a razor blade and 3 μ m diamond polishing grit (notch depth in the range of 0.8–1.2 mm, notch-tip radius of less than 10 μ m). In order to minimize the effect of residual stresses developed during sample preparation, an annealing treatment was applied (1200°C-30 min). According to the ISO standard 6872 [90] no annealing treatment was applied for biaxial strength measurements. The cross-head speed was set to 0.5 mm/min (for toughness) or 1 mm/min (for strength) until failure. In addition, in order to better characterize the *t-m* phase transformation during subsequent steps of loading, the tensile surface of a number of samples of each composition was polished using 1 μ m diamond paste before being submitted to load-unload tests.

Tensile test were also performed on machined “bone-shaped” samples (total length of 60 mm, central diameter 2.5 mm and terminal diameter 5 mm) on a hydraulic MTS tensile machine. A clamping hydraulic pressure of 5 MPa was used to prevent the samples from sliding inside the jaws. The tests were performed at a speed of 0.05 mm/min. Both load-unload and load to failure tests were performed on the tensile samples. Strain was measured directly on the samples by means of a displacement transducer.

As introduced before, and to highlight ceramics exhibiting a relatively high degree of ductility, dental implant prototypes and additive-manufactured samples were also prepared and tested. Both processing and testing will be described in **section V**.

IV. Mechanical behavior of ductile Ce-TZP-Al₂O₃-SrAl₁₂O₁₉ composites

Dopant concentration and microstructural effects on transformation and strength/toughness relations

The development of zirconia-based composites with a significant amount of ductility implies a sufficient propensity towards *t-m* transformation at ambient temperature. Adjusting the *transformation-ability* is possible via the amount of dopant (ceria content) and microstructure control (zirconia grain size). The *t-m* transformation temperature (T_{t-m}) was measured on cylinders suspended above a liquid nitrogen bath, progressively cooled below ambient. The surface temperature of the samples was monitored with thermocouples during cooling and the temperature at which the samples spontaneously cracked (generalized transformation) was recorded. **Figure 7** shows the evolution of the spontaneous *t-m* transformation temperature (without any applied stress) of sintered ceria-doped zirconia / 8 vol.% Al₂O₃ / 8 vol.% SrAl₁₂O₁₉ composites as a function of the ceria content in the zirconia phase and the sintering temperature, for the two types of processing methods described above (*i.e.* surface-coating and powder mixing respectively). As expected and already discussed in the literature on other zirconia systems, T_{t-m} decreases with increasing amount of stabilizer [91-94] and with a refinement of the microstructure, [10, 91-95], which, in turn, can be obtained through a decrease of the sintering temperature and/or by a modification of the powder synthesis (surface-coating route, as proposed in [43, 92] giving a much finer, sub-micron microstructure). As T_{t-m} , and thus the transformability, decreases with the amount of stabilizer, K_{IC} obviously decreases with the amount of CeO₂ in the zirconia phase, as shown in **Figure 8**, obtained for the composites processed through the surface-coating route. On the other hand, **Figure 8** also shows that measured strength passes through a maximum. This peculiar behavior cannot be explained solely by standard fracture mechanics equations, but rather by invoking a transition to a ‘ductile’ behavior (transformation before failure) for low stabilizer content and a ‘brittle’ response (crack propagation and transformation around the propagating crack) for higher stabilizer amount. This is in line with the results and analyses of Swain and co-workers [20, 96] and with those reported in other earlier studies dealing with monolithic Ce-TZP (see **Panel A**).

The limitation of the strength in highly transformable zirconia-based materials is governed by the critical stress necessary to induce the *t-m* zirconia phase transformation. This is shown in **Panel B**,

for which we show that for a high transformability, the mechanical behavior law can be approximated as almost purely elastic-plastic. In other words, the critical stress for transformation σ_c^{t-m} corresponds roughly to the elastic limit σ_y and thus (for a purely elastic-plastic behavior) to the maximum acceptable stress $\sigma_{\max 1}$:

$$\sigma_{\max 1} \sim \sigma_y \sim \sigma_c^{t-m} \quad (2)$$

In this regime, the higher the amount of stabilizer, the higher the critical stress for transformation and thus the higher the possible strength. In contrast, for a larger amount of stabilizer, failure precedes transformation: $t-m$ transition occurs only when a crack propagates from a stress concentration site such as a pre-existing processing flaw. We move then to the more classical theory of phase transformation toughening (transformation around a propagating crack) and the Irwin-Griffith equation, for which the maximum acceptable stress $\sigma_{\max 2}$ is given by:

$$\sigma_{\max 2} \sim \frac{K_{IC}}{\sqrt{\pi c}} \quad (3)$$

In this regime, which is also consistent with eqn. (1) for brittle ceramics, strength decreases when the stabilizer amount increases. This is schematically illustrated in **Figure 8.b**. A maximum in strength is obtained when $\sigma_{\max 1} = \sigma_{\max 2}$. This maximum can also be optimized by careful process control and decrease in defect size. In other words, the lower the defect size induced by the process, the higher the maximum in the strength-toughness relation. The load displacement curves of biaxial bending samples (see **Figure 9**), with different amounts of CeO₂ also illustrate the different mechanical behavior of ductile (10 and 10.5 mol.%) and brittle (11.5 mol.%) composites. Load-unload tests illustrate the inelastic strains in the ductile composites after unloading, with no apparent modification of the stiffness (no apparent damage). This latter aspect is addressed in detail hereafter.

As microstructural features are almost identical in these samples with different ceria amounts, the strength variation is attributed to the different degree of zirconia stabilization. In less-stabilized samples (containing 10.0 and 10.5 mol.% ceria), zirconia transformation starts before crack propagation and the strength depends on the critical transformation stress σ_c^{t-m} . For higher ceria contents (*i.e.* 11.0 and 11.5 mol.% ceria), as zirconia becomes less transformable, the transformation is hindered and it occurs only around the crack as it propagates from a pre-existing

processing flaw. The maximum strength is obtained for the intermediate (10.5 mol.%) ceria content, for which the critical stress for t-m transformation, σ_c^{t-m} and the defect-related strength are equal, *i.e.* when $\sigma_c^{t-m} \sim \sigma_{max1} \sim \sigma_{max2}$. Incidentally, this shows that small variations in dopant content (as well as microstructural features) play a critical role on the mechanical behavior laws in these systems, which emphasizes again the influence of processing robustness on the final properties.

Figure 10.a shows the superposition of an optical microscopy image (Nomarski contrast) and a monoclinic/tetragonal Raman maps obtained by analyzing the tensile surface of a biaxial tested disc (10.5 mol.% ceria) after unloading. These maps were already described in [12]. A large transformation zone is observed (few millimeters in diameter), in which the monoclinic content can reach 60 vol.%, with compressive stresses as high as 1GPa, measured after unloading (**Figure 10.b**). The stress values of **Figure 10.b** are determined for the *t-zirconia* phase. Stress partitioning between the different phases is to be expected; indeed a detailed stress analysis on partly transformed Ce-TZP/Al₂O₃ composites has indicated that the overall average stress, intended as the hydrostatic stress in each phase weighted over the volume fraction of that phase, is indeed very highly compressive in transformed regions [97]. It is noted that these compressive stresses were (and generally are) measured after unloading and not *in-situ*. It is more likely a saturation of the maximum tensile stress at the transformation stress σ_c^{t-m} which occurs in the region of very localized highest applied stresses (*i.e.* starting from the center), is associated with a redistribution of the stress field, as schematically depicted in **Figure 10.c**. This shielding of the applied stress is quite similar to that occurring in metals, when plasticity occurs in regions of high applied stresses. This stress shielding explains, in part (see **Panel B**), the apparent very high biaxial flexural strength. A schematic picture of stress variations across the diameter of the disc, from the center to the border, comparing conventional non-transformable ceramic and with transformable ceramics, during loading and after unloading, is shown in **Figure 10.c**. Such a shielding effect may have important beneficial implications in structures for which the stress field is heterogeneous, with stress concentrations in some areas such as around the notches associated with the screw thread in dental implants. On the other hand, such benefits are only possible if this is true plasticity and if no damage (micro-cracking) is associated with the transformation. The question is all the more important in that the *t-m* transformation is associated with both hydrostatic and deviatoric components (quite large volume expansion and shear strains).

Is it real plasticity?

Figure 11 a. shows the stress-strain curve of a $\text{ZA}_8\text{Sr}_8\text{Ce}_{11}$ -1450°C (84 vol.% ZrO_2 doped with 11 mol.% of Ceria, 8 vol.% Al_2O_3 , 8 vol.% $\text{SrAl}_{12}\text{O}_{19}$, sintered at 1450°C) composite tested in tension, processed here by the powder-mixing method with the aim of obtaining a sufficient number of test specimens. As more comprehensively discussed in **Panel B** this curve shows that the composite processed under these conditions exhibits a significant amount of plasticity for a ceramic before failure (plastic strain of $\sim 0.5\%$). Such a degree of plasticity is related to the capability of the material to transform at low applied stresses, associated with a high T_{t-m} temperature (-42°C , see **Figure 7**), quite close to ambient. Load-unload sequences were conducted at difference stages during the test to evaluate the evolution of the stiffness versus applied strain. A small decrease of the Young's modulus versus applied strain (*i.e.* versus the proportion of transformed monoclinic phase in the material) is observed in the last few load-unload cycles, which could be attributed either to the presence of micro-cracks or to the fact that *m* zirconia exhibits a lower stiffness than that of the *t* phase (**Figure 11.b**). Unfortunately, no experimental data exists in the literature about Young's modulus of ceria-doped monoclinic zirconia and numerical simulations may give different conclusions depending on the binding potentials assumed for atomistic scale simulations [98]. To assess the key question of the absence or presence of micro-cracks (and damage) associated to the transformation, thin foils taken from a transformation band were prepared by Focused Ion Beam (FIB) milling and examined by Scanning Electron Microscopy (SEM) and Transmission Electron Microscopy (TEM) (**Figure 12**). SEM images show that the transformation zone does not exhibit micro-cracks, as it was concluded in the past on Mg-PSZ by Liu et al. [52], except at few grain boundaries located at the surface. These micro-cracks are limited to 1 micron depth. Below 1 micron depth, no micro-cracks are observed. TEM characterization confirmed that no micro- (or nano-) cracks were present inside the transformation bands, except locally at the surface. The mechanical behavior law can therefore be considered as purely elasto-plastic, which is in agreement with a previous paper by Zhe et al. [57] (see also **Panel B**). The presence of a few micro-cracks localized at the surface of the transformation bands cannot explain by itself neither the small variation in Young's modulus, which can then be attributed to a less stiff monoclinic phase, nor the amount of plastic strain observed. However, further static/cyclic fatigue tests are necessary to assess whether micro-cracks of very small dimensions at the surface could be detrimental in the long term.

Transformation Induced Plasticity (TRIP) : relation between transformation bands and plastic strain

Figure B-5 a. shows the features of transformation bands in the composite processed by the mixing route, just after failure by 4-point bending. The bands are clearly visible on the tensile side of the samples. It is interesting to note that the bands are not randomly, but regularly, dispersed. They are absent on the compressive side of the samples (not shown).

Knowing the size of the transformation bands and their density at the surface, as well as the t-m transformation ratio in the bands, it may be possible to calculate the macroscopic strain associated to the transformation. Both Raman spectroscopy and Transmission Kikuchi Diffraction (TKD) in a Scanning Electron Microscope (not shown here) revealed that only a portion ($V_m \approx 25 \text{ vol.}\% \pm 5\%$) of the tetragonal grains were transformed toward the monoclinic symmetry in the bands during the 4 point bending tests (which is below the measured monoclinic content in the transformed zone in biaxial bending). Being V_{ZrO_2} the fraction of zirconia in the composite (84 vol.%) and d_{tb} the density of transformation bands (% of surface transformed) at failure, the strain due to the t-m transformation induced plasticity is given by :

$$\varepsilon = V_m \cdot V_{ZrO_2} \cdot d_{tb} \cdot (\varepsilon_{vol} + \varepsilon_{shear}) \quad (4)$$

In this equation, ε_{vol} and ε_{shear} are the dilatant and shear strain amplitudes of the t-m transformation respectively. More precisely, ε_{vol} is the strain (in the direction of tensile stress) induced by the volume expansion of the grains (i.e. one third of the relative volume expansion) and ε_{shear} is the shear of the lattice associated to the t-m transformation.

Taking only the dilatant strain amplitude ε_{vol} with a value of 0.0167 [59] (i.e. neglecting the shear component of the transformation) and a density of transformation bands (area of the bands divided by the total area in tension) from **Figure B-5 a.** equal to 0.10, gives a macroscopic strain of 0.035%, which is far lower than observed experimentally and calculated by the inverse method described in **Panel B** (0.55% plastic strain). Therefore, the shear component of the transformation is the major part of the observed total strain. Taking a shape strain amplitude of 0.16 [59, 99] then gives a macroscopic strain of 0.37%, which, given the uncertainties in the estimations of V_m , V_{ZrO_2} and d_{tb} is in line with the measured macroscopic strain.

The shear component is often neglected in the analysis of the deformation induced by the t - m transformation [8, 99]. The current analysis clearly shows that it is the Transformation Induced Plasticity (TRIP) effect in zirconia which is the most important contribution to the deformation. Future work may seek to investigate textures of the transformation grains inside transformation zones.

Flaw tolerance

Using the stress superposition argument, the transformation zone in zirconia systems can be considered as a process zone, in which the externally applied stress is “shielded” (that is reduced) by the stress caused by the transformation of tetragonal grains to monoclinic symmetry. The concept of a process (‘plastic’) zone ahead of the crack tip as defined by Ashby [100] is thus relevant to calculate the flaw size above which a given material behaves as fragile or ductile.

Figure 13 is a chart of fracture toughness versus yield stress, often used to compare material’s behavior in relation to the risk of brittle failure. The diagonal lines show the process zone size diameter, d , where:

$$d = \frac{K_{Ic}^2}{\pi\sigma_y^2} \quad (5)$$

The evaluation of the process zone diameter from the toughness (see **Figure 8**) and elastic limit measured for a Ceria content of 11 mol.% (*i.e.* $\sim 10\text{MPa}\cdot\sqrt{\text{m}}$ and 500 MPa respectively, see **Panel B**) gives a process zone diameter of around 100 microns, in line with the transformation zone observed in this system [98] and **section II**. The same consideration for 3Y-TZP ceramics would give a process zone diameter of one to few microns, which is again in line with transformation zones generally observed in this material [60]. Such a simple consideration allows also to predict that $\text{ZA}_8\text{Sr}_8\text{Ce}_{11}$ -1450°C composites processed through the standard powder-mixing route would remain ductile even if processing defects of around 100 microns are present. **Figure 14** illustrates the very high flaw tolerance of such ductile ceramics, by showing two tensile stress-strain curves obtained on samples with and without a large processing defect ($\sim 150\ \mu\text{m}$ observed on the fracture surface). The stress-strain curve is not significantly affected (although the strain to failure is somewhat lower).

Figure 15 is a Weibull plot obtained for the $\text{ZA}_8\text{Sr}_8\text{Ce}_{11}$ -1450°C composite (processed through conventional powder-mixing) and for a benchmark, medical grade (HIPed) 3Y-TZP using two loading configurations (4-point bending and biaxial piston-on-three-balls testing). Strengths were here determined directly from the load to failure and with conventional elastic calculations. From the probability-stress curves, typical Weibull moduli between 12 and 17 are extrapolated for 3Y-TZP, while values around 30 are observed for the Ce-TZP based composite. Such high Weibull moduli were previously reported [12, 22, 101] for highly transformable Ce-TZP systems. The difference between 4-point bending and piston-on-three-balls mechanical behavior cannot be imputed to a size effect in the Weibull analysis (different volumes of samples) but rather to a difference in stress distribution and, hence, to transformation features, as discussed in **Panel B**. It has to be emphasized again that biaxial bending does overestimate real values of strength (see **Panel B**). On the other side, it shows the high reproducibility in the load to failure of the composite, due to a large tolerance to defects, when compared to 3Y-TZP. It has to also be recognized that 4-point bending strength of 3Y-TZP remains almost twice higher than the Ce-based composite and that the benefit of using a ‘ductile’ or ‘fragile’ zirconia ceramic may depend on the actual loading configuration (application, displacement or load controlled, heterogeneous or homogeneous stress distribution), size and geometry of the product and defects generated through the processing. Admittedly, the same comparison *i.e* between 3Y-TZP and the optimal grade of composites processed by surface-coating route would be conclusive, but this was impossible at the time of writing, due to the limits in processing large batches of powders by this synthesis method.

V. Potential Applications of ductile ceramics: case study on implants and additive-manufactured ceramics

Advantages and drawbacks

Case study 1: dental implants with a high tolerance to surface modifications

Implant prototypes were processed from the $\text{ZA}_8\text{Sr}_8\text{Ce}_{11}$ zirconia powder described previously (powder mixing). The powder was granulated by spray drying and cold-isostatically pressed (300 MPa) in the form of cylindrical bars of diameter 5.1 mm. Bars were sintered at 1450°C for 1 hour and then machined in the sintered state to final shape (see **Figure 16**) by hard milling-turning

process on a 5 axis Computer Numerical Control (CNC) milling center. Prototypes were machined to a final diameter of 3.4 mm, which represents the lowest and most challenging dimension for ceramic implants. It is generally accepted that machined surfaces are not optimal to favor bone integration [102-106] and there is a consensus to consider that a certain surface roughness $R_a \sim 1$ -1.5 microns improves osseointegration and mechanical anchorage with bone [102-106]. Several strategies are thus explored to obtain such rough surfaces, the most common being sandblasting and chemical etching. Other surface modifications are today proposed for ceramic implants, as laser patterning [107-109] or injection molding in matrices [110] with the targeted roughness. As sandblasting followed potentially by chemical etching is the most commonly developed strategy, such treatments were tested in this case study. Sandblasting was conducted with 150 μm alumina particles at 3.5 bars, leading to a roughness (S_a) of 1.3 microns (measured using a white-light optical interferometer). When followed by etching (in HF/HNO₃ for 3h at Room Temperature (RT)), S_a was decreased to 1.0 micron, but an additional surface topography was created at the grain scale (see **Figure 17**). An additional thermal treatment was conducted on some of the prototypes to release potential residual stresses associated to different surface treatments. This annealing was performed at 1350°C, (*i.e.* above the *m-t* transformation and below the sintering temperature).

Load to failure tests on hard machined 3.4 mm diameter implants were performed following ISO14801 geometrical prescription [111], so as to follow the most usual and severe testing method for dental implants. The implants were embedded in an epoxy resin having a stiffness similar to bone (RenCast CW 5156/HY5158, with a Young's modulus of 5.8 GPa). The embedding level was 3 mm below the intended initial bone crest position around the implant to simulate bone resorption, as specified in ISO 14801. The implants were loaded to failure at 30° angulation with respect to the vertical axis at a crosshead speed of 5 mm/min. 4 implants were tested for each surface feature. Several surface states were compared: as machined (hard milling process on a 5 axis CNC milling center), machined + sandblasted (alumina particles) or machined + sandblasted + chemically etched.

Figure 17.a shows the load to failure values obtained on the prototypes as a function of the surface treatments conducted. They are compared to publically available data for other ceramic (3Y-TZP based) implants [112-117]. Values are similar irrespective of the surface treatments, ranging from 336 N in average after machining down to 286 N following sandblasting, etched and

then annealed prototypes in which residual machining/sandblasting stresses were relieved. These values appear quite modest when compared to data already reported by manufacturers of 3Y-TZP implants (~ 350 – 450 N [112 - 121]). On the other hand, load to failure results were very reproducible and the strength of implants was minimally affected by the type of surface treatment conducted. Given the limit of the study and the difficulty to compare implant strengths from public datasheets, especially because they have different sizes, designs and surface features, our results are consistent with the main advantages and drawbacks of such ‘ductile’ ceramics: mechanical resistance is modest and associated with the moderate elastic limit of the material tested (≈ 500 MPa). As a reminder, implants were processed using a transformable $\text{ZA}_8\text{Sr}_8\text{Ce}_{11}$ -1450°C composite, processed by a standard powder-mixing route. Given the obtained load to failure value of 295 N for the most common surface treatment (sandblasting followed by etching), these implants of 3.4 mm made with the Ce-zirconia composite would be likely restricted to lateral incisor teeth and at least 4.0 mm diameter would be necessary for other locations [122]. On the other side, thanks to the benefits of flaw tolerance, variability in strength is very low, insuring a high reproducibility and reliability in strength data and a strong robustness against processing variability and surface treatments. At this stage, it must be noted that the prototype implants were not Hot-Isostatically-Pressed as is the case of most commercial 3Y-TZP implants to limit the risk of large defects. Another competitive argument for using Ce-zirconia composites is their resistance to Low Temperature Degradation (aging). Some prototype implants were aged in an autoclave at 134°C-2 bars for 5 hours following ISO 13356 [123]. They showed no evolution, neither in monoclinic content nor change in mechanical strength after the aging treatment. Doping with ceria leads to an absence of susceptibility toward chemically induced Low Temperature Degradation (aging) as ceria addition does not create oxygen vacancies in the lattice, which are associated to water-species diffusion and further destabilization in yttria-doped zirconia with time [59, 61], while 3Y-TZP commercial implants aged, although not visible by XRD but by Raman spectroscopy. Admittedly, there are some signs that large residual stresses, as introduced by a previous t-m transformation, might result in stress-driven (rather than chemical-driven) aging in Ce-TZP composites [124].

Such ductile composites may be seen as a potential option for manufacturing robust dental implants, with an acceptable maximum strength for a zirconia-based ceramic (around 600 MPa in 4-point bending configuration), but a high degree of flaw resistance, reliability and stability.

Certainly, decreasing the ductility to a certain extent (but still in the 'ductile' range of the strength-toughness relationship) would further improve the mechanical resistance of the implants. Again, as for mechanical testing, further development of composites processed through surface-coating route or any method enabling finer microstructures, at a larger, industrial scale, would be welcome for practical applications.

Case study 2: mechanical properties of additive-manufactured scaffolds

In recent years, Additive Manufacturing (AM) techniques have expanded fast, because they enable the customization of complex shapes and may reduce the duration and complexity of the manufacturing process. However, AM of ceramics has many challenges because, compared to metals, ceramics are less tolerant to processing-induced defects, while currently AM results in larger material defects than other well-established industrial technologies. For example, 3Y-TZP commonly exhibits strengths higher than 1 GPa when processed by Cold Isostatic Pressing, while values in the range of 550-850 MPa were reported when shaped by stereolithography [125]. Hence, the ductile Ce-TZP based composites described above may have greater potential for AM, as scaffolds for which defects are inherent to the structure targeted or even as dense materials for which defects are undesired but generally present.

Dense samples and scaffolds were printed using a robotic assisted deposition device (3D inks, Tulsa, OK, USA), often referred as robocasting or Direct-Ink-Writing. The printable paste was prepared by mixing the 33 vol.% $\text{ZA}_8\text{Sr}_8\text{Ce}_{11}$ zirconia powders in a 25 wt.% Pluronic[®] F127-based hydrogel solution. Mixing was performed using SpeedMixer (DAC 150.1 FWZ-K, Flacktek, Germany) at 2500 rpm and the paste was degassed by centrifugal loading at 5000 rpm for 10 min before placing in the syringes. Dense biaxial bending disks and 3D porous structures were built-up by extruding the paste through conical tips of 400 μm diameter at a speed of 10 mm/s on flat Teflon-sprayed substrates in 95 % humidity and at 25°C.

- Disks for biaxial bending were obtained by depositing the filaments in one direction. Distance between the filaments was 320 μm (80% of the filament) in the XY plane and 336 μm (84% of the filament) in the Z direction. The starting filament was placed with 160 μm offset with the previous layer in order to fill the gap between filaments.

- Cylindrical 3D porous structures were deposited with strut-to-strut distance of 800 μm (in the XY plane) and distance between the filaments in the Z direction was 320 μm (*i.e.*, 20 % overlap).
- Two 3D structures with different porosities were printed: one with a reinforcing dense rim and one without rim reinforcement.

Following printing, the structures were dried for 60 hours at a temperature of 60°C while at the same time decreasing the humidity from 95% to 30%. De-binding and sintering were performed at 600°C for 3 h and 1350°C for 1 h, respectively.

Samples of cylindrical 3D structures (\varnothing 10 mm x 10 mm in height after sintering) were used for compression tests at 0.5 mm/min, while disks (\varnothing 12 mm x 1.5 mm in thickness after sintering) were used in piston-on-three-balls bending.

The robocasting method did not develop full density struts after sintering and in case of ‘dense’ biaxial disks only 86 % of theoretical density was achieved. **Figure 18** shows the architecture of the 3D porous structures (with and without the reinforcing rim) and the microstructure of the materials at two scales. Interestingly, although the samples obtained exhibited a relatively high degree of residual micro-porosity (14 %), biaxial flexural strength reached 850 ± 22 MPa (N=8). This is first because the material is highly defect-tolerant (even large defects do not compromise tensile strength, see **figures 13 and 14**), but also and this underlined at different occasions in the paper, because the strength is calculated on the basis of elastic equations. Interestingly, from the load-displacement curves obtained, an elastic-plastic curve was observed with an elastic limit of 550-600 MPa, *i.e.* consistent with that of samples with a higher density. In other words, the plastic strain of these samples was certainly lower than that of dense samples, but the elastic limit remained roughly the same. We also observed dramatic improvements in the compressive strength of the 3D porous scaffold made from this composite, when compared to the literature, even with high porosities (40 % - 60 %) (**Figure 19**). Values obtained for these samples are well above those reported so far in the literature [126-135]. Therefore, such metal-like behavior and defect-tolerant properties of the investigated $\text{ZA}_8\text{Sr}_8\text{Ce}_{11}$ material appear to be an excellent option for additive manufacturing technologies. These preliminary results will be complemented by further analysis of defect size – strength relations in this system, as well as a comparison with Y-TZP processed under the same conditions, in an upcoming paper. Another consequence of these results is that,

contrary to most brittle ceramics including Y-TZP, it is possible to process porous biocompatible structures with a lower stiffness, which is favorable in terms of decreasing stress-shielding with bone, without compromising strength. This can also be exploited for implants in contact with bone, for which the high stiffness of ceramics is generally considered a drawback.

VI. Perspectives and Concluding remarks

Even though, as was sometimes reported in previous literature, transformation-induced ductility of some zirconia ceramics has been certainly under-exploited to date. The high flaw tolerance and higher reliability, along with the associated absence of chemically-driven low-temperature aging, the present work has shown Ceria-doped zirconia based ceramics and composites may be tailored so as to achieve high strength and toughness (for the 'optimum' of the strength-toughness relation), or a larger propensity of transformation induced plasticity associated with still higher toughness. Such ceramic composites with a toughness of more than 10-15 MPa \sqrt{m} , a rising R-Curve and an elastic limit of 500 MPa, may compete with bio-inspired ceramics, which are considered today at the forefront of ceramic research, while being readily accessible using conventional ceramic processes. Better than competing, the combination of phase transformation toughening with a clever microstructural architecture may reveal an interesting field of research, as gradients of transformation from the surface towards the core of a material may be achieved. Laminated structures through tape casting or additive manufacturing or even the combination with self-diagnostic ability by the incorporation of a conductive network or wires inside structures without compromising strengths thanks to the defect-tolerant character of the base-ceramic can be also designed. This paper has confirmed that toughness (and thus ductility) cannot be increased to values exceeding 10 MPa \sqrt{m} without compromising strength, which still remains modest when compared to 3Y-TZP materials. The future of such composites, in order to achieve maximum strength will certainly rely on our capacity to process, with scalable methods, ultra-fine and homogeneous powders and materials, which may then provide even greater potential in term of strength-toughness relations. The concept of strength limitation of transformation-toughened zirconia alloys discussed in the 80's still remains, but the effect of micro- (nano-) structure on such strength-toughness relations is still a matter of scientific and technological interest.

Panel A. Zirconia Systems: Phase Transformation Toughening and Strength-Toughness Relationship

Transformation toughening was first described in TRIP (Transformation-Induced Plasticity) steels and wear-resistant cast irons (1968) [136]. The same phenomenon was then observed in a ceramic material (CaO-partially stabilized zirconia) in 1975 by Garvie et al. [6] and two years later, by Gupta et al. [137] in zirconia containing low percentage of yttria. In these stabilized-zirconia systems, toughening is based on the retention of the metastable tetragonal phase at room temperature: when a crack propagates, the concentrated stress field at the crack tip enables *t*-crystals to transform into a stable *m*-phase and, the associated volume expansion, generates localized compressive stresses, which act against the applied stress intensity factor. This tetragonal-to-monoclinic phase transformation, which can be triggered by shear and/or hydrostatic tensile stresses [138], leads to a significant increase of the strength, due to the increase of the work of fracture rather than the reduction of the defect size, as classically observed in brittle ceramics. Depending on the cation (Ca, Mg, Y, Ce, rare earths oxides...) and the quantity of stabilizing agent added to zirconia, different materials can be developed. If an amount of transformable tetragonal phase is present within a matrix of cubic zirconia, one refers to *Partially Stabilized Zirconia* or PSZ. If zirconia is fully tetragonal following sintering one refers to *Tetragonal Zirconia Polycrystals* or TZP. The term 'TZP' is sometimes incorrectly used for yttria stabilized systems with 3-4 mol.% yttria, while phase diagram and current knowledge of these systems show that they are not fully tetragonal. Finally, *Fully Stabilized Zirconia* or FSZ is developed when the concentration of dopant is high enough for complete cubic stabilization (case of 8Y-FSZ) [139, 140].

In case of ceramics, the stress-shielding effect resulting from the transformation-induced strains near the crack tip was estimated using a linear elastic fracture mechanics model developed by McMeeking and Evans in 1982 [141]. A second model based on energy considerations, developed by Budiansky et al. in 1983 [142], allowed computation of the work of fracture due to the *t-to-m* transformation in zirconia. However, neither of these two models describes with precision the shape, size and volume of the transformation zone at the crack tip. Recently, a two-dimensional elastic phase field model proposed by Mamivand et al. [143] has simulated correctly the phase transformation nucleation at the crack tip and the development of compressive stresses, which lead to crack closure while the crack is under tensile loading. In the 80's, Swain and co-workers [20,

96] showed that the mechanical properties of TZP materials depend on the contribution of the toughening mechanism: (a) at lower toughness (generally less than $8\text{-}10 \text{ MPa}\cdot\sqrt{\text{m}}$ as in 3Y-TZP system [137], see **Fig. A-1**) toughening contribution is modest and the strength is limited by the flaw-size following the Griffith relationship (brittle behavior and transformation follows crack growth) while (b) at higher toughness (case of 9-10 Ce-TZP systems showing ductile-like behavior, see **Fig. A-1**), the strength is limited by the critical transformation stress to induce the *t-m* zirconia phase transformation taking place before crack propagation.

The critical stress to trigger the *t-m* transformation (σ_c^{t-m}) is primarily a function of the grain size and the type and quantity of stabilizing agent but can be also modified by residual stresses due to thermal expansion mismatch between grains and/or the presence of secondary phases. For a given dopant concentration, σ_c^{t-m} decreases with increasing grain sizes (grains smaller than a critical size cannot undergo the phase transformation under a given stress field) and at similar grain size and dopant concentration, the degree of stabilization depends on the type of dopant (*e.g.* adding yttria creates oxygen vacancies, which is the most efficient means to stabilize the tetragonal phase, while ceria relies only on lattice parameter changes [144, 145]). Obviously, for a given type of dopant, the lower the dopant concentration the lower the σ_c^{t-m} .

In composites, σ_c^{t-m} decreases if residual tensile stresses are generated or increase when zirconia is put under compression. The magnitude and sign of internal residual stresses depends on *i*) secondary phase compositions, *ii*) the associated thermal expansion coefficients and *iii*) the presence of a preexisting *t-m* transformation [97].

The plot of strength versus fracture toughness for various PSZ and TZP systems (see **Fig. A-2**) shows that in Y-TZP, Ce-TZP and Mg-PSZ transformable zirconia, increasing toughness above $8\text{-}10 \text{ MPa}\cdot\sqrt{\text{m}}$ is associated with a decrease in strength. This toughness values represent the frontier between the two different behaviors proposed by Swain and Rose [20]: it should be taken into account when designing zirconia-toughened-based engineering ceramics. In practical terms, if the objective is to develop maximum strength, it will be necessary to limit the transformability of the material while improving the processing, machining and final surface treatments applied to the product in order to reduce the critical flaw size. On the contrary, if the material to be developed must be flaw and damage tolerant (that is less sensitive to processing, machining and surface modifications), it will be more beneficial to increase the transformability and to adapt the product

design to guarantee the maximum strength that will be limited by the σ_c^{t-m} . Practically, in the latter materials, the $t-m$ phase transformation will take place before failure.

Among the more classical transformable zirconia systems, Y-TZP shows the highest mechanical strength (more than 1 GPa) but relatively moderate toughness [146, 147]. On the contrary, Ce-TZP can be very transformable (high fracture toughness) but at a lower maximum strength [148, 149]. In Ce-TZP the optimum fracture strength was observed for ceramics containing 10-12 mol.% CeO₂ (about 500-600 MPa). This relative modest strength (in comparison to Y-TZP) is mostly related to the larger grain size of Ce-TZP. Therefore, from the late 1980s, many researchers have worked on hindering grain growth in Ce-TZP by adding one or more secondary phases (Al₂O₃, MgAl₂O₃, SrAl₁₂O₁₉...), developing Ce-TZP-based composites with strengths higher than 1 GPa [12, 35, 38, 43-45].

Another important feature shown in **Fig. A-2** is that the addition of a secondary phase to Y-TZP increases also the strength to 2.4 GPa, as reported by Tsukuma and Ueda [150] in 2Y-TZP composites containing 20-40 wt.% of alumina. According to these authors, the improvement of the strength from 1.4 GPa (pure 2Y-TZP) to 2.4 GPa is related to the presence of smaller flaws and the suppression of crack initiation by alumina. The effectiveness of Y-TZP additions to Al₂O₃ has also been studied and maximum bending strengths of ~1.6 GPa and toughness of 6.5 MPa.m^{1/2} were reached with 70 vol.% of Al₂O₃-3Y-TZP systems [151]. 3Y-TZP is one of the most commonly used ceramics to boost the strength of Zirconia Toughened Alumina (ZTA).

Panel B. Mechanical behavior laws of highly transformable zirconia ceramics - importance of the test methods

Different methods are proposed in standards and publications for the strength measurements of ceramics. Among them, three- or four-point and biaxial bending tests are the most popular. They are schematized in the **Appendix**. They provide the advantage, for ceramics, to create tensile stresses on one side of the sample, without having to proceed with more difficult, pure tensile tests. The biaxial flexural strength tests also have the advantage of not being sensitive to the specimen edge preparation as is the case for three- and four-point bending tests. ISO standards for dental ceramics (ISO 6872 [90]), and more specifically for zirconia as an implant material (ISO 13356 [123]), specify the use of bending tests to obtain strength data, using linear elastic equations. However, with non-linear behavior, and this is the case of very transformable zirconia, stresses and strain cannot be calculated simply and directly from load and displacement hypothesizing a purely elastic behaviour. As already indicated by Fett and Munz [9] and later by Rauchs et al. [10], plastic deformation on the tensile side of the bending samples leads to an overall stress re-distribution and to overestimated values of the tensile stress, and thus of real strength, when using elastic-behavior equations given in the **Appendix**. In the case of biaxial bending tests with supporting balls, additional errors associated with indentation of the material by the balls is generally not considered but may be significant and compromise (underestimate) the measurement of beam deflection.

Figure B-1 shows apparent stress-strain curves obtained on a $\text{ZA}_8\text{Sr}_8\text{Ce}_{11}$ -1450°C composite processed through conventional powder mixing (thus exhibiting high transformability) with different loading configurations, when both stress and strain are calculated through standard equations considering elastic hypotheses in the case of the bending tests. The $\text{ZA}_8\text{Sr}_8\text{Ce}_{11}$ -1450°C composition was chosen as a model material with transformation before failure and a high level of transformation-induced plasticity. It is noted that the displacements were accurately measured by Linear Voltage Displacement Transducer (LVDT) just under the samples in bending tests and with an extensometer in the case of tension. A significant indentation of the samples by the supporting balls was noted in biaxial bending and taken into consideration in the actual measured displacement. **Figure B-2** illustrates a load-displacement curve of a ball of the same diameter as the one used for biaxial bending on a flat $\text{ZA}_8\text{Sr}_8\text{Ce}_{11}$ -1450°C support, for a maximum load

applied on the ball similar to that reached during biaxial bending. A permanent penetration of the ball of 20 μm is observed. This shows that under biaxial bending, a portion of the measured displacements is due to indentation effects. From a practical point of view, strength calculation following ISO standards would result in values of roughly 400 MPa in tension, 540 MPa in 3 or 4-point bending and more than 1 GPa in biaxial bending.

Tensile tests are very sensitive to misalignment and lead to a larger scatter of results (as schematized by the dashed area in **Figure B-1**). On the other hand, stresses calculated in bending overestimate true values of strength and do not capture relevant mechanical behavior laws without further analysis. Finite Element Methods (FEM) can be used to simulate a load-displacement response during a loading test, by integrating a given stress-strain (constitutive) mechanical behavior law of the material. **Figure B-3** shows the load-displacement curve experimentally measured during a 4-point bending test and the ones calculated from the knowledge of the stress-strain curves determined in tension. Plasticity was modeled as cast-iron behavior, which considers plasticity with isotropic hardening in tension and only elasticity (no transformation) in compression.

The simulations based on stress-strain curves obtained through the tensile tests are consistent with the experimental load-displacement curve, especially for the upper stress-strain curve (best alignment), but do not fully match with it. In fact, a simulation of tensile tests by FEM shows that small misalignments, even imperceptible, may lead to stress gradients and thus transformation (plasticity) onset near the upper and lower edges of the narrowing of the sample. This was checked with Raman Spectroscopy where the onset of phase transformation was heterogeneous in the case of the strongest misalignment, as shown in **Figure B-4**. In other words, bending stresses superimpose onto the applied tensile stresses and lead to a certain under-estimation of the real tensile stress. An alternate approach to the issue stems from the following question: what would be the strain–stress curve to enter in the FEM simulation to fit the experimental load-displacement curve in bending? The best fit was obtained with a cast-iron model, exhibiting a yield (transformation) stress of 500 MPa in tension with minimal hardening (maximum stress of 540 MPa) and a pure elastic behavior in compression. This result is important since it shows that the effective stress-strain curve does not show significant hardening and that the mechanical behavior law of such highly transformable ceramic is almost purely elastic-plastic in tension. It shows also that 4-point bending does not over-estimate the real strength significantly as the maximum stress determined is

of 540 MPa. On the other hand, it shows that tensile tests may underestimate yield and maximum stresses if very careful attention is not given to misalignment. Finally, it shows that biaxial bending should be avoided, as it overestimates strength to an unacceptable extent, unless a similar inverse approach is performed (considering an elastic-plastic, cast-iron mechanical behavior law instead of pure elasticity). Though not shown here, this approach has been adopted in our case, and taking the stress-strain curve obtained through the analysis of the 4-point bending test (inverse method) agrees exceptionally well with the experimental load-displacement curve, provided that the penetration of the supporting balls into the material is also considered.

From a general point of view, the mechanical behavior law is the same whatever the type of loading condition (*i.e.* transformation starts when the maximum tensile stress reaches a critical value - here 500 MPa – and the behavior can then be described by a cast-iron model without strain hardening). The difference between biaxial bending, 4-point bending and tension is not due to a different intrinsic mechanical behavior law, but different loading configurations, which in turn generates a different transformation zone and associated different stress distribution, as explained by Touaiher et al. [152] and highlighted in the main core of the text (see also **Figure 10**). The features of the transformation zones in 4-point and biaxial bending are illustrated in **Figure B-5 a**. It was unfortunately not possible to observe the transformation features on the tensile samples, since polishing of the cylindrical samples revealed not enough, despite large efforts. Transformations bands, perpendicular to the main tensile stress direction, are visible and increase rapidly in number and depth between the onset of transformation and the end of the test (fracture) for the 4-point bending configuration. A much larger zone is observed in piston-on-three ball (**Figure B-5.b**), starting on the tensile side of the sample and increasing progressively in size with increasing load. This large transformation acts to shield the applied tensile stresses and leads to stress redistribution, which explains the high loads that can withstand the samples in this configuration. We may expect another shape of the transformation bands in pure tension.

In practical terms, such considerations may have two implications:

- The use of Biaxial bending in the conditions of the ISO standards should be avoided in highly transformable zirconia ceramics, because it overestimates to a large extent the real strength of the material if elastic equations are used to compute stresses,

- From a product point of view, the benefits of the transformation-induced plasticity depend on the loading conditions, with a better potential reinforcement for complex loading configurations and stress distribution. If pure tension is considered, the load necessary for transformation and for failure will be almost the same. On the other hand, if peak stresses are generated, as it is the case of biaxial bending, transformation will shield the applied stresses and allow a redistribution of the stress field through a large portion of the material.

Acknowledgements

The research leading up to these results was undertaken in the framework of the LONGLIFE project (<http://www.longlife-project.eu>) funded by the European Community's Seventh Framework Program (FP7/2007-2013) under the grant agreement n. 280741 and SISCERA project (<http://siscera-project.eu>) also funded by E.U. (H2020-FTIPilot-2016, grant agreement n. 737954). Even if this paper concentrates on mechanical properties of the materials, the research effort conducted by our other partners in the field of powder synthesis and processing is deeply appreciated and acknowledged. In particular, we warmly thank our colleagues and friends from Politecnico di Torino, Marta Fornabaio, Paola Palmero, Laura Montanaro, from Swerea IVF, Erik Adolfsson, and Doceram AG, Tobias Fuerderer and Sven Schomer. We also deeply thank our colleagues from INSA, Sylvain Meille, Laurent Gremillard, Arnaud Doko, and Christian Olagnon, who took part on some of these projects at different steps of their achievements. V.S. and V.L. thank Alois Bonifacio for his contribution in the analysis of the Raman mapping data. We acknowledge the CLYM (Centre Lyonnais de Microscopie), supported by the CNRS, the "Grand Lyon" and the Rhône-Alpes Region for the access to the FIB/SEM device used in this study. Some of the Raman data shown were collected by Francesca Russo Cirillo for her undergraduate thesis, and her work is gratefully acknowledged.

References

1. Dann GE. Martin Heinrich Klaproth: (1743-1817.) Ein deutscher Apotheker und Chemiker. Sein Weg und seine Leistung. Berlin: Akademie-Verlag; 1958.
2. The use of zirconia as a refractory material. *Nature*. 1917; 99 (2488):375-376.
3. Phillips AJ. The partial purification of zirconium oxide. *J Am Ceram Soc*. 1918;1(11):791-800.
4. Ryshkewitch E, inventor; Degussa, assignee. A process for Overpass of zirconia in the plastic state. *Deutsch Patent 519796C*. 1926 Dec 18.
5. Hannink RHJ, Kelly PM., Muddle BC. Transformation toughening in ZrO_2 -containing ceramics. *J Am Ceram Soc*. 2000;83(3):461-487.
6. Garvie RC, Hannink RHJ, Pascoe RT. Ceramic Steel. *Nature*. 1975; 258(5538):703-704.
7. Grathwohl G, Liu T. Crack Resistance and Fatigue of Transforming Ceramics: II, CeO_2 -Stabilized Tetragonal ZrO_2 . *J Am Ceram Soc*. 1991;74(12):3028–3034.
8. Gogotsi GA, Zavadaa VP, Swain MV. Mechanical Property Characterization of a 9 mol% Ce-TZP Ceramic Material -I. Flexural Response. *J Eur Ceram Soc*. 1995;15(12):1185-1192.
9. Fett T, Munz D. Influence of time-dependent phase transformations on bending tests. *Mat Sci Eng A-Struct*. 1996; 219(1-2): 89–94.
10. Rauchs G, Fett T, Munz D, Oberacker R. Tetragonal-to-monoclinic phase transformation in CeO_2 -stabilised zirconia under uniaxial loading. *J Eur Ceram Soc*. 2001;21(12):2229-2241.
11. Palmero P, Fornabaio M, Montanaro L, Reveron H, Esnouf C, Chevalier J. Towards long lasting zirconia-based composites for dental implants. Part I: Innovative synthesis, microstructural characterization and in vitro stability. *Biomaterials*. 2015;50:38-46.
12. Reveron H, Fornabaio M, Palmero P, et al. Towards long lasting zirconia-based composites for dental implants: Transformation induced plasticity and its consequence on ceramic reliability. *Acta Biomater*. 2017; 48:423-432.
13. Evans AG. Structural Reliability:A Processing-Dependent Phenomenon. *J Am Ceram Soc*. 1982;65(3):127-137.
14. Evans AG. Perspective on the Development of High-Toughness Ceramics. *J Am Ceram Soc*. 1990;73():187-206.
15. Niihara K. New Design Concept of Structural Ceramics. *J Ceram Soc Jpn*. 1991;99(10):974-982.
16. Jaafar M, Reveron H, Esnouf C, Fantozzi G. Highly creep-resistant alumina–SiC nanocomposites processed by spark plasma sintering. *Scripta Mater*. 2013;68(2):134-137.

17. Bai X, Huang C, Wang J, Zou B, Liu H. Fabrication and characterization of Si₃N₄ reinforced Al₂O₃-based ceramic tool materials. *Ceram Int*. 2015;41(10):12798-12804.
18. Gogotsi Y. Particulate silicon nitride-based composites. *J Mat Sci*. 1994;29(10):1573-4803.
19. Yin Z, Huang C, Zou B, Liu H, Zhu H, Wang J. Preparation and characterization of Al₂O₃/TiC micro-nano-composite ceramic tool materials. *Ceram Int*. 2013;39(4):4253-4262.
20. Swain V, Rose LRF. Strength Limitations of Transformation-Toughened Zirconia Alloys. *J Am Ceram Soc*. 1986;69(7):511-518.
21. Cutler RA, Mayhew RJ, Prettyman KM, Virkar AV. High-Toughness Ce-TZP/Al₂O₃ Ceramics with Improved Hardness and Strength *J Am Ceram Soc*. 1991;74(1):179-86.
22. Touaiher I, Saadaoui M, Chevalier J, Preiss L, Reveron H. Fracture behavior of Ce-TZP/alumina/aluminate composites with different amounts of transformation toughening. Influence of the testing methods. *J Eur Ceram Soc*. 2018;38(4):1778-1789.
23. Dietrich M. What Can We Learn from R-Curve Measurements? *J Am Ceram Soc*. 2007;90(1):1-15.
24. Yu CS, Shetty DK. Transformation yielding, plasticity and crack-growth-resistance (R-curve) behaviour of CeO₂-TZP. *J Mater Sci*. 1990;25(4):2025-2035.
25. Readey MJ, McCallen CL. Microstructure, Flaw Tolerance, and Reliability of Ce-TZP and Y-TZP Ceramics. *J Am Ceram Soc*. 1995;78(10):2769-2776.
26. Tsai JF, Chon U, Ramachandran N, Shetty DK. Transformation Plasticity and Toughening in CeO₂-Partially-Stabilized Zirconia-Alumina (Ce-TZP/Al₂O₃) Composites Doped with MnO. *J Am Ceram Soc*. 1992;75(5):1229-1238.
27. Eichler J, Hoffman M, Eisele U, Rödel J. R-curve behaviour of 2Y-TZP with submicron grain size. *J Eur Ceram Soc*. 2006;26(16):3575-3582.
28. Yu CS, Shetty DK. Transformation Zone Shape, Size, and Crack-Growth-Resistance [R-Curve] Behavior of Ceria-Partially-Stabilized Zirconia Polycrystals. *J Am Ceram Soc*. 1989;72(6):921-928.
29. Nawa M, Kurizoe N, Okamoto Y, Ueno A. Transformation-induced plastic deformation in Ce-TZP/alumina nanocomposite generated during fatigue tests at room temperature. *J Eur Ceram Soc*. 2014;34(16):4337-4345.
30. Benzaid R, Chevalier J, Saadaoui M, et al. Fracture toughness, strength and slow crack growth in a ceria stabilized zirconia-alumina nanocomposite for medical applications. *Biomaterials*. 2008;29(27):3636-3641.
31. Ramachandran N, Chao LY, Shetty DK. R-Curve Behavior and Flaw Insensitivity of Ce-

- TZP/Al₂O₃ Composite. *J Am Ceram Soc.* 1993;76(4):961-969.
32. Sato T, Endo T, Shimada M. Postsintering Hot Isostatic Pressing of Ceria-Doped Tetragonal Zirconia/Alumina Composites in an Argon Oxygen Gas Atmosphere. *J Am Ceram Soc.* 1989;72(5):761-764.
 33. Tsai JF, Yu CS, Shetty DK. Fatigue Crack Propagation in Ceria-Partially-Stabilized Zirconia (Ce-TZP)-Alumina Composites” *J Am Ceram Soc.* 1990;73(10):2992-3001.
 34. Yu CS, Shetty DK, Shaw MC, Marshall DB. Transformation Zone Shape Effects on Crack Shielding in Ceria-Partially-Stabilized Zirconia (Ce-TZP)/Alumina Composites. *J Am Ceram Soc.* 1992;75(11):2991-2994.
 35. Nawa M, Nakamoto S, Sekino T, Niihara K. Tough and strong Ce-TZP/Alumina nanocomposites doped with Titania. *Ceram Int.* 1998;24(10):497-506.
 36. NANOZR brochure. Panasonic Healthcare. Available from <https://www.phchd.com>
 37. Nawa M, Nakanishi H, Suehiro Y, inventors; Panasonic Electric Works Co., Ltd. (Osaka, JP) assignee. ZrO₂-Al₂O₃ composite ceramic material and production method therefor. US Patent 7928028. 2004 March 23.
 38. Apel E, Ritzberger C, Courtois N, et al. Introduction to a tough, strong and stable Ce-TZP/MgAl₂O₄ composite for biomedical applications. *J Eur Ceram Soc.* 2012;32(11):2697-2703.
 39. Mazaheri M, Mari D, Hesabi ZR, Schaller R, Fantozzi G. Multi-walled carbon nanotube/nanostructured zirconia composites: Outstanding mechanical properties in a wide range of temperature. *Compos Sci Technol.* 2011;71(7):939-945.
 40. Yang G, Li JC, Wang GC, Yashima M, Min SL, Chen TC. Investigation on strengthening and toughening mechanisms of Ce-TZP/Al₂O₃ nanocomposites. *Metall Mater Trans A.* 2006;37(6):1969-1975.
 41. Guo R, Guo D, Chen Y, Yang Z, Yuan Q. In situ formation of LaAl₁₁O₁₈ rodlike particles in ZTA ceramics and effect on the mechanical properties. *Ceram Int.* 2002;28(7):699-704.
 42. Magnani G, Brillante A. Effect of the composition and sintering process on mechanical properties and residual stresses in zirconia-alumina composites. *J Eur Ceram Soc.* 2005;25(15):3383-3392.
 43. Kern F. A comparison of microstructure and mechanical properties of 12Ce-TZP reinforced with alumina and in situ formed strontium- or lanthanum- hexaaluminate precipitates. *J Eur Ceram Soc.* 2014;34(2):413-423.
 44. Cutler RA, Lindemann JM, Ulvensøen JH, Lange HI. Damage-resistant SrO-doped Ce-TZP/Al₂O₃ composites. *Mater Design.* 1994;15(3):123-133.

45. Burger W, Richter HG. High strength and toughness alumina matrix composites by transformation toughening and “in situ” platelets reinforcement (ZPTA)-the new generation of bioceramics. *Key Eng Mat.* 2011;192-195:545-548.
46. Munch E, Launey ME, Alsen DH, Saiz E, Tomsia AP, Ritchie RO. Tough, Bio-Inspired Hybrid Materials. *Science.* 2008;322(5907):1516-1520.
47. Bouville F, Maire E, Meille S, Van de Moortèle B, Stevenson AJ, Deville S. Strong, tough and stiff bioinspired ceramics from brittle constituents. *Nat Mater.* 2014;13:508-514.
48. Le Ferrand H, Bouville F, Niebel TP, Studart AR. Magnetically assisted slip casting of bioinspired heterogeneous composites. *Nat Mater.* 2015;14:1172-1179.
49. Wegst, UGK, Bai H, Saiz E, Tomsia AP, Ritchie RO. Bioinspired structural materials. *Nat Mater.* 2014;14:23-36.
50. Launey ME, Ritchie RO. On the Fracture Toughness of Advanced Materials. *Adv Mater.* 2009;21(20):2103-2110.
51. Hannink RHJ, Swain MV. Metastability of the Martensitic Transformation in a 12mol% Ceria-Zirconia Alloy - I Deformation and Fracture Observations. *J Am Ceram Soc.* 1989;72(8):90-98.
52. Liu SY, Chen IW. Fatigue Deformation Mechanisms of Zirconia Ceramics. *J Am Ceram Soc.* 1992;75(5):1191-1204.
53. Liu T, Mai YW, Swain MV, Grathwohl G. Effects of grain size and specimen geometry on the transformation and R-curve behaviour of 9Ce-TZP ceramics. *J Mater Sci.* 1994;29(3):835-843.
54. Reyes-Morel PE, Chen IW. Transformation plasticity of CeO₂-stabilized tetragonal zircona polycrystals: I, Stress assistance and autocatalysis. *J Am Ceram Soc.* 1988;71(5):343-353.
55. Wang JS, Tsai JF, Shetty DK, Virkar AV. Effect of MnO on the microstructures, phase stability, and mechanical properties of ceria-partially-stabilized zirconia (Ce-TZP) and Ce-TZP-Al₂O₃ composites. *J Mater Res.* 1995;5(9):1948-1957.
56. Lankford J. Plastic Deformation of Partially Stabilized Zirconia. *J Am Ceram Soc.* 1983;66(11): C212-C213.
57. Zhe X, Wang C, Hendry A. Dislocation-Related Plasticity of Ceria-Stabilized Zirconia Polycrystals. *J Am Cer Soc.* 1996;79(6):1726-1728.
58. Camosilvan E, Anglada M. Size and plasticity effects in zirconia micropillars compression. *Acta Mater.* 2016;103:882-892.
59. Chevalier J, Gremillard L, Virkar AV, Clark DR. The Tetragonal-Monoclinic Transformation in Zirconia: Lessons Learned and Future Trends. *J Am Ceram Soc.* 2009;92(9):1901-1920.

60. Shimozono T, Ikeda J, Pezzotti G. Evaluation of transformation zone around propagating cracks in zirconia biomaterials using Raman microprobe spectroscopy. *Key Eng Mater.* 2006;309-311:1207-1210.
61. Chevalier J, Gremillard L. Ceramics for medical applications: A picture for the next 20 years. *J Eur Ceram Soc.* 2009;29(7):1245-1255.
62. Rossi M, Rainforth W, McComb DW, Scott AJ, Brydson R. The role of trace additions of alumina to yttria-tetragonal zirconia polycrystals (Y-TZP). *Scripta Mater.* 2001;45(6):653-660.
63. Tsubakino H, Nozato R, Hamamoto M. Effect of Alumina Addition on the Tetragonal-to-Monoclinic Phase Transformation in Zirconia- 3 mol% Yttria". *J Am Ceram Soc.* 1991;74(2):440-443.
64. Matsui K, Yoshida H, Ikuhara Y. Nanocrystalline, Ultra-Degradation-Resistant Zirconia: Its Grain Boundary Nanostructure and Nanochemistry, *Scientific Reports* volume 4, Article number: 4758 (2014).
65. Paul A, Vaidhyathan B, Binner JGP. Hydrothermal Aging Behavior of Nanocrystalline Y-TZP Ceramics. *J Am Ceram Soc.* 2011;94(7):2146-2152.
66. Lughì V, Sergo V. Low temperature degradation -aging- of zirconia: a critical review of the relevant aspects in dentistry. *Dent Mater.* 2010;26(8):807-820.
67. Maschio S, Pezzotti G, Sbaizero O. Effect of LaNbO₄ addition on the mechanical properties of Ceria-Tetragonal Zirconia Polycrystal Matrices. *J Eur Ceram Soc.* 1998;18(12):1779-1785.
68. Miura M, Hongoh H, Yogo T, Hirano S, Fujii T. Formation of plate-like lanthanum-β-Aluminate crystal in Ce-TZP matrix. *J Mater Sci.* 1994;29(1):262-268.
69. Ori S, Kojima T, Hara T, Uekawa N, Kakegawa K. Fabrication of Ce-TZP/β-hexaaluminate composites using amorphous precursor of the second phase. *J Ceram Soc Jpn.* 2012;120:111-115.
70. Yamaguchi T, Sakamoto W, Yogo T, Fujii T., Hirano TS. In situ formation of Ce-TZP/Ba hexaaluminate composites. *J Ceram Soc Jpn.* 1999;107:814-916.
71. Chevalier J, Grandjean S, Kuntz M, Pezzotti G. On the kinetics and impact of tetragonal to monoclinic transformation in an alumina/zirconia composite for arthroplasty applications", *Biomaterials.* 2009;30(29):5279-5282.
72. Thuan WH, Chen Z, Wang TC, Cheng CH, Kuo PS. Mechanical properties of Al₂O₃/ZrO₂ composites. *J Eur Ceram Soc.* 2002;22(16):2827-2833.
73. Rafferty A, Alsebaie AM, Olabi AG, Prescott T. Properties of zirconia toughened-alumina prepared via powder processing and colloidal processing routes. *J Colloid Interf Sci.*

2009;329(2):310-315.

74. Yuan Z, Vleugels J, Van Der Biest O. Synthesis and characterization of CeO₂-coated ZrO₂ powder-based TZP. *Mater Lett*. 2000;46(5):249-254.
75. Palmero P, Naglieri V, Chevalier J, Fantozzi G, Montanaro L. Alumina-based nanocomposites obtained by doping with inorganic salt solutions: application to immiscible and reactive systems. *J Eur Ceram Soc*. 2009;29(1):59-66.
76. Torrecillas R, Diaz Rodriguez LA, inventors; CSIC, assignee. Nanostructured composite material of stabilized zirconia with cerium oxide and doped alumina with zirconia, use, and procedure for obtaining same. United States patent US8546285B2. 2013 Oct 1.
77. Schehl M, Díaz L.A, Torrecillas R. Alumina nanocomposites from powder-alkoxide mixtures. *Acta Mater*. 2002;50(5):1125-1139.
78. Bartolomé JF, De Aza AH, Martín A et al., Alumina/Zirconia Micro/Nanocomposites: A New Material for Biomedical Applications With Superior Sliding Wear Resistance. *J Am Ceram Soc*. 2007;90(10):3177-3184.
79. Palmero P, de Barra E, Cambier F. *Advances in ceramic biomaterials : Materials, Devices and Challenges*. Woodhead Publishing; 2017.
80. Benazzo F, Falezio F, Dietrich M. *Bioceramics and alternative bearings in joint arthroplasty: 11th biolox symposium-proceeding, ceramics in orthopaedics*. Springer Science and Business Media; 2006.
81. De Aza AH, Chevalier J, Fantozzi G, Schehl M, Torrecillas R. Slow-crack growth behavior of zirconia toughened alumina ceramics processed by different methods *J Am Ceram Soc*. 2003;86(1):115-120.
82. Deville S, Chevalier J, Fantozzi G et al. Low temperature ageing of zirconia toughened alumina ceramics and its implication in biomedical implants. *J Eur Ceram Soc*. 2003;23(15):2975-2982.
83. Goyos L, Diaz LA, TorrecillasR. Alumina-Ceria-TZP nano composites obtained in an alcohol medium by two different processing routes. Paper presented at: *ECCMIS 15th*. 2012 Jun 24-28; Venice, Italie. p. 24-28.
84. Rouanet A. Etude du système zircone oxide de cerium à haute temperature. *C R Hebd Seances Acad Sci*. 1968;18(C908).
85. Leonov AI, Keler EK, Andreeva AB. The system La₂O₃-ZrO₂, Ce₂O₃-ZrO₂ and Nd₂O₃-ZrO₂. *Izv Akad Nauk USSR Neorg Mater*. 1966;2:1047-1054. (pp. 893-897 on the English edition).
86. Heussner KH, Claussen N. Strengthening of ceria-doped tetragonal zirconia polycrystals by

- reduction-induced phase transformation. *J Am Ceram Soc.* 1989;72(6):1044-1046.
87. Sergo V, Schmid C, Meriani S, Evans AG. Mechanically Induced Zone Darkening of Alumina/Ceria-Stabilized Zirconia Composites. *J Am Ceram Soc.* 1994;77(11):2971-2976.
 88. Maschio S, Lucchuni E, Sergo V. Piezospectroscopic Analysis of the Residual Stresses in the Strontium Hexaluminate / Zirconia (SrAl₁₂O₁₉/ZrO₂) System. *J. Am. Ceram. Soc.* 1999;82:3145 – 3149.
 89. Montanaro L, Palmero P, Chevalier J, Reveron H, Fuerderer T, inventors ; Politec di Torino et al., assignee. Procedimento di produzione di compositi ceramici multifasici a base di zirconia. Italien patent TO2014A00145. 2014 Feb 21.
 90. International Organization for Standardization. ISO 6872:2015._Dentistry-Ceramic materials -. Geneva: ISO; 2015.
 91. Becher PF, Swain MV, Ferber MK. Relation of transformation temperature to the fracture toughness of transformation-toughened ceramics. *J Mater Sci.* 1987;22(1):76-84.
 92. Alexander KB, Becher PF, Wang X, Hsueh C. Internal Stresses and the Martensite Start Temperature in Alumina-Zirconia Composites: Effects. *J Am Ceram Soc.* 1995;78(2):291-269.
 93. Becher PF, Swain MV. Grain-Size-Dependent Transformation Behavior in Polycrystalline Tetragonal Zirconia. *J Am Ceram Soc.* 1992;75(3):493-502.
 94. Li LF, Yang K, Li YY. Microstructure and toughening of Ce-TZP ceramics at low temperatures. In: Balachandran UB, Hartwig KT, Gubser DU, Bardos VA, editors. *Advances in Cryogenic Engineering Materials*. Boston: Springer, 2000; p.259-266.
 95. Li B, Zhe X, Ishii K, Sasaki Y. Transformation characteristics of Ce-TZP during shape memory cycles. *Mater Trans JIM.* 1997;38(10):906-909.
 96. Swain MV. Inelastic deformation of Mg-PSZ and its significance for strength-toughness relationship of zirconia toughened ceramics. *Acta Metall.* 1985;33(11):2083-2091.
 97. Sergo V, Clarke DR, Pompe W. Deformation Bands In Ceria-Stabilized Tetragonal Zirconia/Alumina: I. Measurement of Internal Stresses. *J Am Ceram Soc.* 1995;78(3):633-640.
 98. Gebresilassie AG. Atomic scale simulations in zirconia : Effect of yttria doping and environment on stability of phases. *Mechanics of materials [physics.class-ph]*. Université de Lyon, 2016.
 99. Chevalier J, Cales B, Drouin JM. Low-Temperature Aging of Y-TZP Ceramics. *J Am Ceram Soc.* 1999;82(8):2150-2154.
 100. Ashby MF. *Materials Selection in Mechanical Design*, 3rd ed. Waltham, MA: Butterworth-

Heinemann; 2005.

101. Lambrigger M. Evaluation of Weibull master curves of zirconia ceramics and zirconia/alumina composites. *J Mater Sci Lett*. 1997;16(11):924-926.
102. Wennerberg A, Albrektsson T, Wennerberg AT. Suggested guidelines for the topographic evaluation of implant surfaces. *Int J Oral Maxillofac Implant*. 2000;15:331-344.
103. Wennerberg A, Albrektsson T. On Implant Surfaces: A Review of Current Knowledge and Opinions. *Int J Oral Maxillofac Implant*. 2009;24:63-74.
104. Sennerby L, Dasmah A, Larsson B, Iverhed M. Bone tissue responses to surface-modified zirconia implants: a histomorphometric and removal torque study in the rabbit. *Clin Implant Dentistry Related Res*. 2005;7:13-20.
105. Depprich R, Zipprich H, Ommerborn M, et al. Osseointegration of zirconia implants compared with titanium: an in vivo study. *Head Face Med*. 2008;4(30):1-8.
106. Yamashita D, Machigashira M, Miyamoto M, et al. Effect of surface roughness on initial responses of osteoblast-like cells on two types of zircon2009;28:461-470.
107. Kurella A, Dahotre NB. Review paper: Surface modification for bioimplants: The role of laser surface engineering. *J Biomater Appl*. 2005;20(1):5-50.
108. Roitero E, Lasserre F, Anglada M, Mücklich F, Jiménez-Piqué E. A parametric study of laser interference surface patterning of dental zirconia: Effects of laser parameters on topography and surface quality. *Dent Mater*. 2017;33(1):e28–e38.
109. Roitero E, Lasserre F, Roa JJ, Anglada M, Mücklich F, Jiménez-Piqué E. Nanosecond-laser patterning of 3Y-TZP: Damage and microstructural changes. *J Eur Ceram Soc*. 2017;37(15):4876-4887.
110. Park YS, Chung SH, Shon WJ. Peri-implant bone formation and surface characteristics of rough surface zirconia implants manufactured by powder injection molding technique in rabbit tibiae. *Clin Oral Implants Res*. 2013;24(5):586-591.
111. International Organization for Standardization. ISO 14801:2008. *Dentistry-Implants-Dynamic fatigue test for endosseous dental implants*. Geneva: ISO; 2008.
112. Rosa LB, Batiglioni C, Siéssere S, et al. Bite force and masticatory efficiency in individuals with different oral rehabilitations. *Open J Stomatol*. 2012;2(1):21-26.
113. Ferrario VF, Sforza C, Serrao G, Dellavia C, Tartaglia GM. Single tooth bite forces in healthy young adults. *J Oral Rehabil*. 2004;31(1):18-22.
114. Biswas BK, Bag S, Pal S. Biomechanical Analysis Of Normal And Implanted Tooth Using Biting Force Measurement. *Int J Eng Appl Sci*. 2013;4(2):17-23.
115. Luraschi J, Schimmel M, Bernard JP, Gallucci GO, Belser U, Müller F. Mechanosensation

and maximum bite force in edentulous patients rehabilitated with bimaxillary implant-supported fixed dental prostheses. *Clin Oral Implants Res.* 2012;23(5):577-583.

116. Jofré J, Hamada T, Nishimura M, Klattenhoff C. The effect of maximum bite force on marginal bone loss of mini-implants supporting a mandibular overdenture: A randomized controlled trial. *Clin Oral Implants Res.* 2010;21(2):243-249.
117. Fontijn-Tekamp FA, Slagter AP, Van Der Bilt A, et al. Biting and chewing in overdentures, full dentures, and natural dentitions. *J Dent Res.* 2000;79(7):1519-1524.
118. <https://www.straumann.com>
119. <https://zsystems.com>
120. <https://www.zeramex.com>
121. <https://www.camlog.fr>
122. International Organization for Standardization. ISO3950:2016._Dentistry-Designation system for teeth and areas of the oral cavity_.Geneva:ISO; 2016.
123. International Organization for Standardization. ISO 13356:2015._Implants for surgery-Ceramic materials based on yttria-stabilized tetragonal zirconia (Y-TZP)_.Geneva:ISO; 2015.
124. Harrer W, Schwentenwein M, Lube T, Danzer R. Fractography of zirconia-specimens made using additive manufacturing (LCM) technology. *J Eur Cer Soc.* 2017;37(14):4331-4381.
125. Goyos-Ball L, García-Tuñón E, Fernández-García E, et al. Mechanical and biological evaluation of 3D printed 10CeTZP-Al₂O₃ structures. *J Eur Ceram Soc.* 2017;37(9):3151-3158.
126. Tarafder S, Balla VK, Davies NM, Bandyopadhyay A, Bose S. Microwave-sintered 3D printed tricalcium phosphate scaffolds for bone tissue engineering. *J Tissue End Ren M.* 2013;7(8):631-41.
127. Khalyfa A, Vogt S, Weisser J, et al. Development of a new calcium phosphate powder-binder system for the 3D printing of patient specific implants. *J Mater Sci-Mater M.* 2007;18(5):909-916.
128. Miranda P, Pajares A, Saiz E, Tomsia AP, Guiberteau F. Fracture modes under uniaxial compression in hydroxyapatite scaffolds fabricated by robocasting. *J Biomed Mater Res A.* 2007;83(3):646-655.
129. Farzadi A, Solati-Hashjin M, Asadi-Eydivand M, Abu Osman NA. Effect of layer thickness and printing orientation on mechanical properties and dimensional accuracy of 3D printed porous samples for bone tissue engineering. *Plos One.* 2014;9(9):e108252.
130. Zocca A, Colombo P, Gomes CM, Günster J. Additive Manufacturing of Ceramics: Issues, Potentialities, and Opportunities. *J Am Ceram Soc.* 2015;98(7):1983-2001.

131. Fielding GA, Bandyopadhyay A, Bose S. Effects of silica and zinc oxide doping on mechanical and biological properties of 3D printed tricalcium phosphate tissue engineering scaffolds. *Dent Mater.* 2012;28(2):113-122.
132. Kolan KC, Leu MC, Hilmas GE, Brown RF, Velez M. Fabrication of 13-93 bioactive glass scaffolds for bone tissue engineering using indirect selective laser sintering. *Biofabrication.* 2011;3(2):025004.
133. Chu TMG, Orton DG, Hollister SH, Feinberg SE, Halloran JW. Mechanical and in vivo performance of hydroxyapatite implants with controlled architectures. *Biomaterials.* 2002;23(5):1283-1293.
134. Genet M, Houmard M, Eslava S, Saiz E, Tomsia AP. A two-scale Weibull approach to the failure of porous ceramic structures made by robocasting: possibilities and limits. *J Eur Ceram Soc.* 2013;33(4):679-688.
135. Deville S, Saiz E, Tomsia AP. Freeze casting of hydroxyapatite scaffolds for bone tissue engineering. *Biomaterials.* 2006;27(32):5480-5489.
136. Gerberich WW, Hemings PL, Merz MD, Zackay VF. Preliminary toughness results on TRIP steel. *Trans Am Soc Metal.* 1968;61:843-847.
137. Gupta TK, Bechtold JH, Kuznickii RC, Cadoff LH, Rossing BR. Stabilization of tetragonal phase in polycrystalline zirconia. *J Mater Sci.* 1977;12:2421-2426.
138. Chen IW, Reyes Morel PE. Implications of transformation plasticity in ZrO₂-containing ceramics : I, Shear and dilatation effects. *J Am Ceram Soc.* 1986;69(3):181-189.
139. Claussen N. Microstructural Design of Zirconia-Toughened Ceramics (ZTC). In: Claussen N, Ruhle M, Heuer AH, editors. *Advances in Ceramics, Vol. 12. Science and Technology of Zirconia 11.* Columbus OH: American Ceramic Society, 1984; p. 325-351.
140. Heuer AH. Transformation toughening in ZrO₂ -containing ceramics. *J Am Ceram Soc.* 1987;70(10): 689-698.
141. McMeeking RM, Evans AG. Mechanics of Transformation-Toughening in Brittle Materials. *J Am Ceram Soc.* 1982;65(5):242-246.
142. Budiansky B, Hutchinson JW, Lambropoulos JC. Continuum theory of dilatant transformation toughening in ceramics. *Int J Solids Struct.* 1983;19:337-355.
143. Mamivand M, Asle Zaeem M, El Kadiriab H. Phase field modeling of stress-induced tetragonal-to-monoclinic transformation in zirconia and its effect on transformation toughening. *Acta Mater.* 2014;64:208-219.
144. Maekawa H, Kawata K, Xiong YP, Sakai N, Yokokawa H. Quantification of local oxygen defects around Yttrium ions for yttria-doped ceria-zirconia ternary system. *Solid State*

Ionics. 2009;180(4-5): 314-319.

145. Li P, Chen IW, Penner-Hahn JE, Tien TY. X-ray Absorption Studies of Ceria with Trivalent Dopants. *J Am Ceram Soc.* 1991;74(5): 958-967.
146. Tsukuma K, Kubota Y, Tsukidate T. Thermal and mechanical properties of Y_2O_3 -stabilized tetragonal zirconia polycrystals. In: Claussen N, Ruhle M, Heuer AH, editors. *Advances in Ceramics, Vol. 12. Science and Technology of Zirconia 12.* Columbus OH: American Ceramic Society, 1984; p.382-390.
147. Gross V, Swain MV. Mechanical Properties and Microstructure of Sintered and Hot Isostatically Pressed Ytria-Partially Stabilized Zirconia. *J Aust Ceram Soc.* 1986;22:1-12.
148. Tsukuma K, Shimada M. Strength, fracture toughness and Vickers hardness of CeO_2 -stabilized tetragonal ZrO_2 polycrystals (Ce-TZP). *J Mater Sci.* 1985;20(4):1178-1184.
149. El Attaoui H, Saâdaoui M, Chevalier J, Fantozzi G. Static and cyclic crack propagation in Ce-TZP ceramics with different amounts of transformation toughening. *J Eur Ceram Soc.* 2007;27(2-3):483-486.
150. Tsukuma K, Ueda K, Matsushita K, Shimada M. High-Temperature Strength and Fracture Toughness of Y_2O_3 -Partially-Stabilized ZrO_2/Al_2O_3 Composites. *J Am Ceram Soc.* 1985;68(2): C56-C58.
151. Tsukuma K, Takahata T. Mechanical Property and Microstructure of TZP and TZP/ Al_2O_3 Composites. Paper presented at MRS; 1986. *MRS Proceedings.* 1986;78:12-135.
152. Touaiher I, Saâdaoui M, Chevalier J, Reveron H. Effect of loading configuration on strength values in a highly transformable zirconia-based composite. *Dent Mater.* 2016;32(9):e211-e219.
153. Fünfschilling S, Fett T, Hoffmann M, et al. Bridging stresses from R-curve of silicon nitrides. *J Mater Sci.* 2009;44(14):3900-3904.

Table 1.

Materials	Toughness (MPa·m ^{1/2})	Strength (MPa)	Weibull modulus	Inelastic deformation	Grain size (μm)	
					ZrO ₂	Al ₂ O ₃
3Y-TZP ^[27]	4-6	800-1200	~8 ^[27]	-	~ 0.3	-
Ce-TZP ^[27, 28]	7-16	400-600	~20 ^[27]	0.25-0.45 % (4PB) ^[28]	~ 2	-
10Ce-TZP/30Al₂O₃ nanocomposite ^[29, 30, 35]	9.8*	950	12.6 (4PB) 23.0 (P3B)	~ 0.1-0.3 % (4PB)	0.42 ± 0.08	0.59 ± 0.09
NANOZR ^[37]	8.6	1290	-	-	-	-
10.5Ce-TZP/8Al₂O₃/ SrAl₁₂O₁₉ ^[11, 12]	10.2*	1100 (P3B)	-	-	0.6 ± 0.2	0.3 ± 0.1 lm
MnO-doped 12Ce- TZP/10Al₂O₃ ^[26, 31]	7.6-10*	650	40 (4PB)	(4PB) (Uniaxial tension)	1.5-2.5	-
10Ce-TZP/16 vol.% of MgAl₂O₄ ^[38]	15 [§]	900	-	-	0.5	0.2
12Ce-TZP/SrO/Al₂O₃ ^[21]	8.3-14.0	500-700	-	0.5%-1.5% (compression)	~ 2	-

*Measured by single edge V-notch beam (SEVNB); § Measured by double torsion; 4PB: four-point bending; P3B: piston-on-three-balls

FIGURES AND TABLES CAPTIONS

FIGURES CAPTIONS

Figure 1. Transformation-induced plasticity in 9 mol % Ce-TZP, as shown by different papers: (a) Stress-strain diagrams in four-point bending test of 9Ce-TZP sintered at various conditions [7]. (b) Cyclic load-displacement in four-point bending test [8]. (c) Stress-strain curve with acoustic emission signal in four-point bending test. The acoustic emission signals were produced by the burst formation of transformation bands at the onset of elastic-plastic deformation [10]. (d) Load-displacement in double cantilever beam test [53]. Note that only works using 9Ce-TZP were representatively shown in this figure, but several works also showed the transformation-induced plasticity effect on other zirconia ceramics including Ce-TZP, Ce-TZP-based composite and Mg-PSZ [9, 20, 21, 26, 52, 54-57, 28-31].

Figure 2. (a) R-curve illustration of zirconia ceramics. Extent of crack-shielding due to stress-induced transformation (*i.e.* transformation toughening ΔK_{CT}) is proportional to $h^{1/2}$, which then depends on the critical stress for phase transformation (σ_c) in the relationship of $h \propto (K_{app}/\sigma_c)^2$, where K_{app} is the applied stress intensity factor. As a consequence of the tangency condition, the strength is directly related to the slope of the R-curve [5, 23]. (b) R-curves of 12Ce-TZP [23, 24] with two different cracks (natural crack and macrocrack) and (c) R-curves of Y-TZP materials (2Y-TZP and 3T-TZP [27]) compared with Si_3N_4 [153]. Ce-TZP has high ΔK_{CT} and a_{ss} (crack extension at the steady-state or plateau value, K_{RMax}) resulting in high fracture toughness and defect tolerant characteristics, whereas, 3Y-TZP has steep slope in R-curve, contributing to its high strength.

Figure 3. Microstructural features of 10Ce-TZP-alumina based composites developed by Nawa et al. [35] from which the commercial product NANOZR derives (figure from NANOZR brochure [36]).

Figure 4. Microstructural features of BIOLOX Delta[®] ZTA composite, adapted from [71].

Figure 5. (a) TEM (STEM-HAADF) and (b) SEM microstructural features of Zr_8Sr_8 composites [11, 12] prepared at the lab-scale from powder surface-coating route and then through slip-casting and sintering (1450°C-1h). Z stands for Zirconia grains, A for Alumina grains and S for Strontium aluminate grains. Figure adapted from [11].

Figure 6. SEM microstructural features of Zr_8Sr_8 composites prepared at the industrial level from powder mixing and then spray-drying granulation, CIP and sintering (1450°C-1h) [22]. Z stands for Zirconia grains, A for Alumina grains and S for Strontium aluminate grains.

Figure 7. Evolution of the spontaneous t - m transformation temperature (i.e. without any applied stress) of Ceria-doped zirconia / alumina / Strontium Aluminate composites as function of the Ceria content in the zirconia phase and of the sintering temperature, for two types of powder-synthesis methods.

Figure 8. (a) Biaxial strength and toughness as function of the ceria content for ZA8Sr8Ce11-1450°C composite obtained by surface-coating route. (b) Schematic illustration of the “ductile-brittle” transition in Ce-TZP composites. σ_R stands for the maximum strength, K_{IC} the toughness, c the critical defect size, σ_c^{t-m} the critical transformation stress, σ_y the yield strength, c_0 and c_1 two different defect sizes with $c_1 < c_0$.

Figure 9. Biaxial bending load-unload-displacement curves for different ceria-containing Ce-TZP composites obtained by post-doping and after a sintering at 1450°C. A clear difference in the mechanical behavior is observed depending on the Ceria concentration.

Figure 10. (a) Superposition of an optical microscopy image (Nomarski contrast) and a monoclinic/tetragonal Raman map obtained by analyzing the tensile surface of a biaxially tested disc (10.5 mol.% ceria). (b) Corresponding stress distribution obtained by Raman mapping. Results were obtained on Ce-TZP processed by surface-coating route and after a sintering at 1450°C. (c) Schematic picture of stress variations along the distance from the center for a conventional non-transformable ceramic and for the transformable Ce-TZP ceramic tested here. The residual stress field represented here is the difference between the stress field of the elasto-plastic material and the purely elastic case.

Figure 11. (a) Stress-strain load-unload curve of a ZA8Sr8C11-1450°C composite obtained by the mixing route during a tensile test, exhibiting a significant amount of plasticity before failure (b) Corresponding variations of the Young’s modulus as function of the applied strain (measurements performed during re-loading).

Figure 12. (a) Location of the FIB lift-out of the thin foils inside a transformation band. (b) Preparation of the TEM foil by FIB. (c) SEM image of the prepared TEM foil showing micro-cracks of approximately 1 μm at the upper surface and no micro-cracks inside the foil. (d) TEM image of the central part of the foil showing that no micro-cracks are visible. TEM foil was prepared on a ZA8Sr8Ce11-1450°C composite obtained by mixing route.

Figure 13. Fracture toughness versus yield strength chart for different materials. Blue figures are referring to 3Y-TZP ceramics while orange figures refer to Ce-TZP composites. The diagonal lines show the process-zone size diameter, d , in mm.

Figure 14. Tensile Stress-Strain curve of two different Ce-TZP composite samples (ZA8Sr8Ce11-1450°C obtained by mixing route). Sample 1 doesn’t show any internal defect whereas sample 2 exhibits a large internal defect of $\sim 150 \mu\text{m}$. It can be noted that sample 2

does not show any significant decrease of the mechanical properties compared to sample 1, even though it contains a large internal defect, illustrating the large flaw tolerance.

Figure 15. Weibull plot: probability of failure as function of the calculated stress for Ce-TZP composite: $\text{ZA}_8\text{Sr}_8\text{Ce}_{11}$ -1450°C obtained by mixing route (round orange symbols) compared to 3Y-TZP (blue square symbols) obtained with two different loading conditions: 4 point bending test (full symbols) and biaxial bending tests using a piston-on-3-balls set up (half black symbols). The Ce-TZP composite shows a very high Weibull modulus compared to 3Y-TZP explaining its lower sensitivity to the presence of defects. Clearly the overall strengths of Ce-TZP composites are relatively lower than 3YTZP.

Figure 16. Image of a prototype dental implant made of the Ce-TZP composite ($\text{ZA}_8\text{Sr}_8\text{Ce}_{11}$ -1450°C-mixing route) and machined in the sintered state.

Figure 17. (a) Load to failure of implant prototypes as function of the surface treatments for the $\text{ZA}_8\text{Sr}_8\text{Ce}_{11}$ -1450°C composite obtained by mixing route. Available data for 3Y-TZP dental implants fall in the dashed region. “M” stands for hard machining, “S” for sandblasting (with 150 μm alumina particles), “E” for etching (in HF/HNO₃ for 3h) and “A” for annealing at 1350°C for one hour respectively. 3 to 4 samples were tested in each conditions. **(b)** and **(c)** SEM image of a dental implant prototype after sandblasting. **(d)** and **(e)** SEM image of a dental implant prototype after sandblasting + etching.

Figure 18. Additive-manufactured (Robocasting) lattice structures (top 3 optical pictures) and microstructure of $\text{ZA}_8\text{Sr}_8\text{Ce}_{11}$ (11Ce-TZP/Al₂O₃/ SrAl₁₂O₁₉) composite (bottom 2 SEM pictures).

Figure 19. Compressive strength of $\text{ZA}_8\text{Sr}_8\text{Ce}_{11}$ scaffolds achieved by Direct Ink Writing (DIW) for two porosity contents. Higher strength was obtained with the scaffold with a rim and the scaffold without rim had lower compressive strength. Comparison with literature values of porous ceramics made from additive manufacturing and freeze casting techniques is reported for comparison [126-135]. *TCP* stands for TriCalciumPhosphate, *DLM* for dianhydro-D-glucitol [bis(dilactoylmethacrylate), *TTCP* for TetraCalciumPosphate, *3DP* for 3D printing, *HA* for hydroxyapatite, *CaP* for CalciumPhosphate, *SLS* for selective laser sintering and *SLA* for stereolithography.

Panel A - Figure A-1. Strength-toughness relationship for zirconia materials. Linear curves are predicted from Griffith equation considering different flaw-sizes (5-100 microns, Y-TZP) whereas the hyperbolic curve is predicted theoretically using the expression proposed by Swain and Rose [20].

Panel A - Figure A-2. Summary of the strength-toughness results for various PSZ and TZP systems and for 2Y-TZP-20 wt.% Al₂O₃ composites [20, 151].

Panel B - Figure B-1. Apparent ‘stress-strain’ curves obtained on the $\text{ZA}_8\text{Sr}_8\text{Ce}_{11}$ -1450°C composite obtained by mixing route with different loading configurations, when both stress and strain in bending are calculated through standard equations considering elastic hypotheses. The dashed area corresponds to the variation obtained with tensile tests.

Panel B - Figure B-2. Applied load as function of the penetration depth after a 1 ball-indentation test on the $\text{ZA}_8\text{Sr}_8\text{Ce}_{11}$ -1450°C composite obtained by mixing route. For an applied load of 350 N, a permanent penetration depth of the ball of approximately 20 μm is observed. This displacement should be subtracted from the displacement measured by the LVDT.

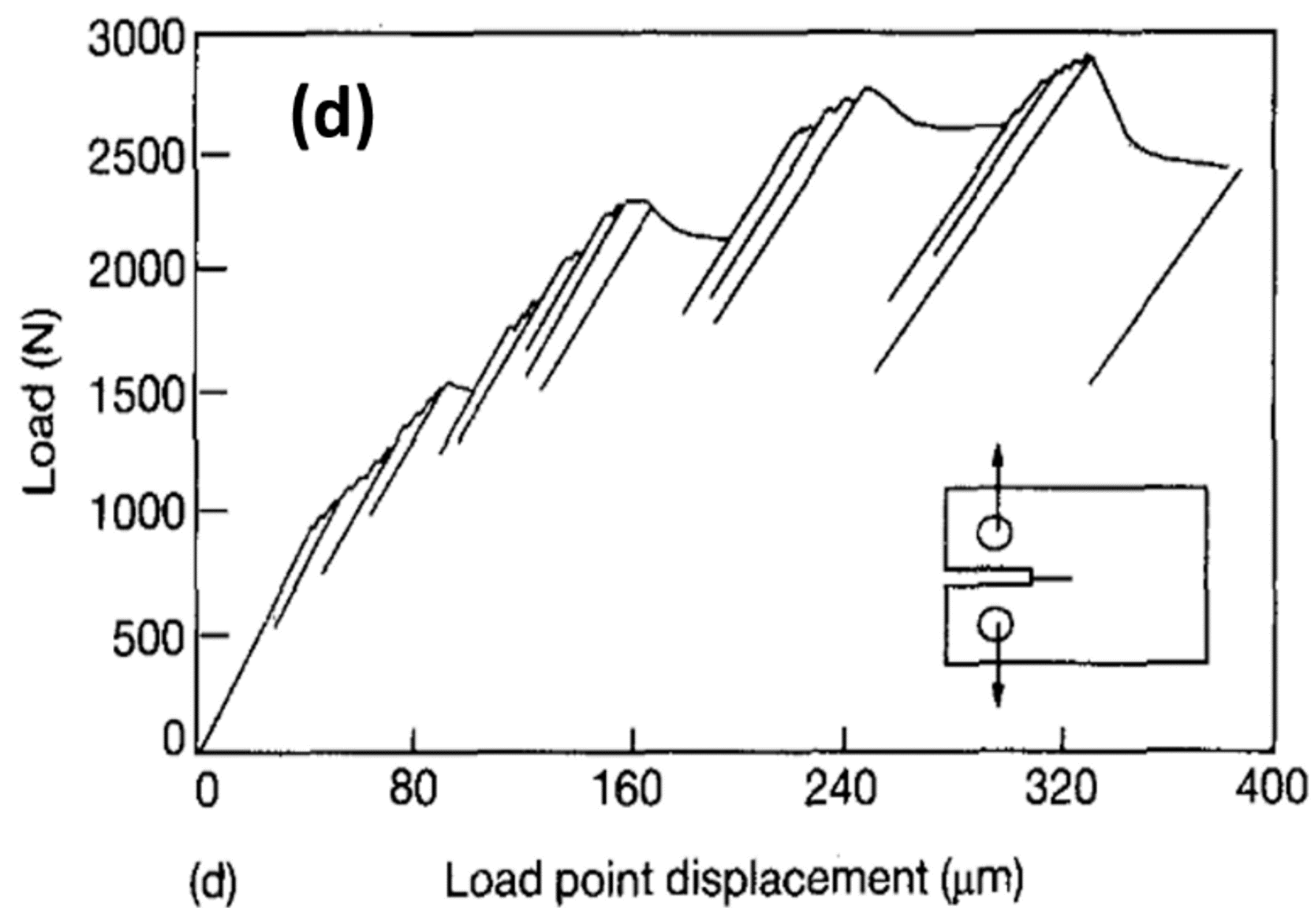
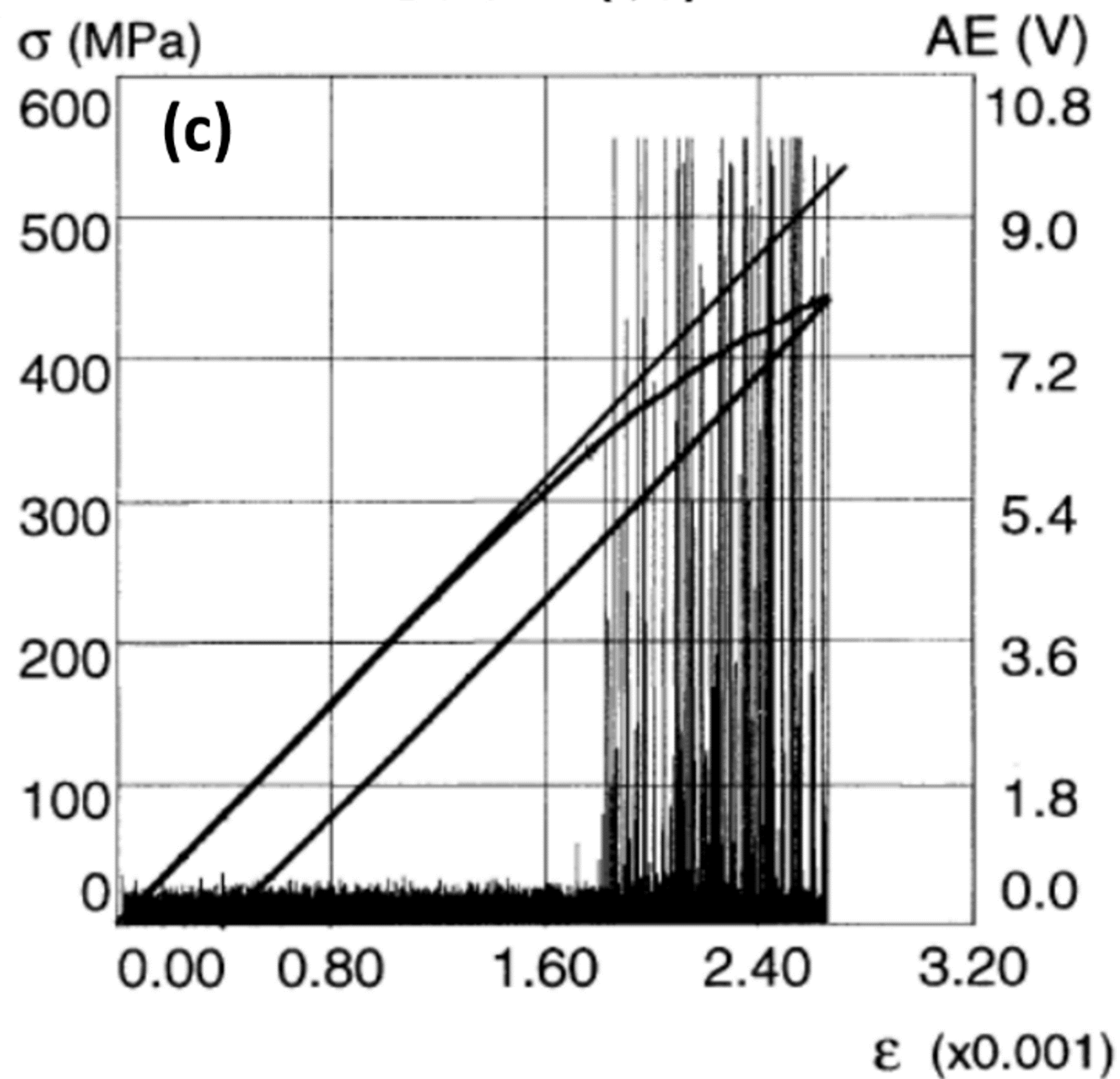
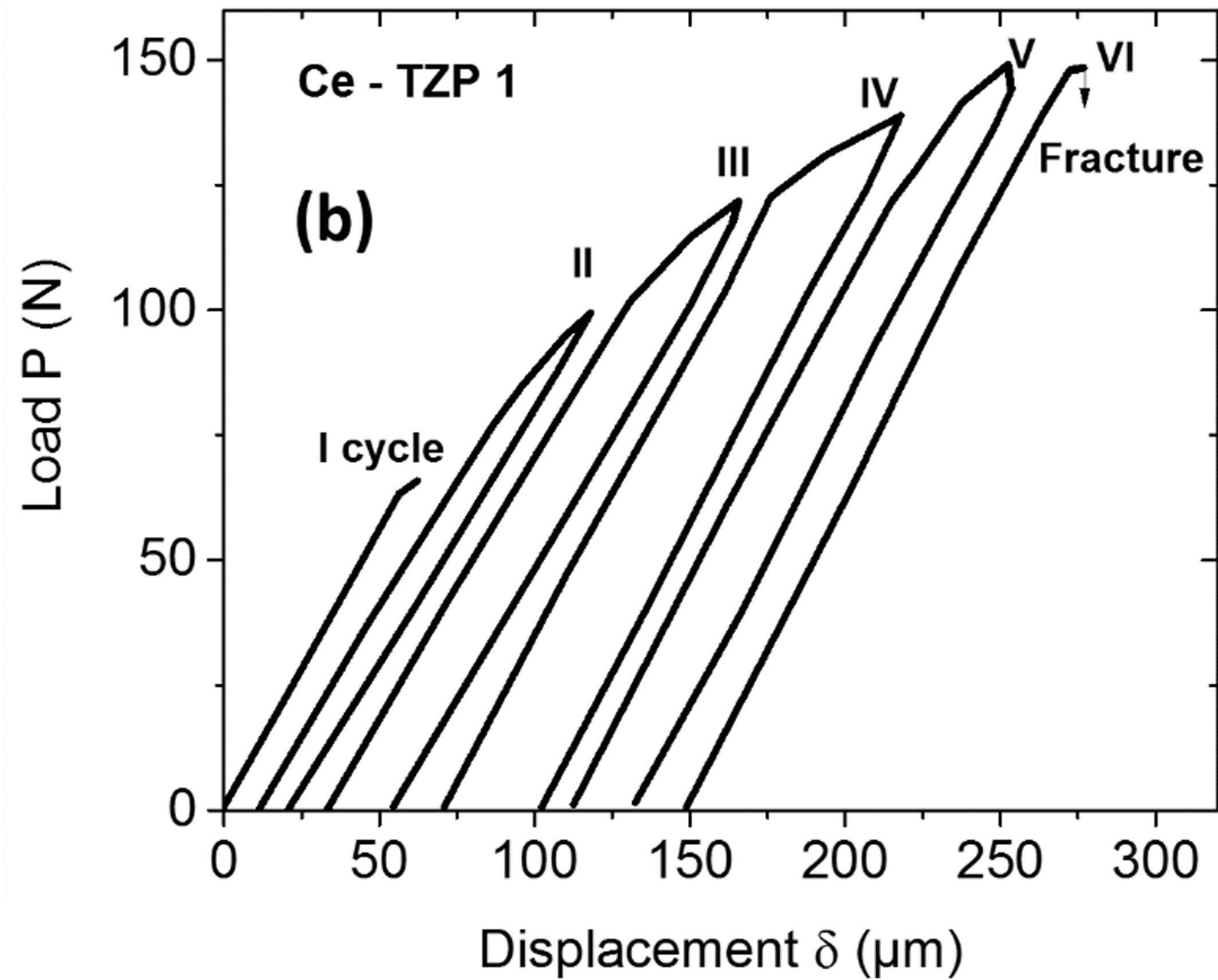
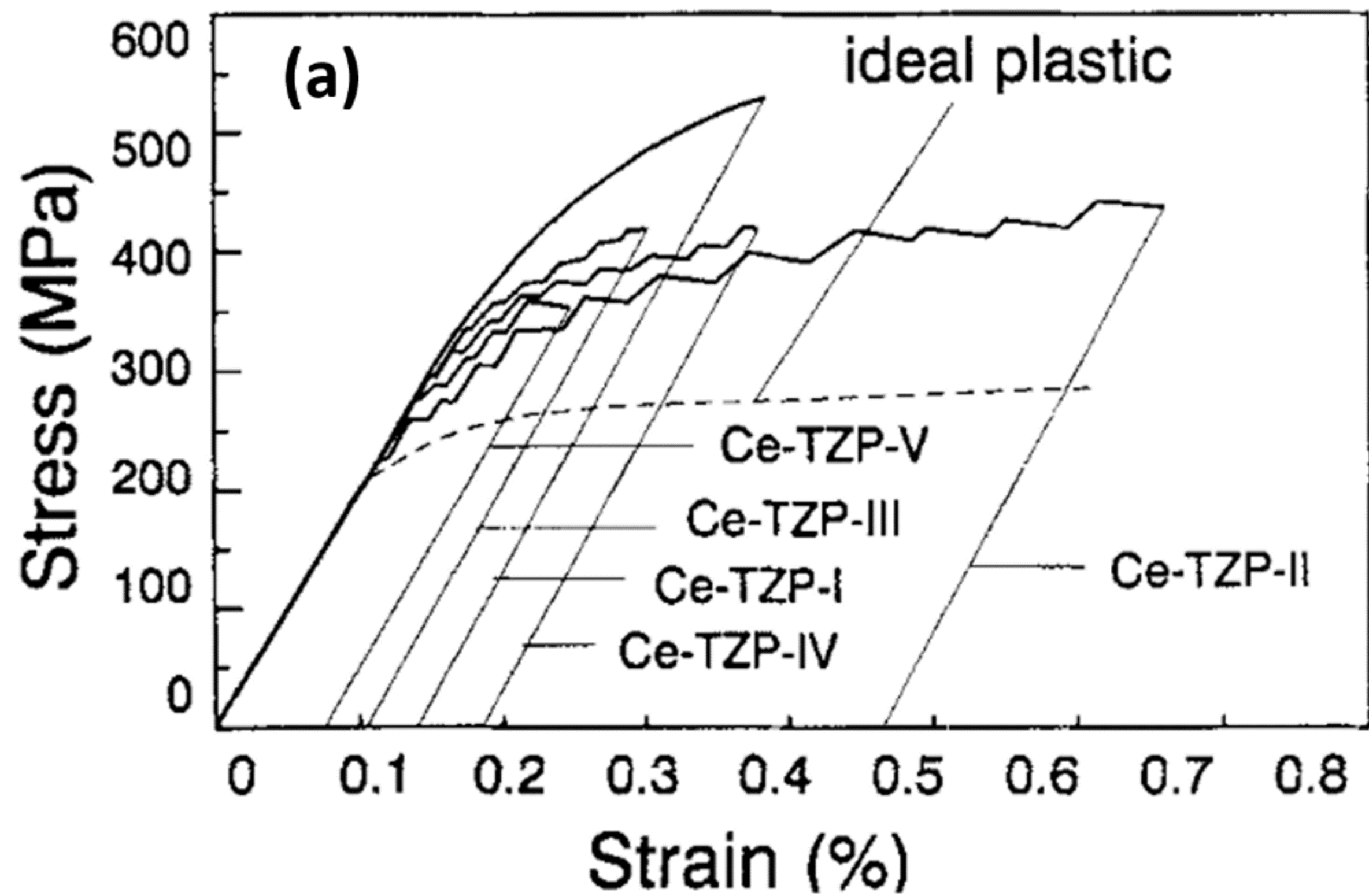
Panel B - Figure B-3. (a) Experimental (solid black line) and FEA-simulated load-displacement curves in 4 point bending for the $\text{ZA}_8\text{Sr}_8\text{Ce}_{11}$ -1450°C composite obtained by mixing route. FEA-simulated curves are obtained by using a CAST-IRON material’s model (elastic in compression and elasto-plastic in tension) and effective load-displacement curve recorded in tension (Figure (b), red and orange symbols). In blue, the results of the inverse method, showing that the behavior can be well described by an elasto-plastic behavior, with a yield stress of 500 MPa and almost no hardening.

Panel B - Figure B-4. Effect of misalignment on the onset of transformation and apparent yield stress measured in tension on $\text{ZA}_8\text{Sr}_8\text{Ce}_{11}$ -1450°C composite obtained by mixing route. (a) Experimental Stress-strain curve with the lowest apparent yield (transformation) stress in all out set of data. (b) Monoclinic content versus position along the sample measured by Raman spectroscopy for two opposite line-scans along the same sample. (c) Finite Element Simulation of maximal principal stress in a tensile sample with a parasite misalignment of 30 microns.

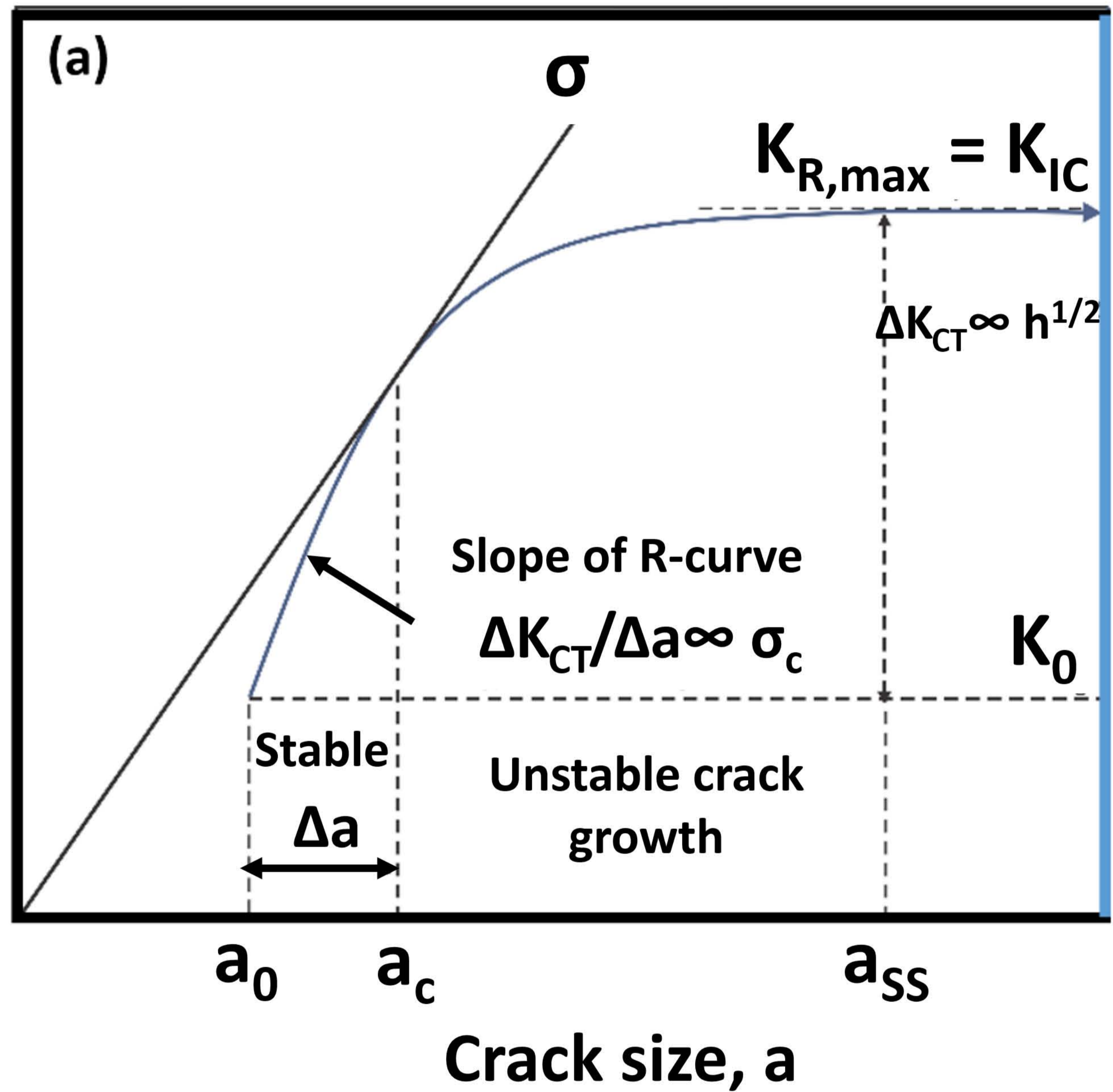
Panel B - Figure B-5. Specific features of the transformation zones observed by optical microscopy (Nomarski contrast) on $\text{ZA}_8\text{Sr}_8\text{Ce}_{11}$ -1450°C composite obtained by mixing route in pure bending (a) and biaxial bending (b)

TABLES CAPTIONS

Table 1. The properties of some Ce-TZP composites developed in the past compared to 3Y-TZP and Ce-TZP ceramics.

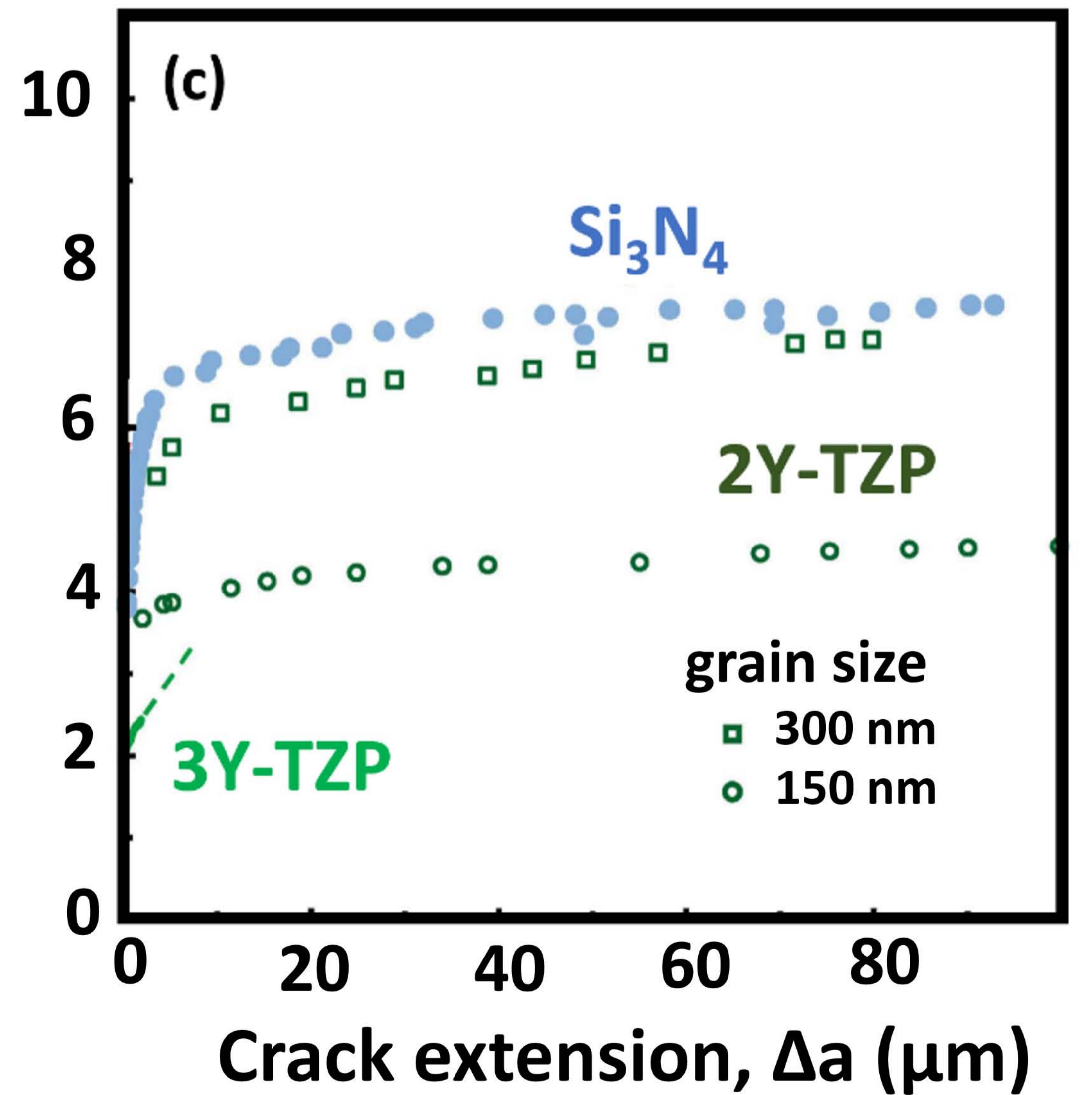
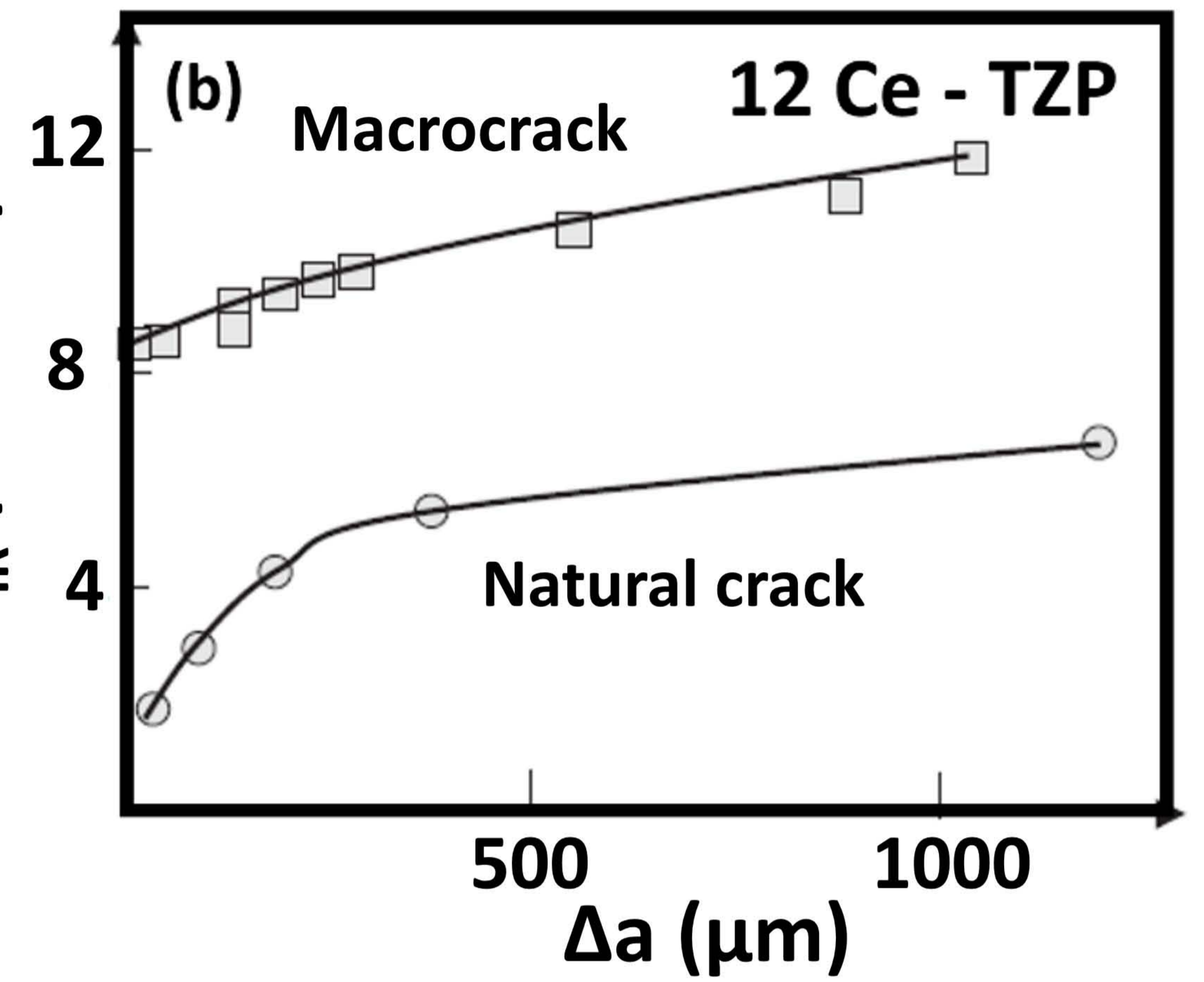


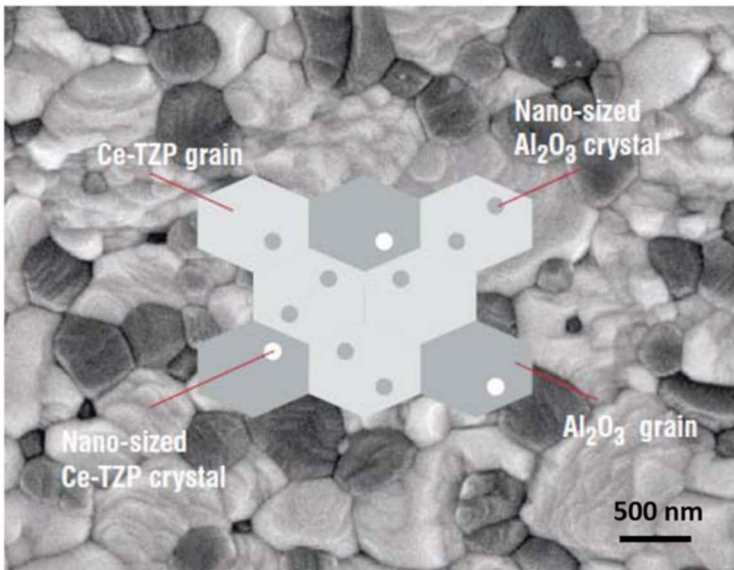
Applied stress intensity, K_{app} (MPa \sqrt{m})

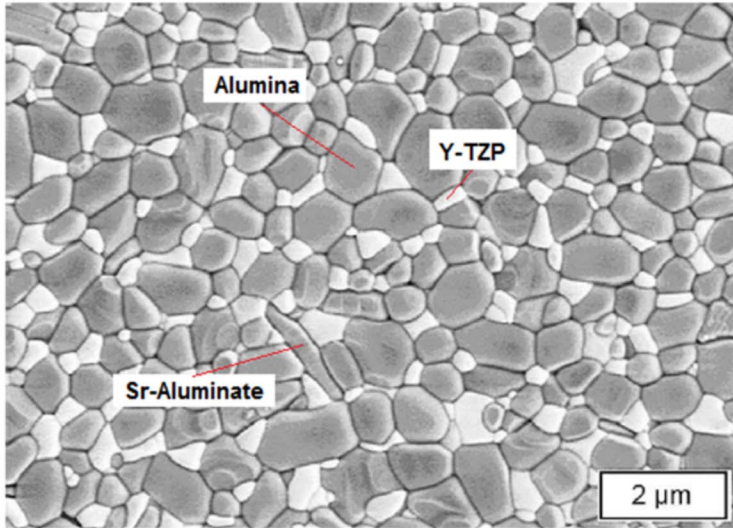


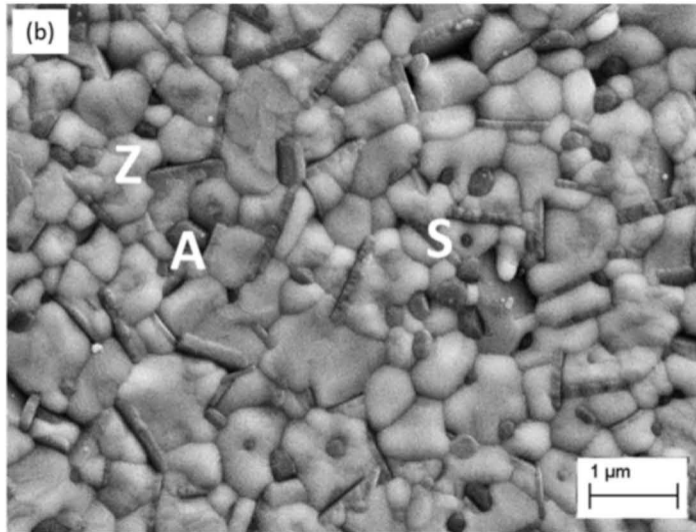
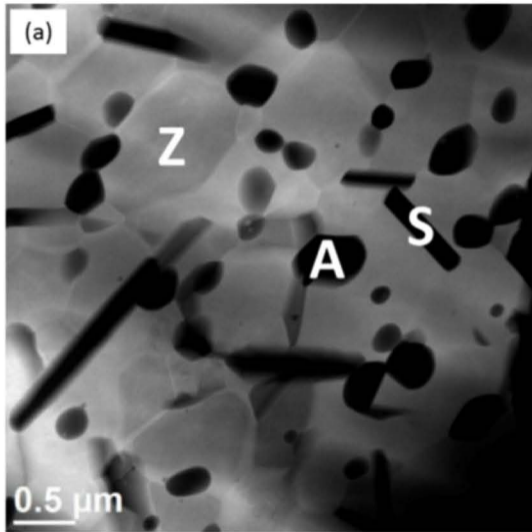
Crack-growth resistance, K_R (MPa $\cdot\sqrt{m}$)

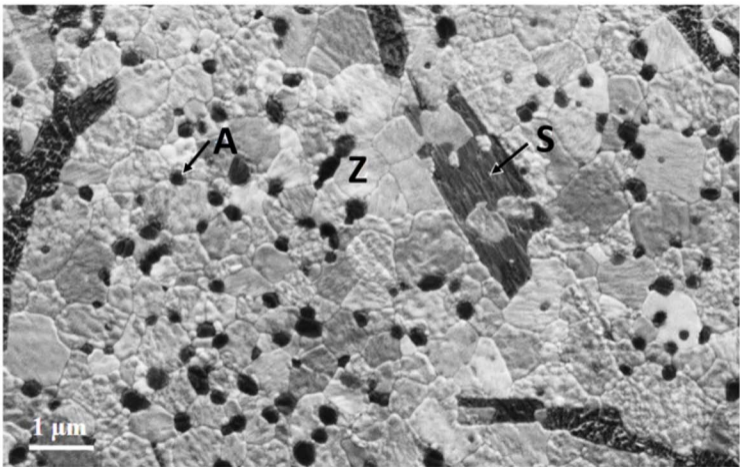
Crack growth resistance, K_R (MPa \sqrt{m})

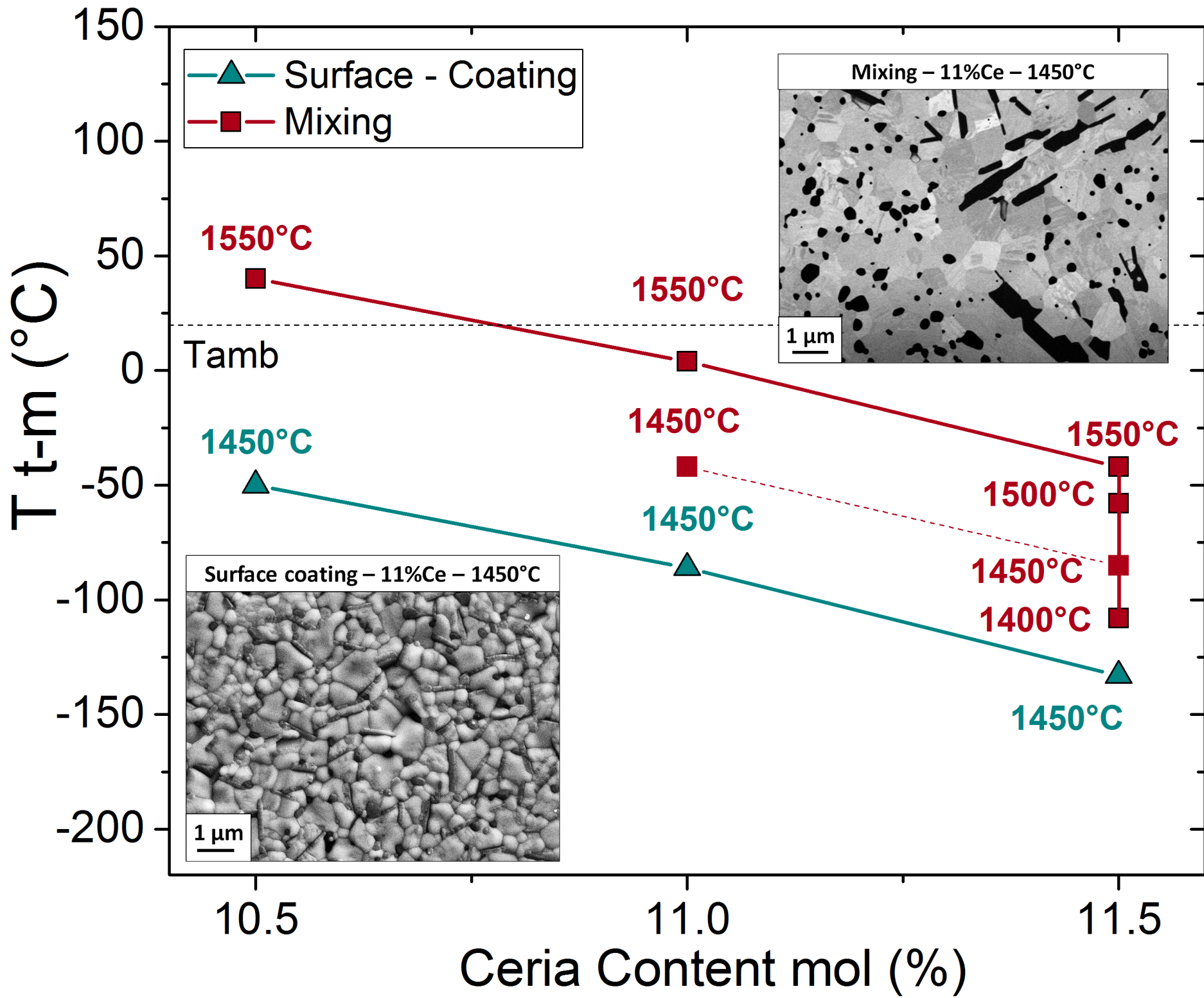


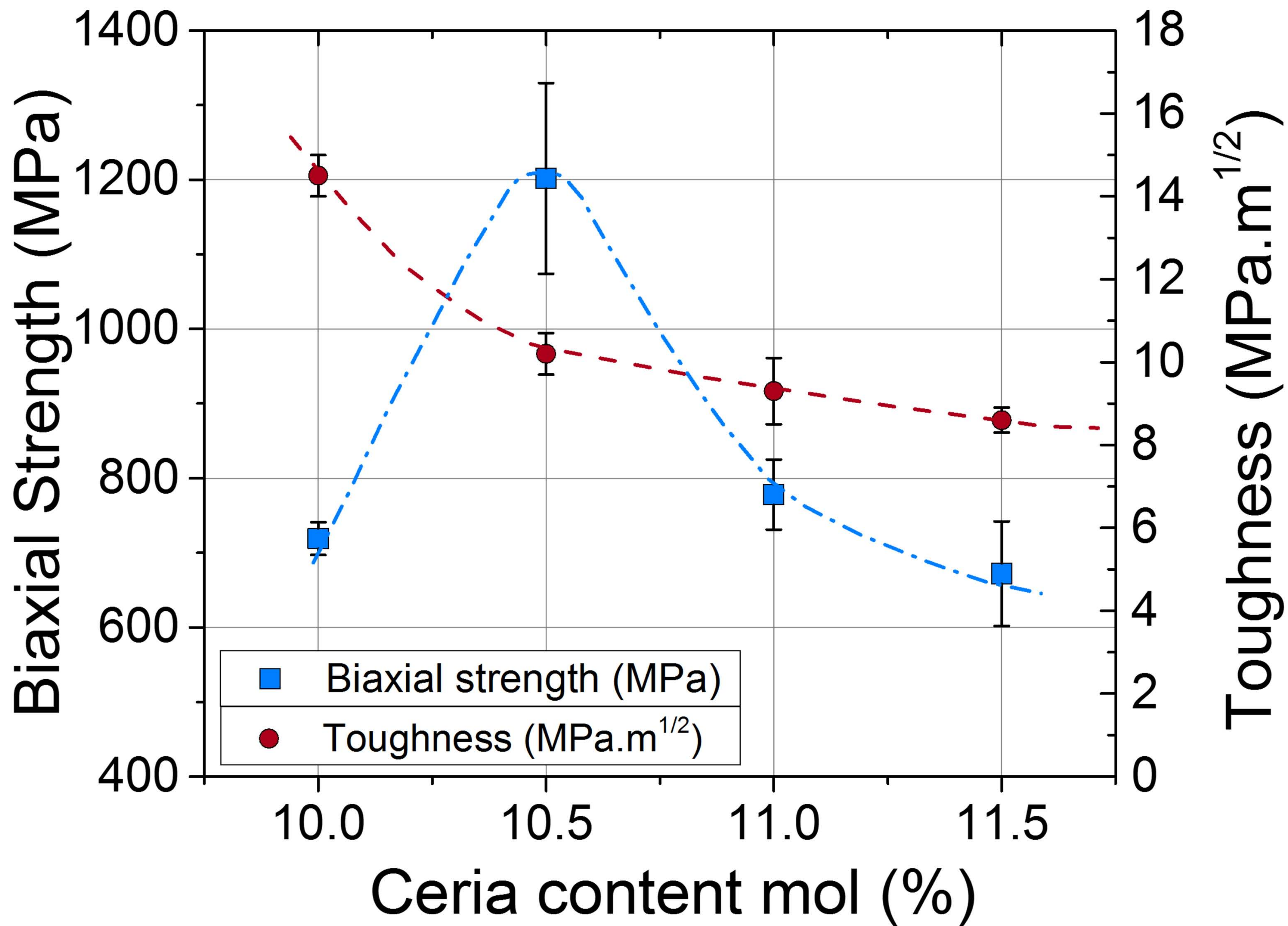


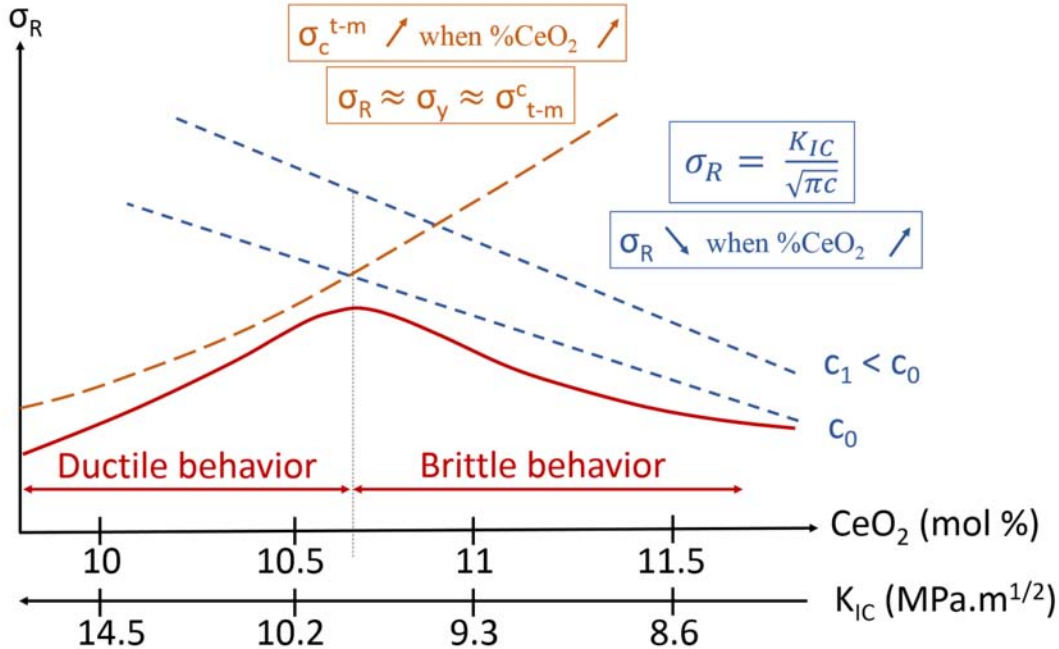


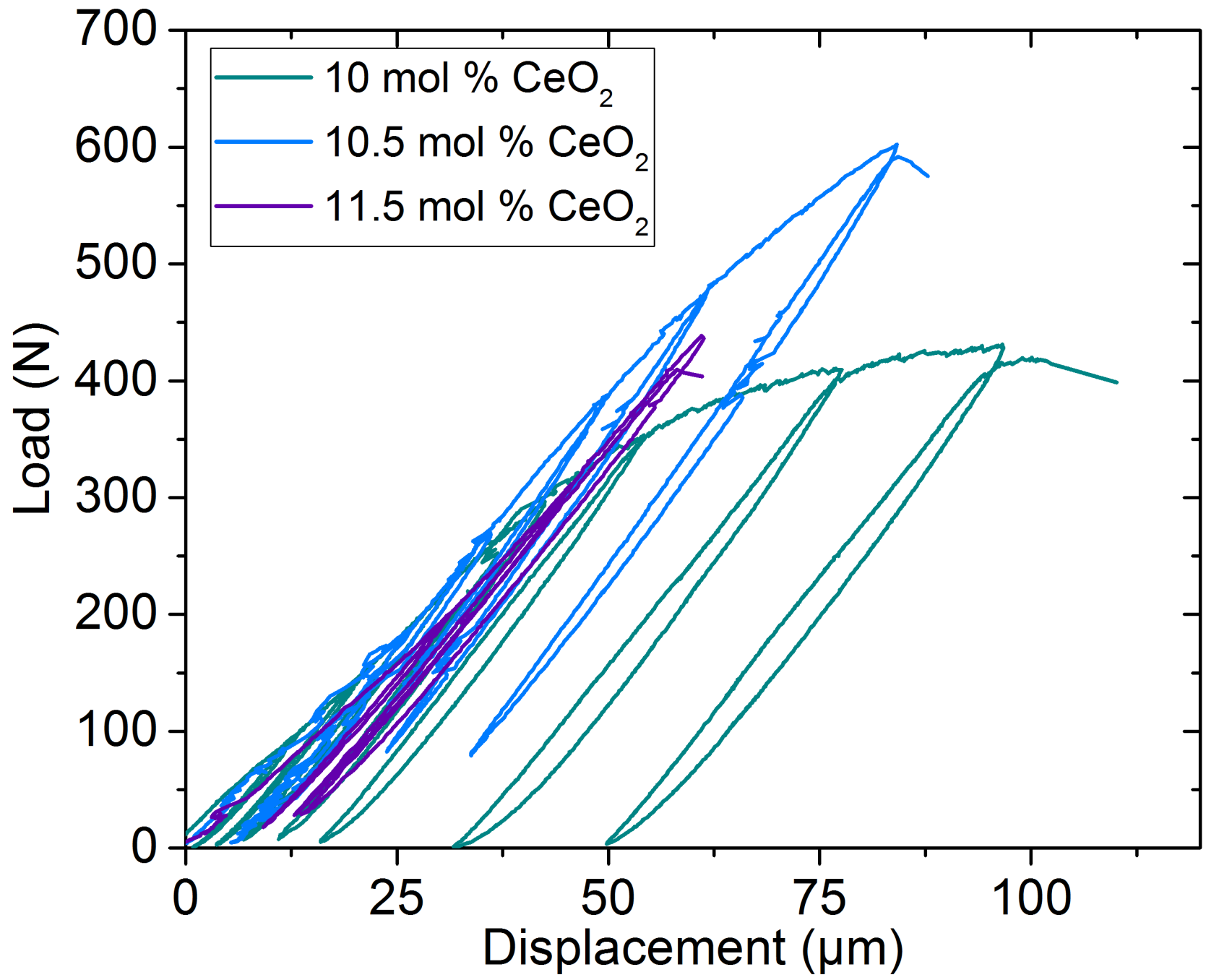




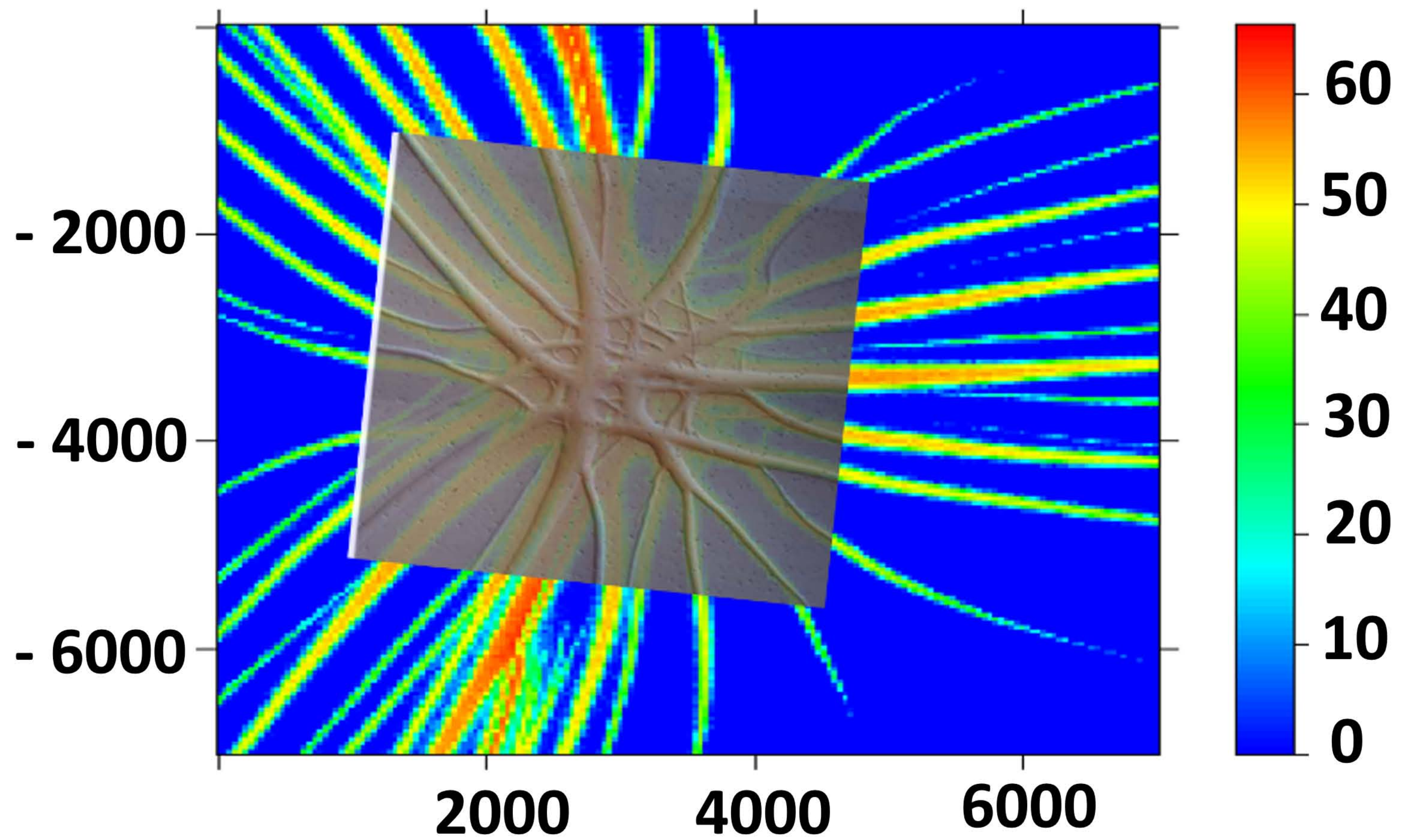




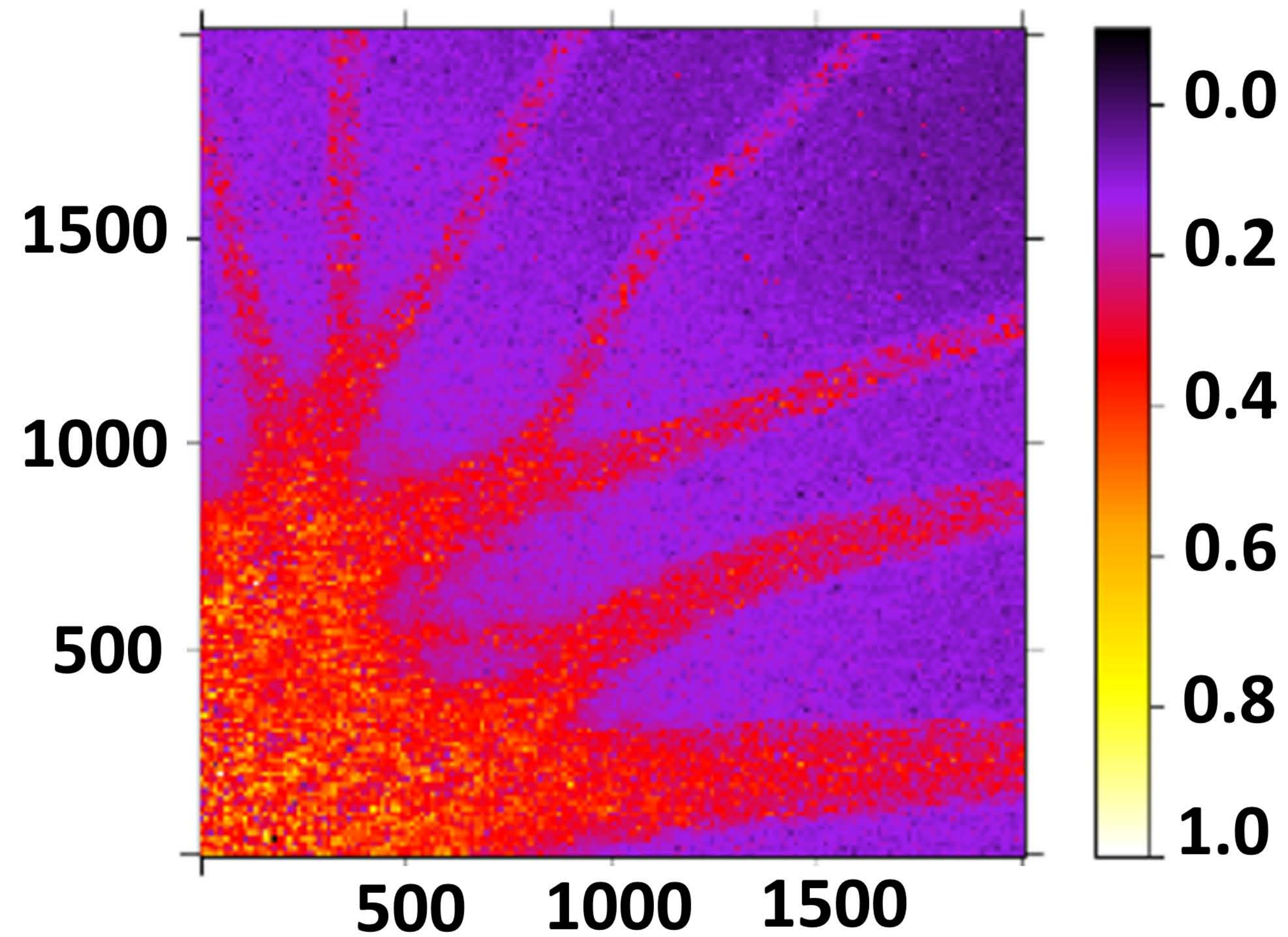




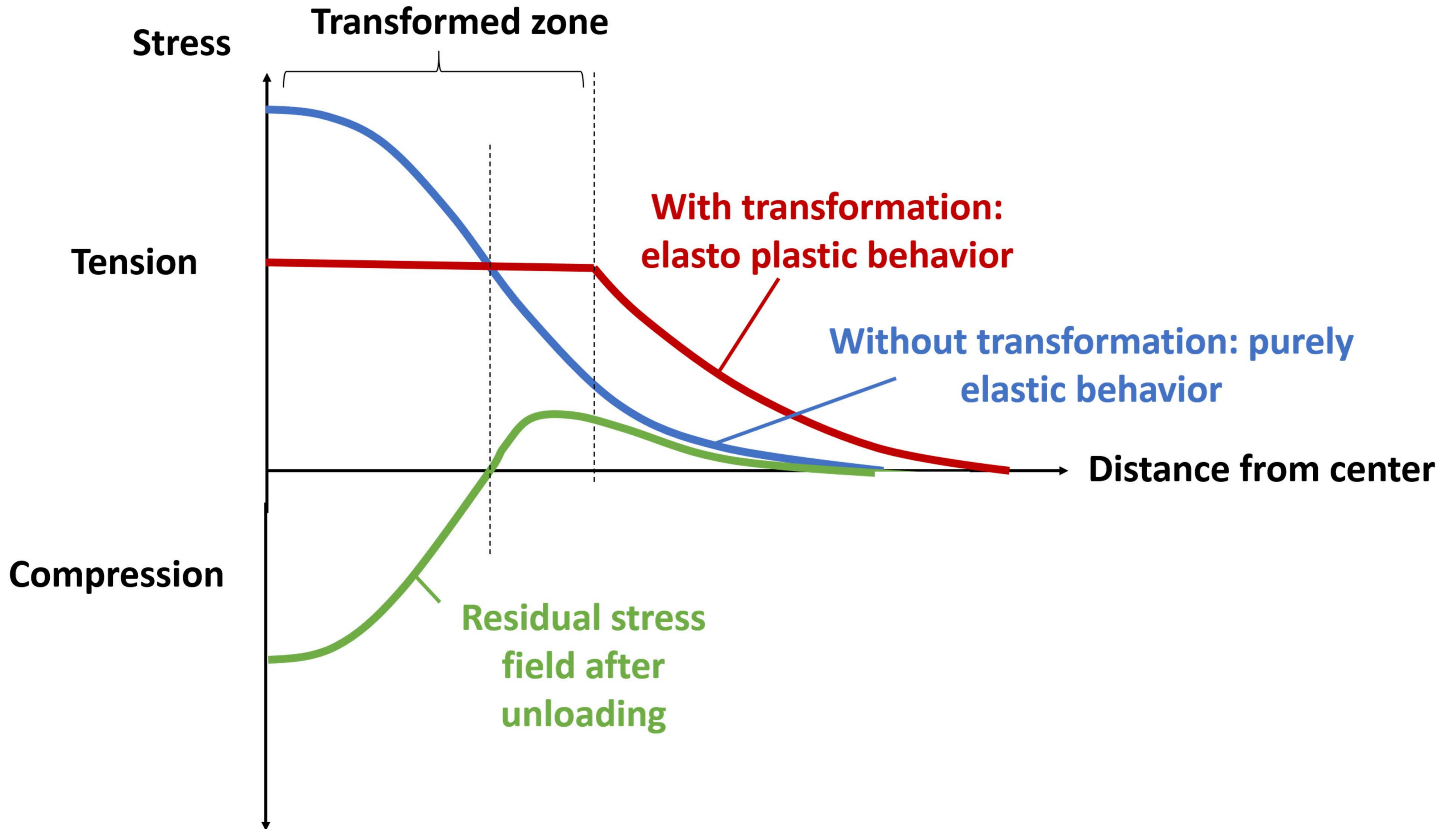
(a) Monoclinic (%)

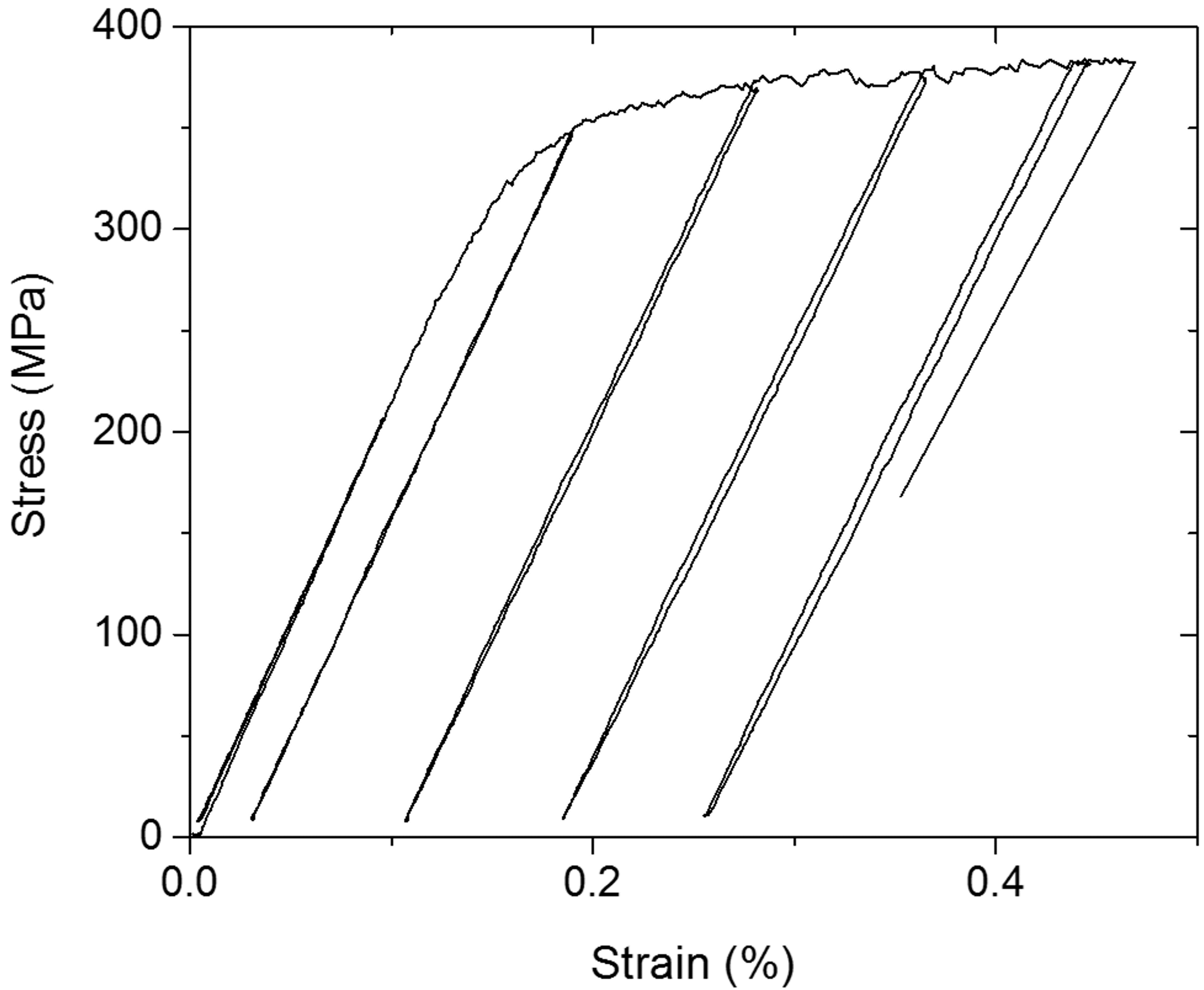


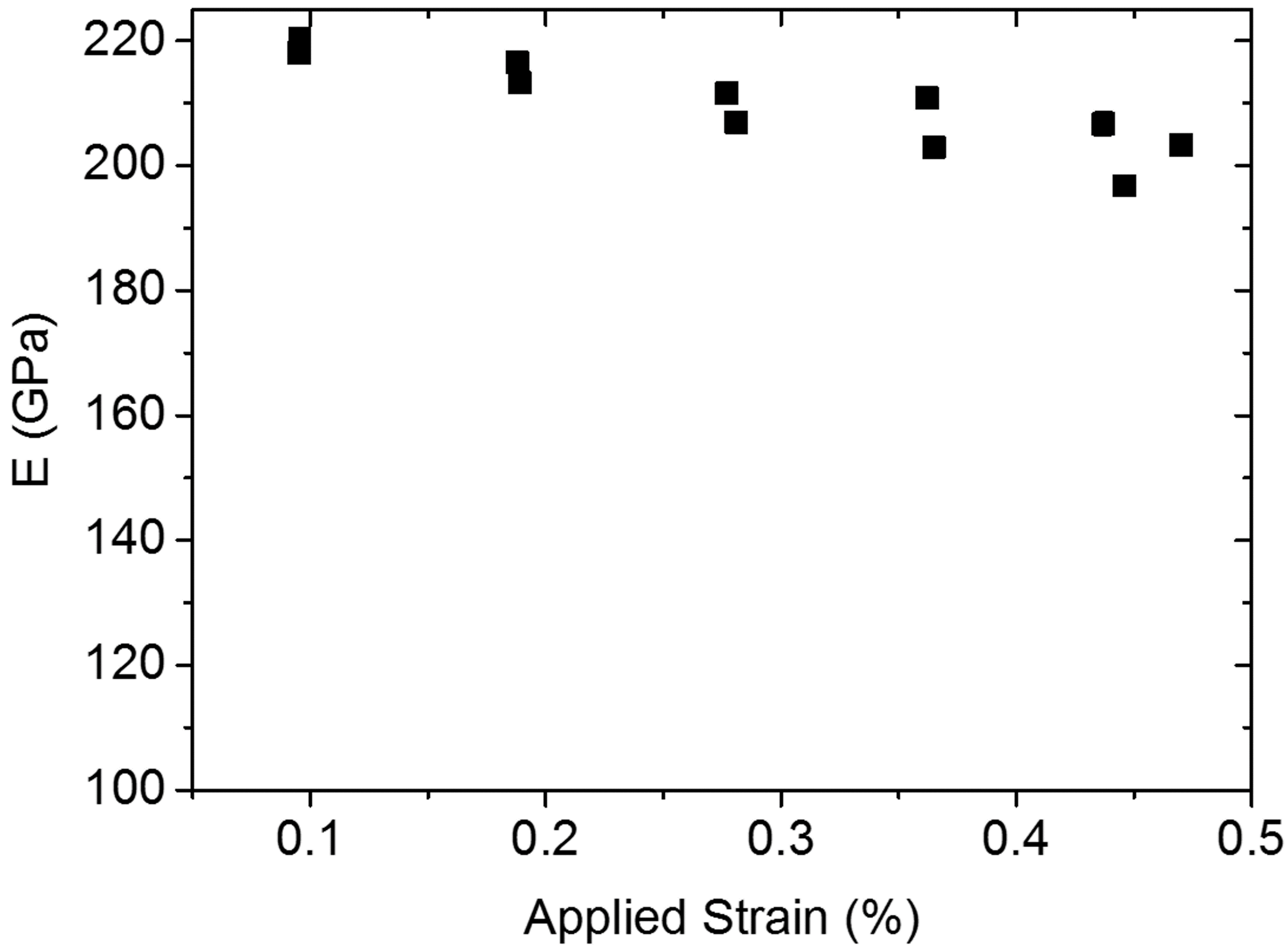
(b) Stress (GPa)

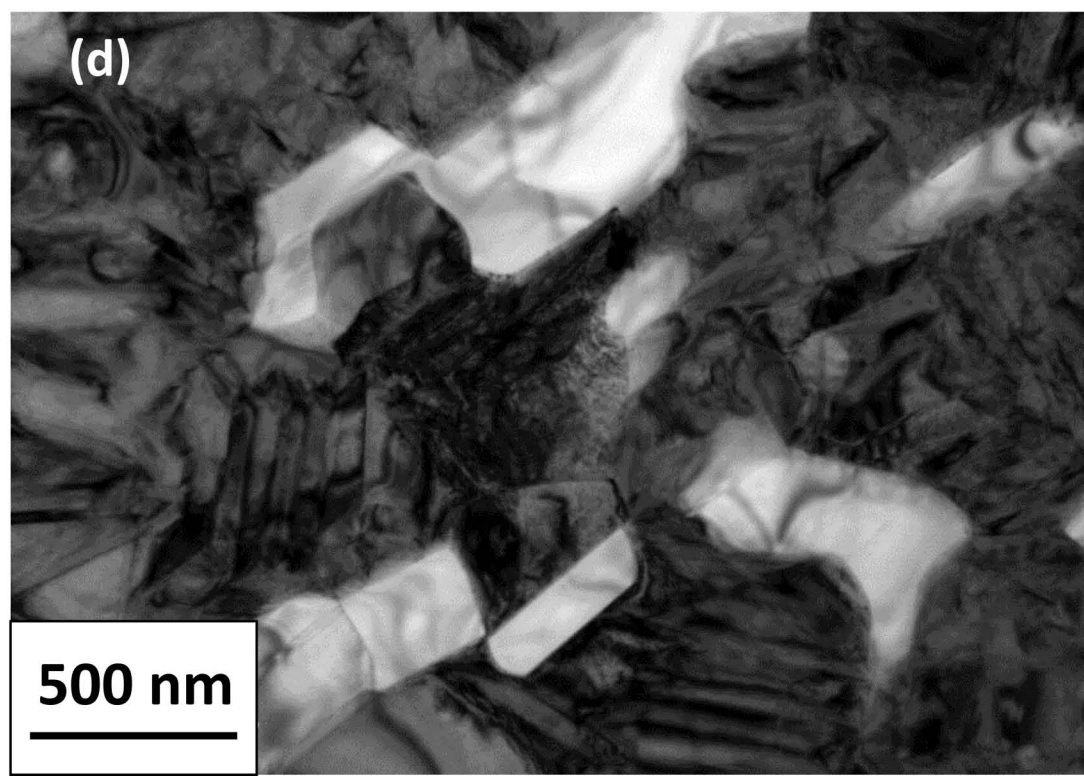
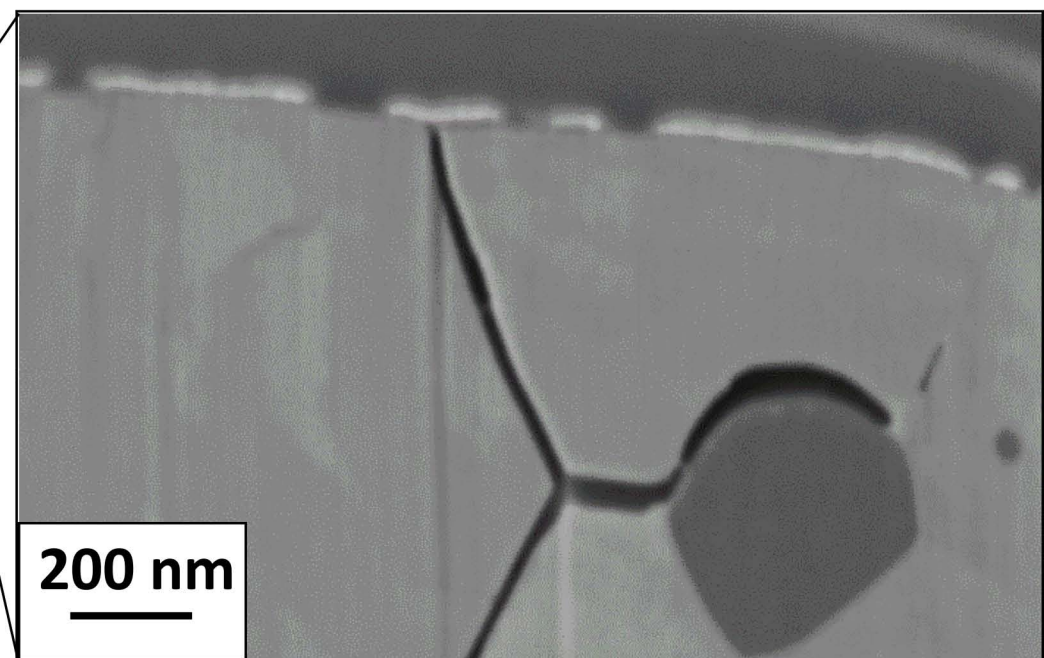
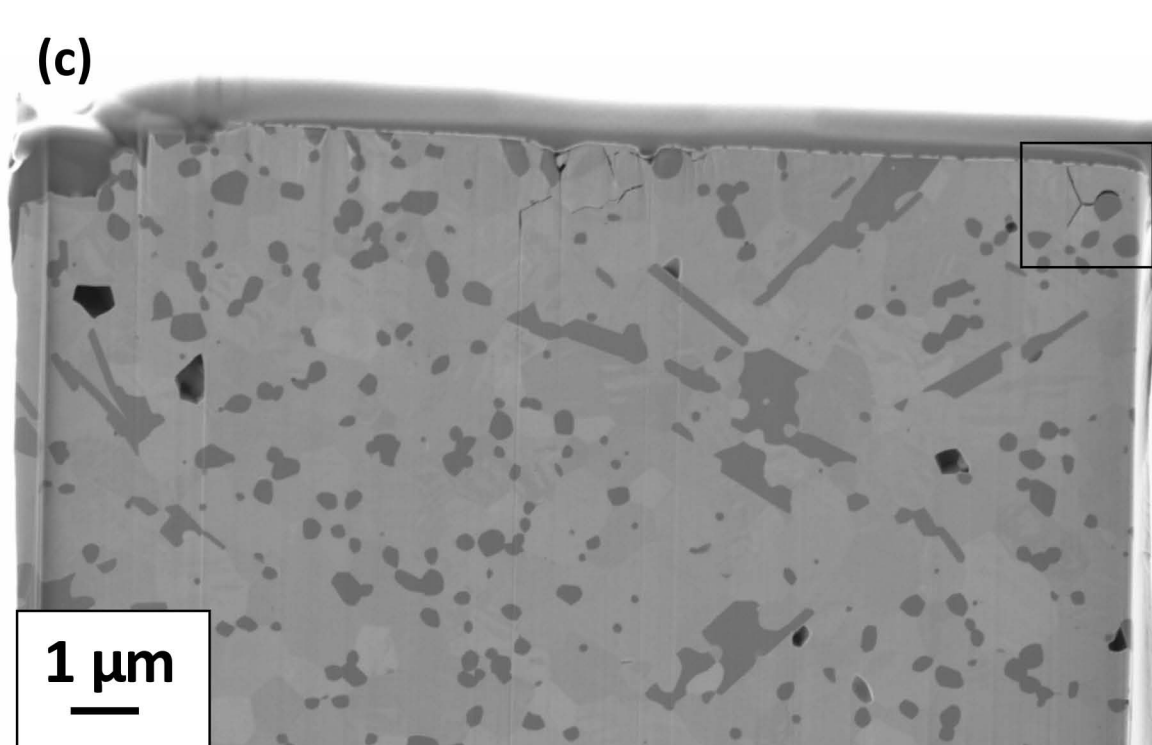
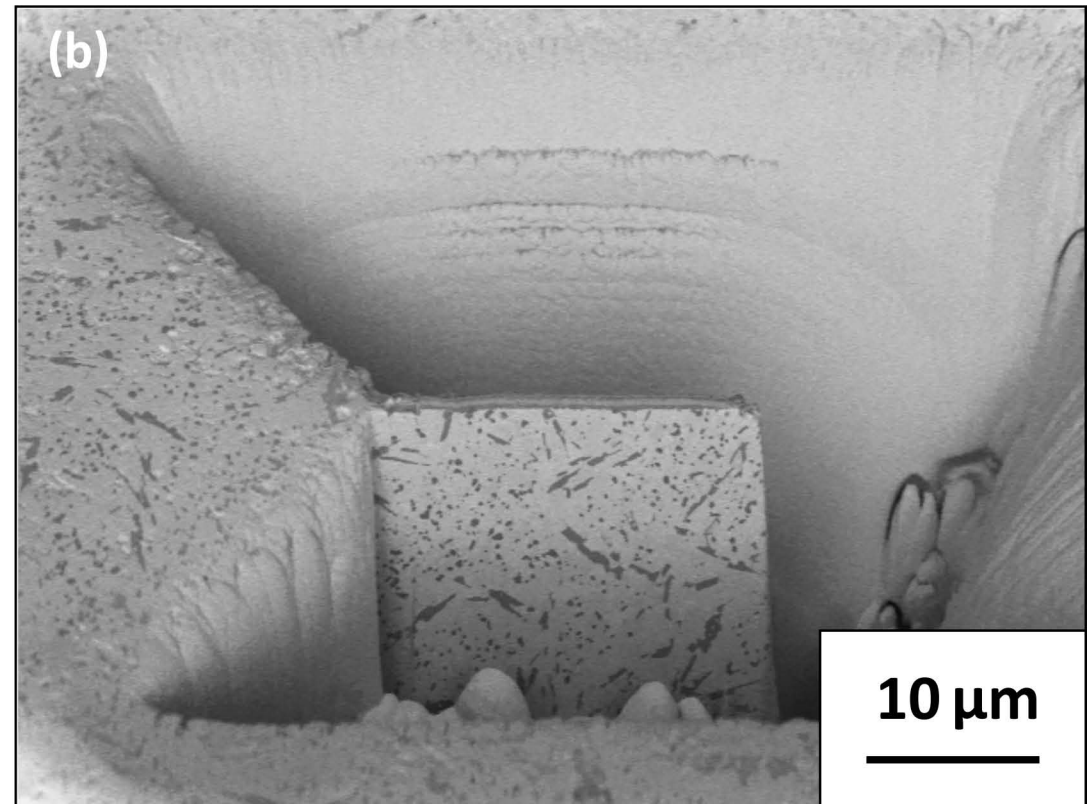
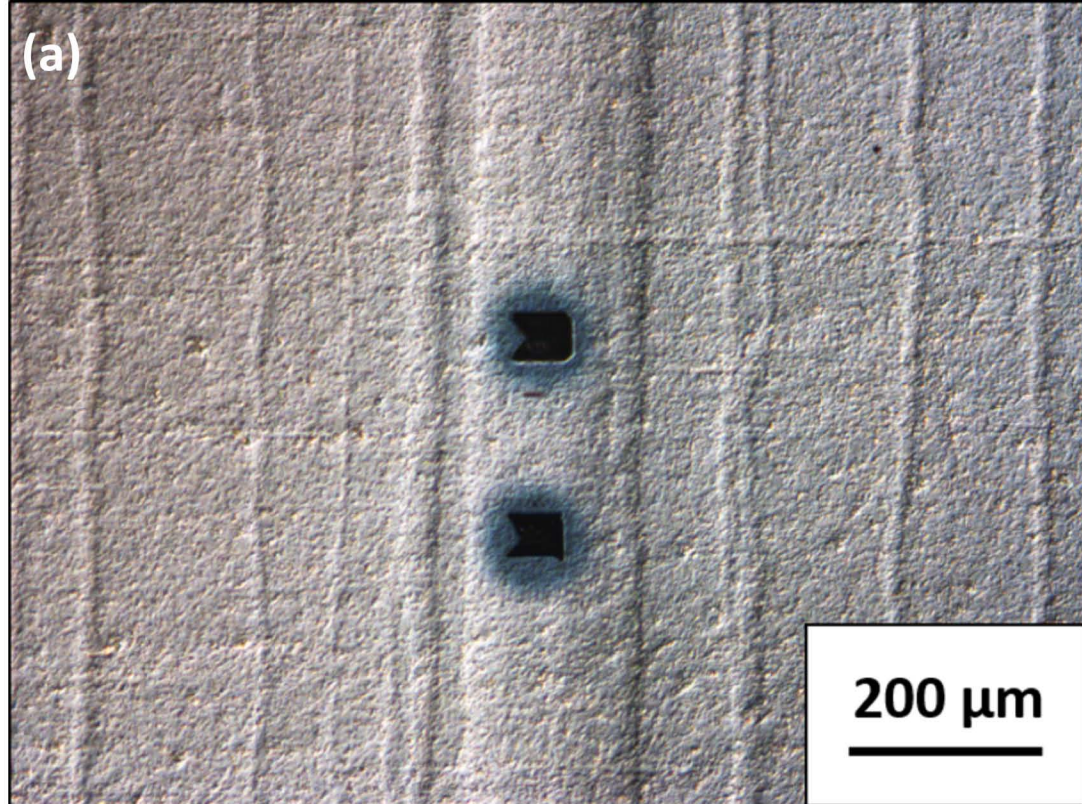


Stress variations









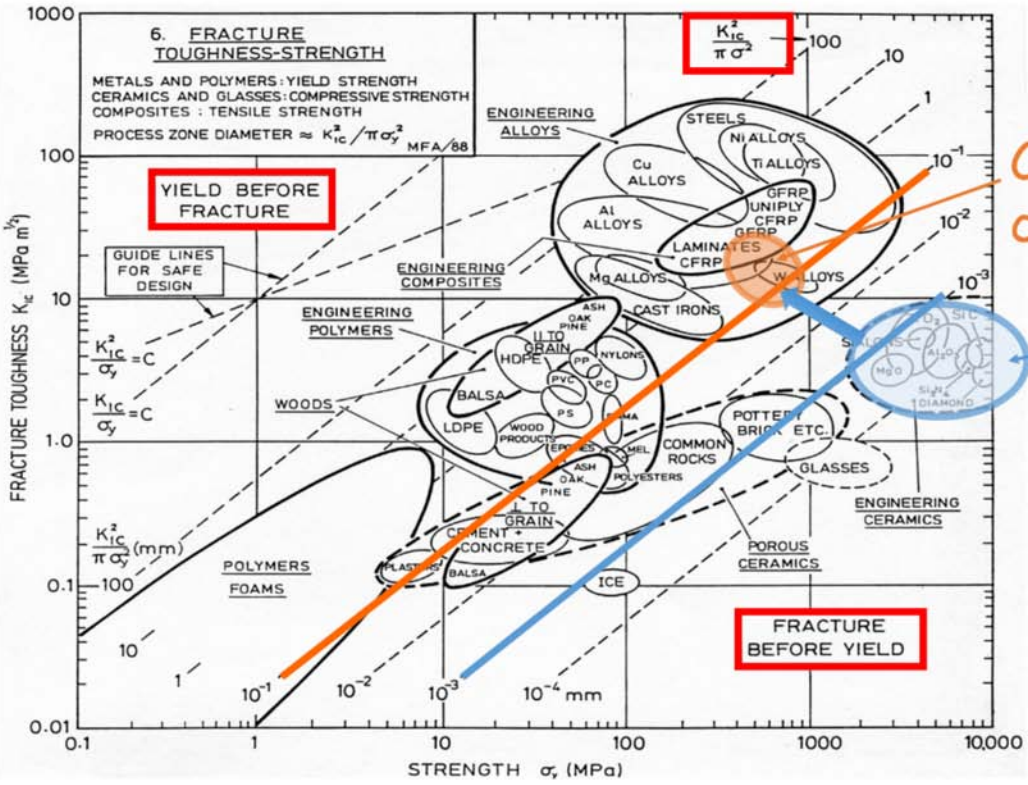
6. FRACTURE TOUGHNESS-STRENGTH

METALS AND POLYMERS: YIELD STRENGTH
 CERAMICS AND GLASSES: COMPRESSIVE STRENGTH
 COMPOSITES: TENSILE STRENGTH
 PROCESS ZONE DIAMETER $\approx K_{IC}^2 / \pi \sigma_y^2$ MFA/88

YIELD BEFORE FRACTURE

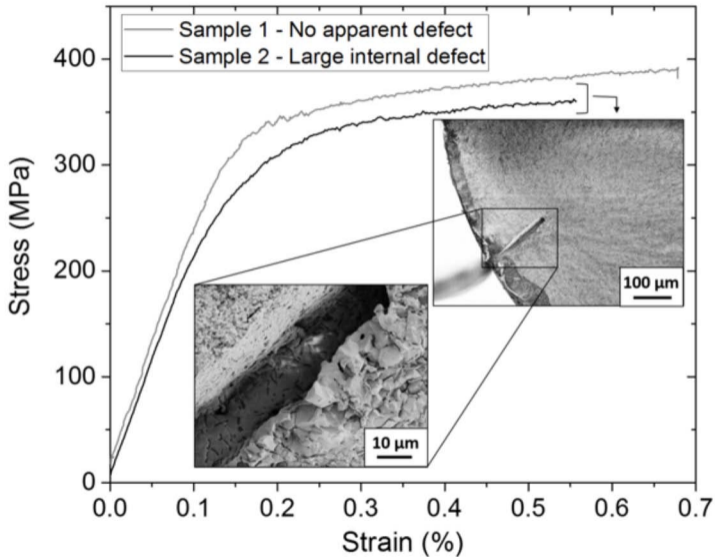
GUIDE LINES FOR SAFE DESIGN

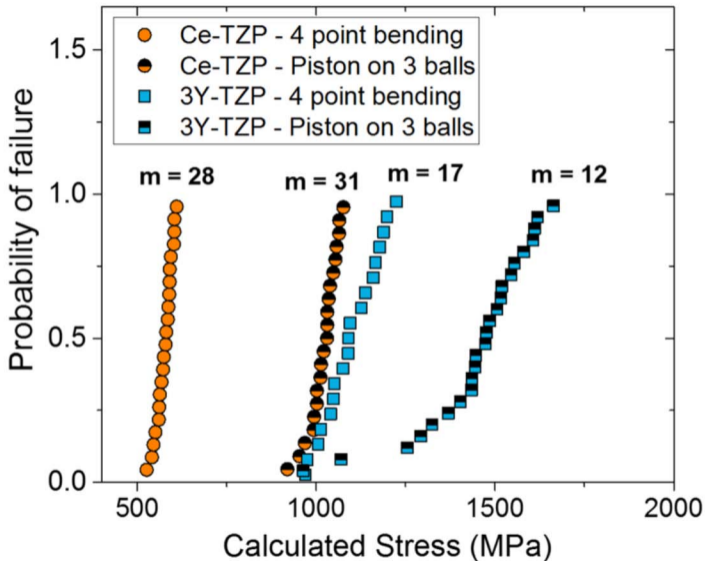
$\frac{K_{IC}^2}{\pi \sigma^2}$



Ce-TZP composites

3Y-TZP







mm

1

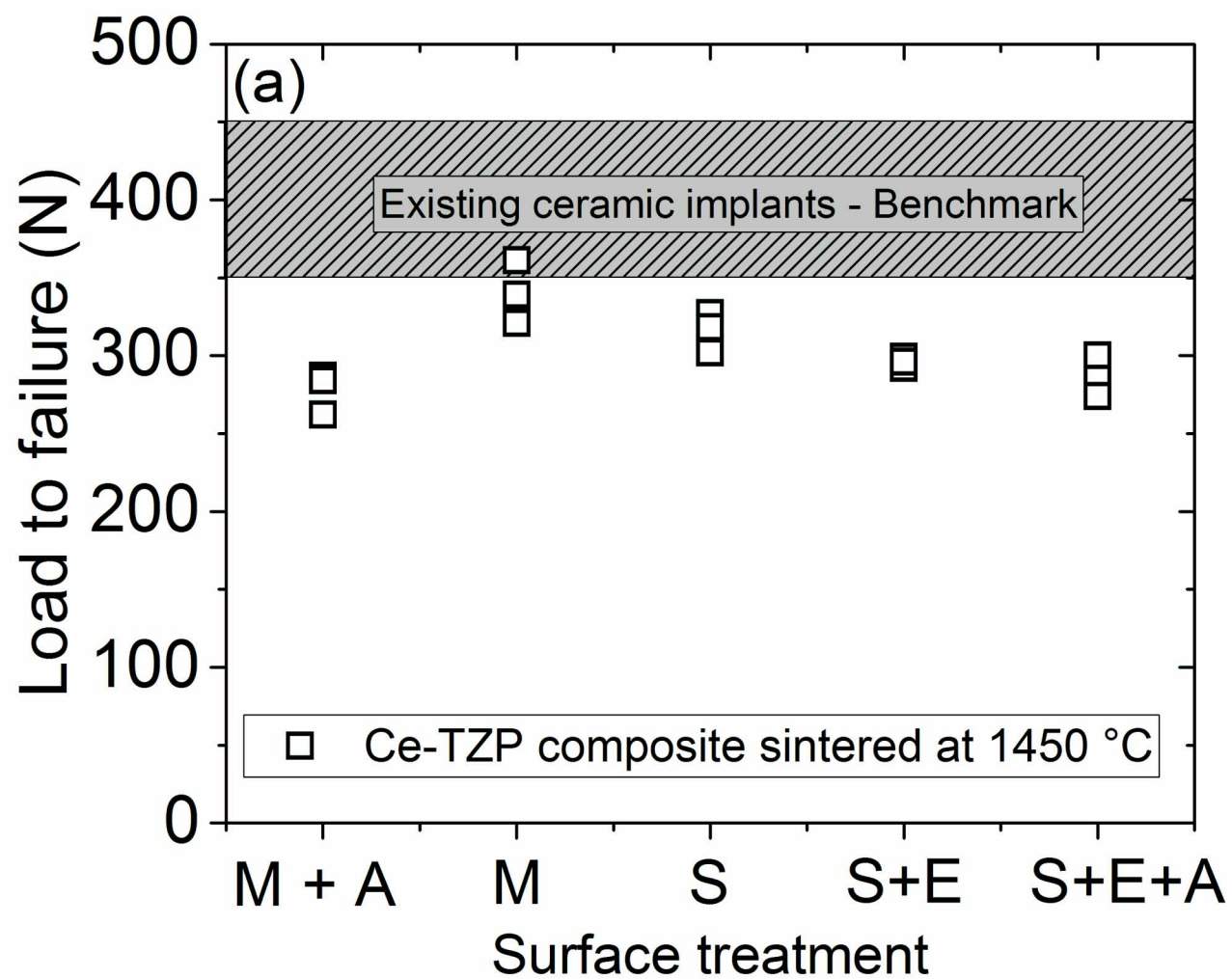
0.2m

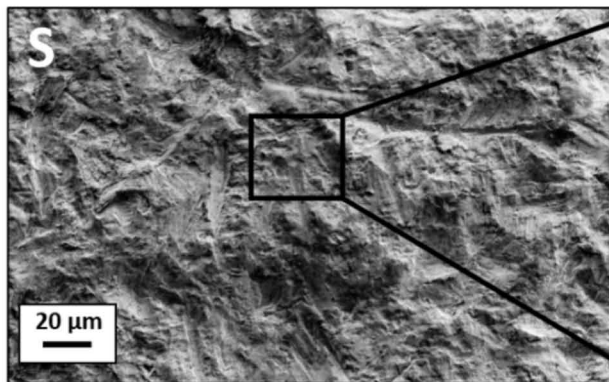
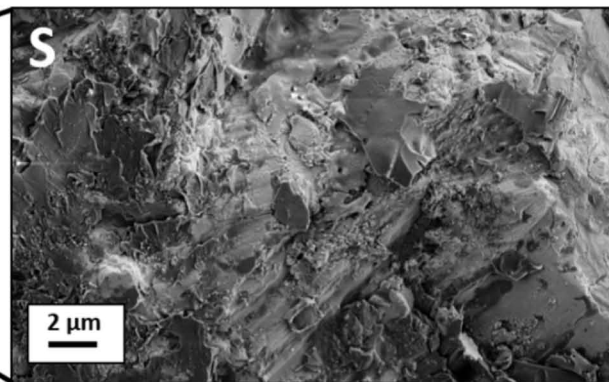
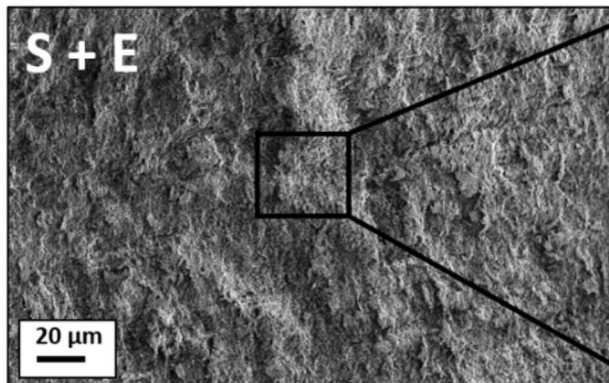
2

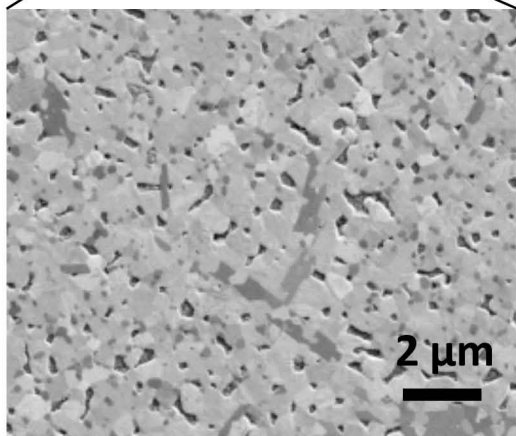
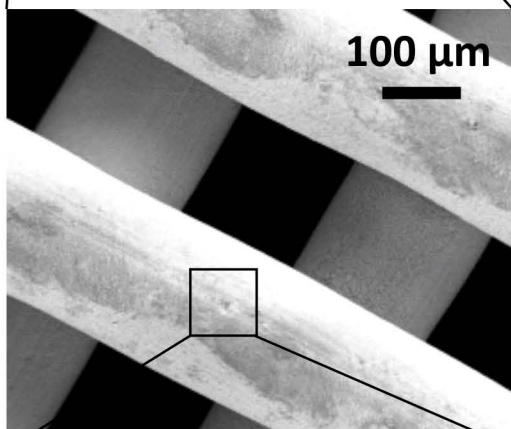
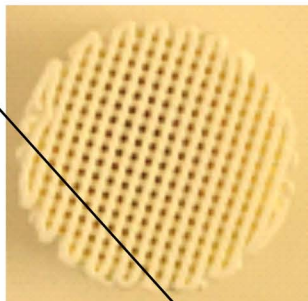
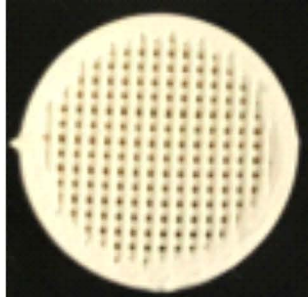
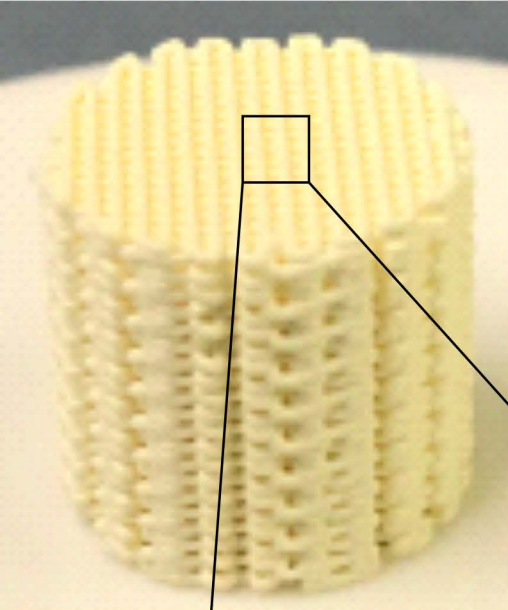
STANLEY

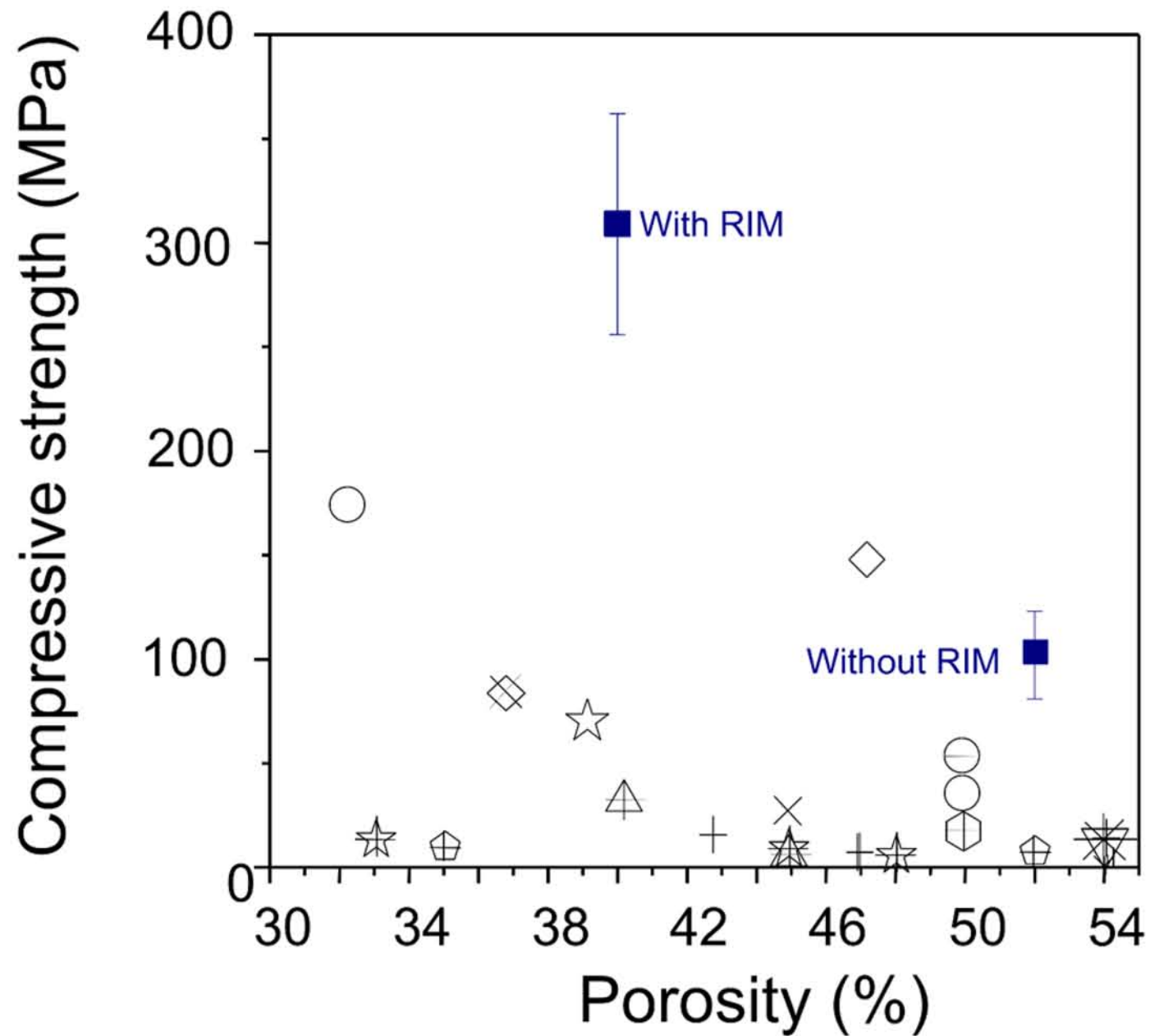
3

mm



(b)**(c)****(d)****(e)**

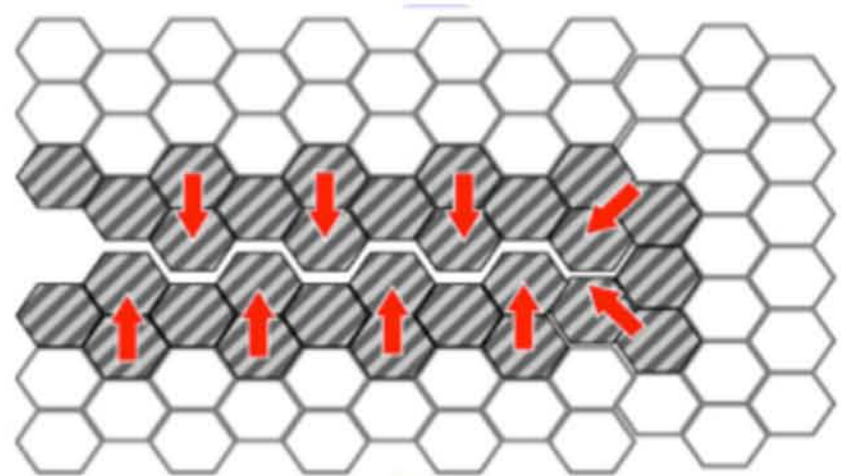




- ZA8Sr8Ce11 DIW, this work
- 10Ce-TZP-Al₂O₃ DIW [127]
- + TCP, microwave sintering Binder jetting [128]
- ▽ TCP, conventional sintering Binder jetting [128]
- ◇ DLM infiltrated TTCP/b-TCP 3DP [129]
- ☆ HA DIW [130]
- ✱ CaP Binder jetting [131, 132]
- ⬠ TCP Binder jetting [132]
- ☆ TCP+ZnO Binder jetting [133]
- ⬠ Bioglass SLS [134]
- △ HA SLA [135]
- × TCP DIW [136]
- ◇ Lamellar HA Freeze casting [137]

Flaw limited strength

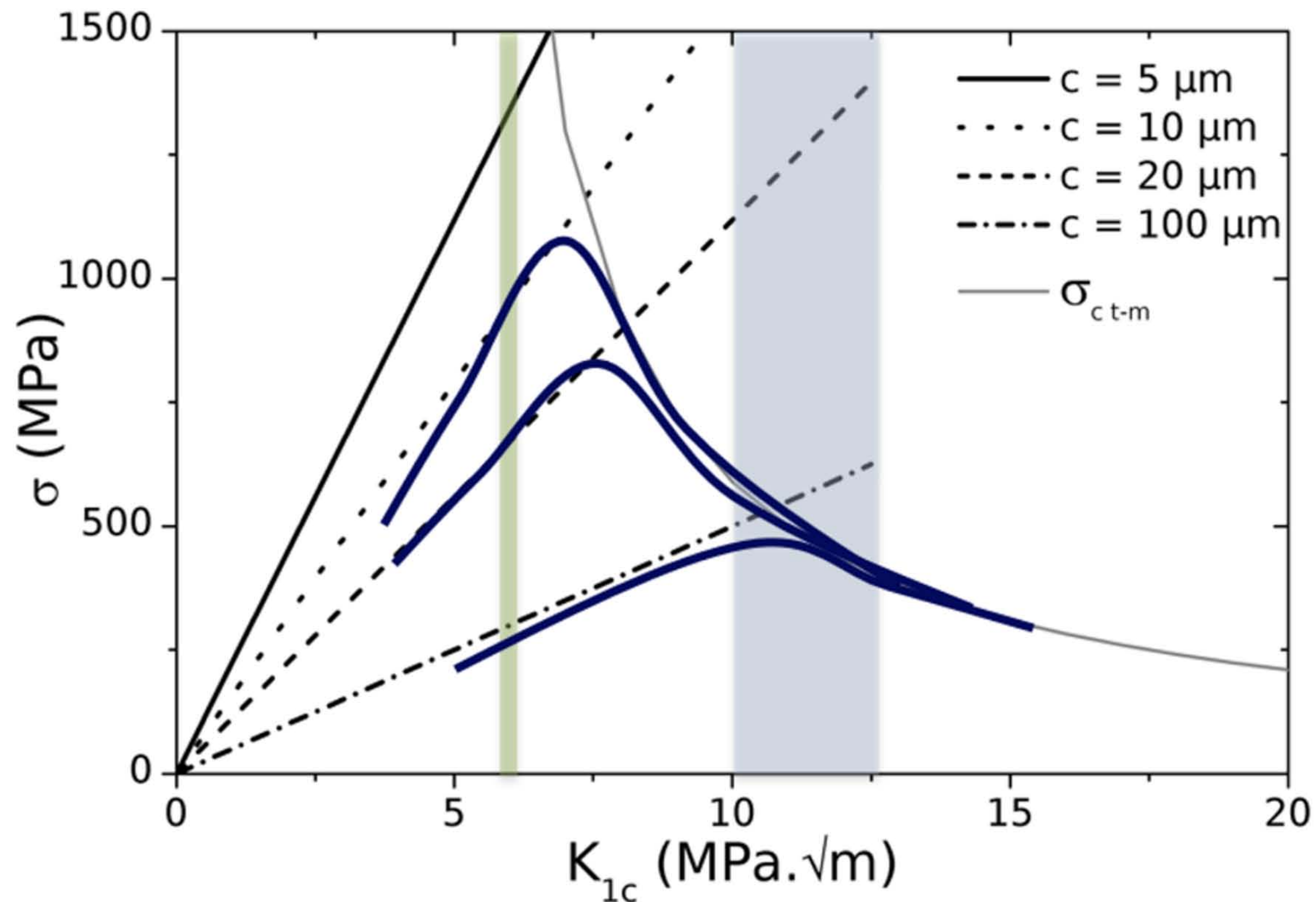
Transformation follows crack growth



Key parameter:
Flaw size

$$\sigma_R = \frac{K_{IC}}{\sqrt{\pi \times c}}$$

3Y-TZP 9-10 Ce-TZP



Transformation limited strength

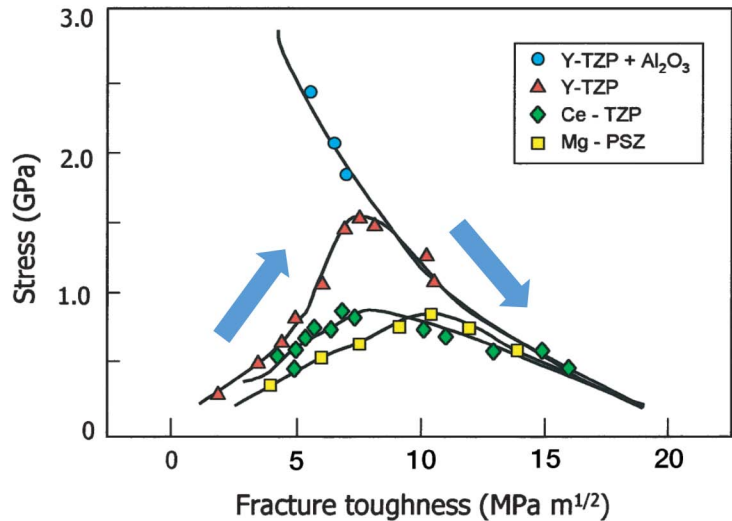
Transformation precedes failure

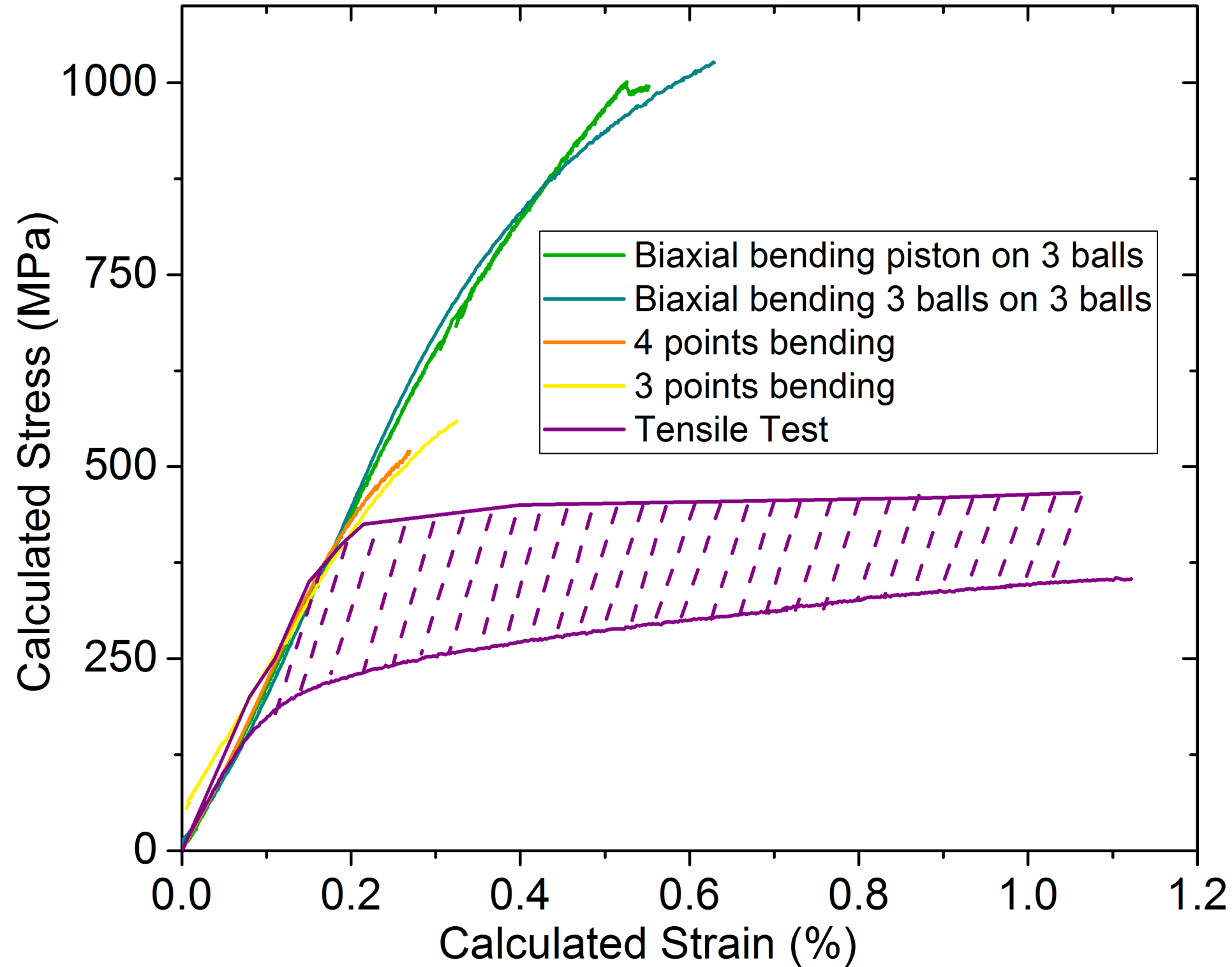


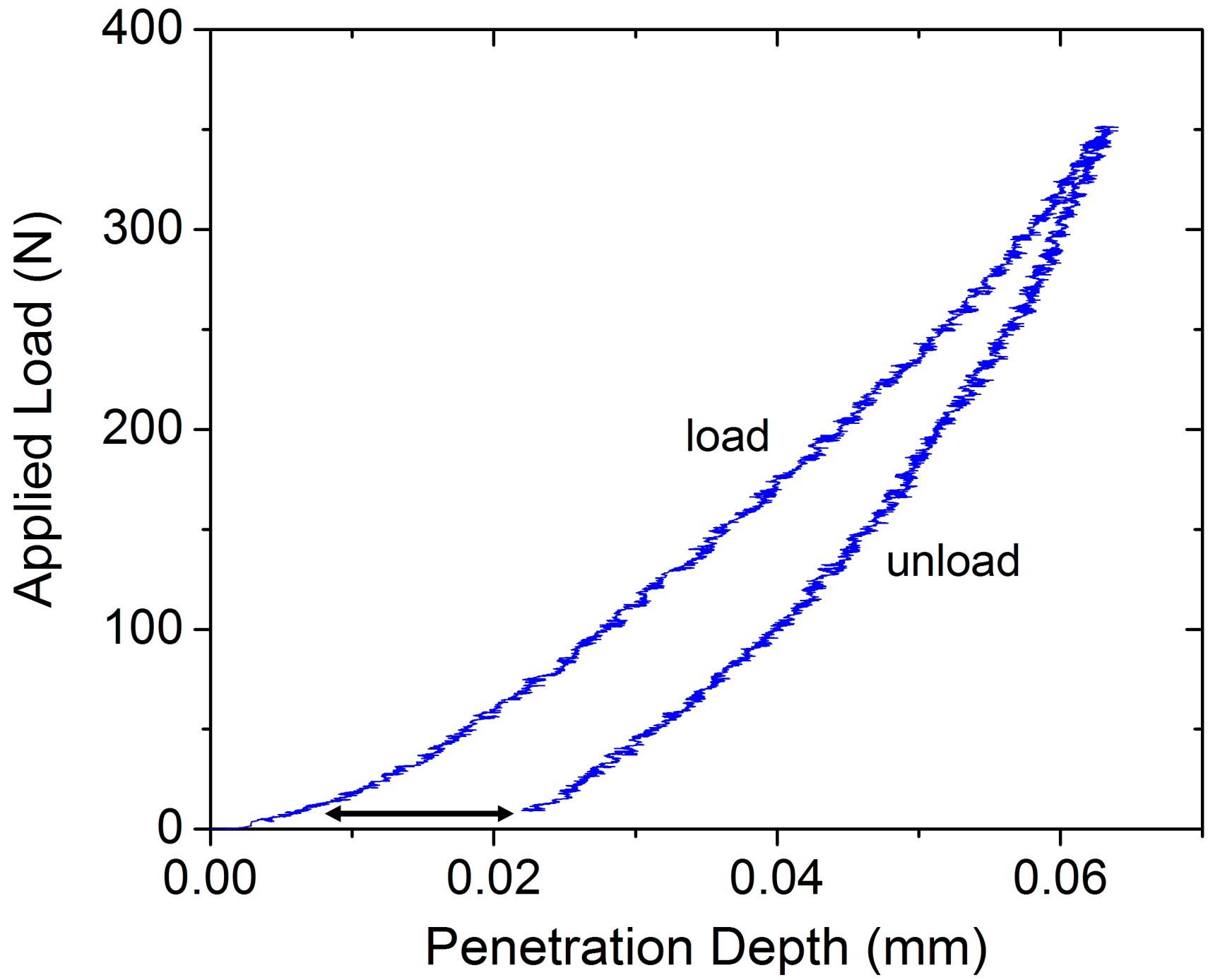
Key parameter:
 σ_c^{t-m}

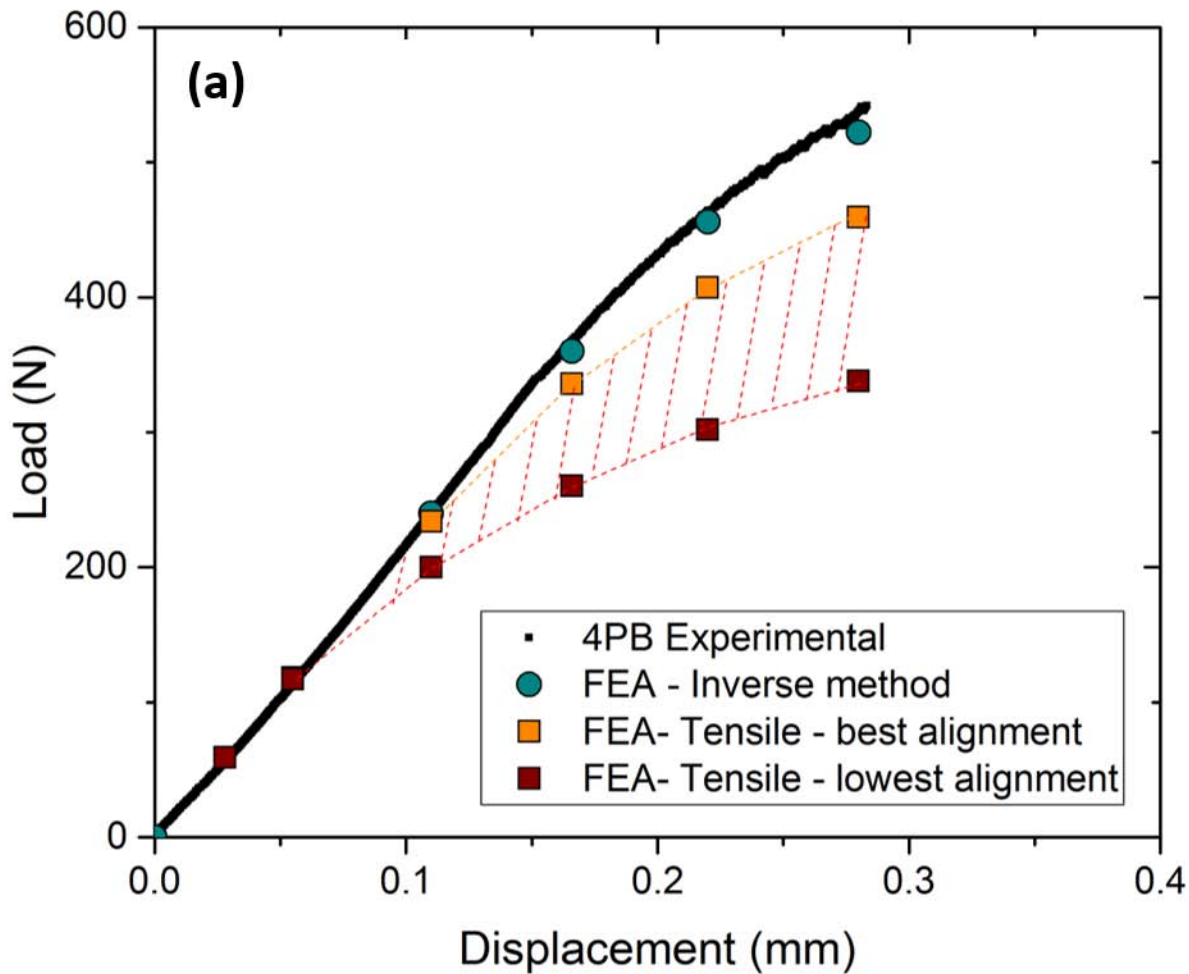
$$\sigma_R = \alpha \times \sigma_{c-t-m}$$

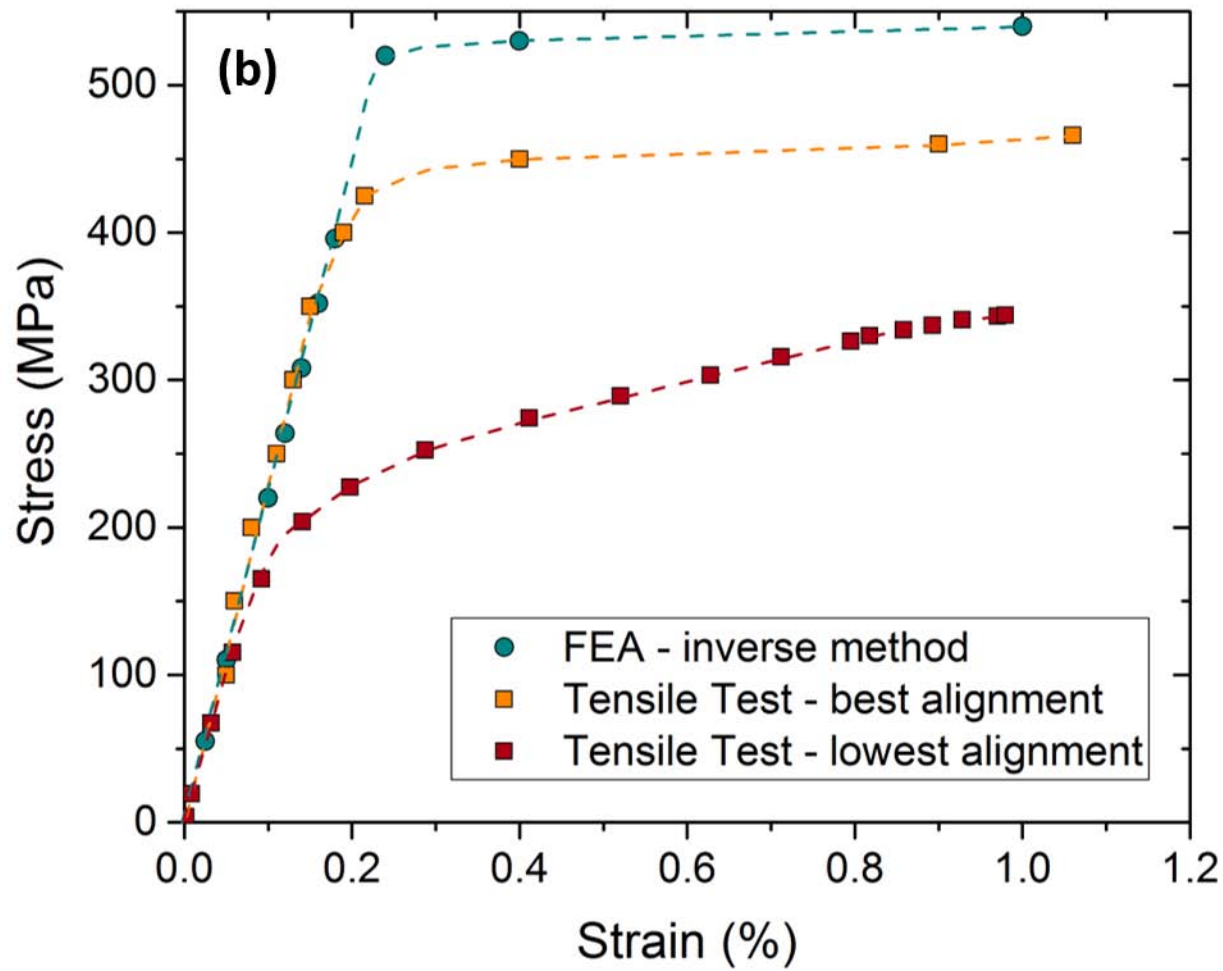
$$\alpha \sim 1$$

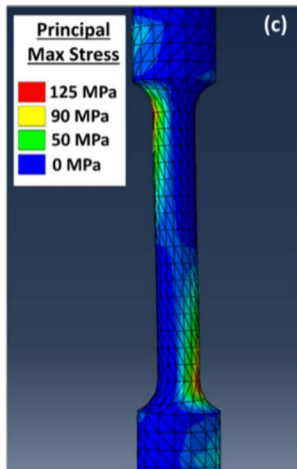
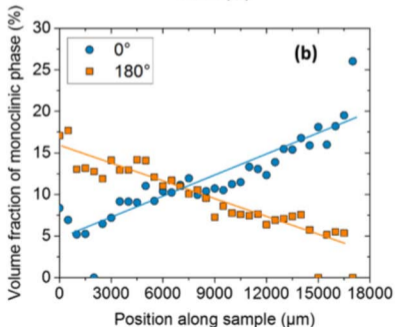
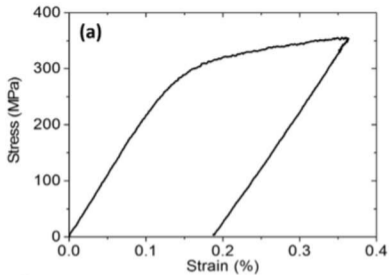













4 Point Bending


450 N

3 mm




500 N

3 mm

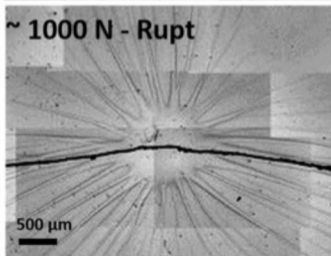
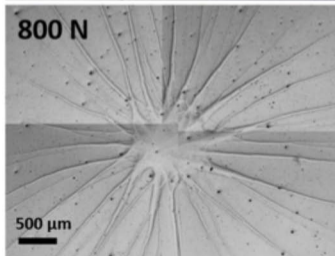
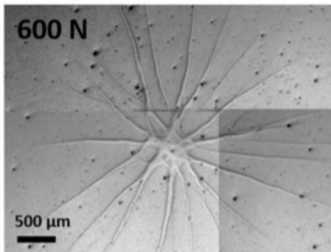
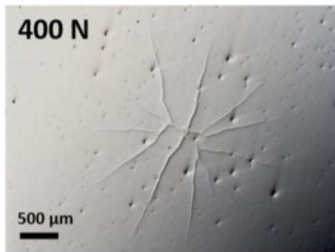


545 N - Rupt

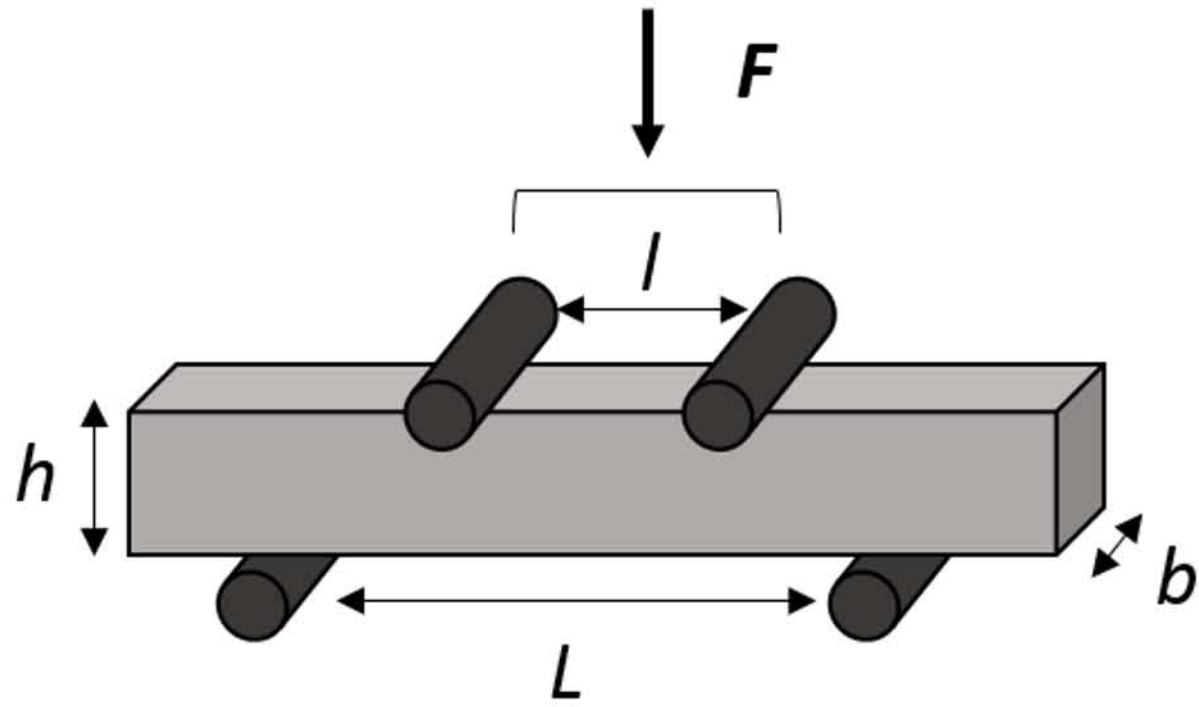
3 mm



Biaxial Bending – Piston on 3 balls



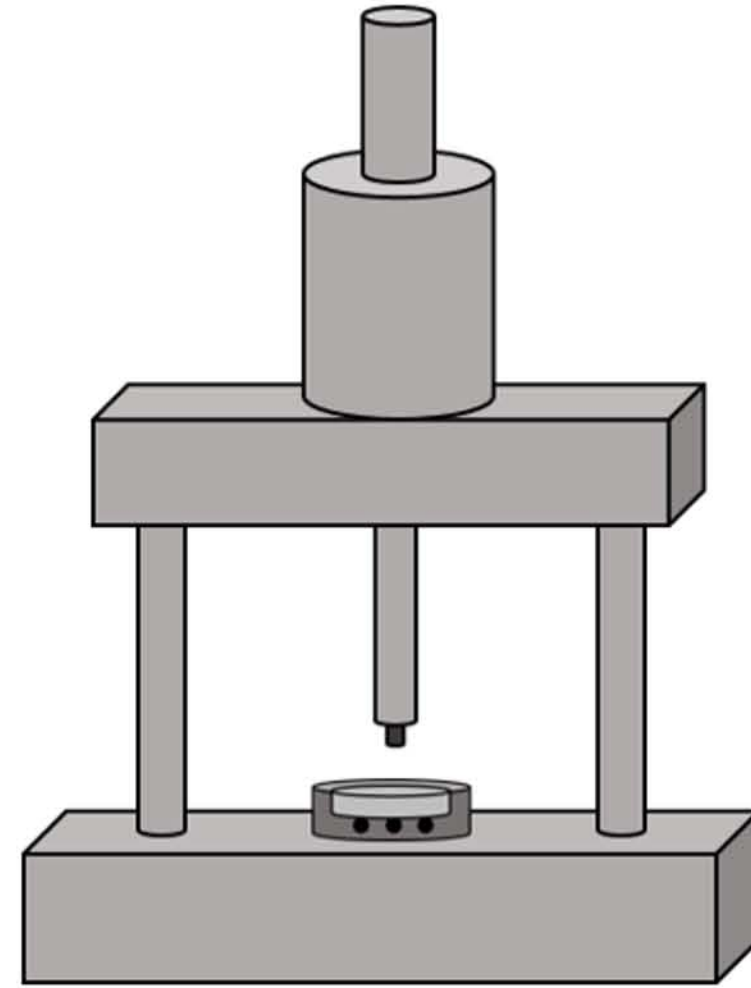
4 Point Bending



$$\sigma_{max} = \frac{3 F(L-l)}{2 b h^2} \quad (1)$$

With F the load to failure, b the width, h the thickness of the sample, L and l the outer and inner spans

Biaxial Bending Piston on 3 balls



$$\sigma_{max} = \frac{-0.2387 F(X-Y)}{t^2} \quad (2)$$

$$X = (1 + \nu) \ln\left(\frac{r_2}{r_3}\right)^2 + \left[\frac{(1 - \nu)}{2}\right] \left(\frac{r_2}{r_3}\right)^2$$

$$Y = (1 + \nu) \left[1 + \ln\left(\frac{r_1}{r_3}\right)^2\right] + (1 - \nu) \left(\frac{r_2}{r_3}\right)^2$$

With F the load to failure, t the thickness of the disk sample, r_1 the radius of the supported circle, r_2 the radius of the piston, r_3 the radius of the disk sample and ν the Poisson's coefficient

Tensile Test

